X-ray crystallographic studies of toxic shock syndrome toxin-1 and related superantigens

Passalacqua, Edward F.

Award date:
1995

Awarding institution:
University of Bath

X-ray Crystallographic Studies of Toxic Shock Syndrome Toxin-1 and Related Superantigens.

Submitted by Edward F. Passalacqua

for the degree of Ph.D.

of the

University of Bath 1995.

COPYRIGHT

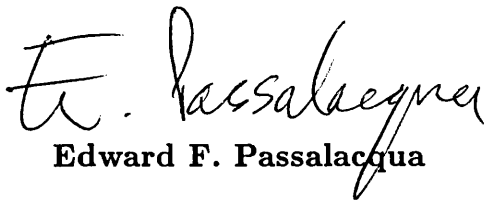

Edward F. Passalacqua

ProQuest LLC
789 East Eisenhower Parkway
P.O. Box 1346
Ann Arbor, MI 48106-1346

Abstract

Three staphylococcal enterotoxins (SE) A, B and C2 and the toxic shock syndrome toxin-1 (TSST-1) were purified to homogeneity by a simple two-step procedure involving dye ligand and fast protein liquid chromatography. These toxins were all shown to be $> 99\%$ pure as shown by SDS-PAGE. Crystallization trials were prepared for all four purified toxins. Crystals of TSST-1 and SEC2 suitable for X-ray diffraction work were grown. Crystals of SEB were found to be highly disordered and further trials were not pursued. No crystals of SEA were obtained.

The 3D structure of TSST-1 was determined using X-ray crystallography to 2.5Å and a final crystallographic R-factor of 0.213. This toxin has a two domain structure characteristic of SE. A structural basis for the superantigenic properties of TSST-1 was elucidated. Based on our structural data in combination with other available data on TSST-1, a trimolecular model consisting of TSST-1, the major histocompatibility complex class II (MHC II) and T cell receptor (TcR) was proposed. Subsequent X-ray crystallographic studies of the MHC II/TSST-1 complex have validated this general model. A brief comparison of the wild type TSST-1 structure with that of TSST-1 complexed to MHC II was undertaken. This highlighted some significant differences on the TSST-1 structure to accommodate the MHC II-bound peptide fragment.

Attempts were also made to elucidate the 3D structure of SEC2 by molecular replacement, using the refined TSST-1 structure as the search model. This proved to be ambitious and the structure of SEC2 could not be determined.

A TSST-1 mutant (Lys 105 Glu) was crystallized, and the structure

was determined to 2.8Å resolution.

Dedication

This thesis is dedicated in its entirety to my mother,

Honora,

whose many, many sacrifices over the years have allowed

me to achieve my goals.

Acknowledgements

First and foremost I would like to thank my main supervisor Ravi Acharya for his enthusiasm, dedication and tenacity, all of which rightly culminated in this successful project. Special thanks must go to Ashley Pike for his help with computing. I would like to express my appreciation to Demetri and Tassos for their helpful discussion. I would like to acknowledge Vasanta Subramanian for her help and lab facilities with the gel filtration work.

Next to Salisbury. I would first like to thank my industrial supervisor, Howard Tranter, for reading this thesis, his helpful discussion and his understanding. A very special thank-you must go to Rossalyn Brehm for the time I spent in her lab purifying the toxins. I would like to acknowledge Gerald Adams for lyophilizations and Andy Gorringe for assistance with photographs. I must not forget everyone at Centre for Applied Microbiology and Research (CAMR) for making my stay there a most enjoyable and memorable one.

Oxford. Special thanks has to go to the Laboratory of Molecular Biophysics, in particular Dave Stuart for the two weeks of dedicated use of the image plate time, extensive use of his unpublished computer programs and computer time. Thanks to Karl Harlos for all his help with heavy atom data collection work. Yvonne Jones' contribution to computing was crucial to the structure presented here.

Don Wiley kindly provided DR1/TSST-1 complex coordinates.

I would like to thank the Science and Engineering Research Council and CAMR for their awards which allowed me the great privilege to work on this Ph.D. project.

Finally, thank-you to all my family and friends who have encouraged me and followed my progress throughout this project.

Symbols and Abbreviations

(hkl)	Unique reflection plane (or Miller indices)
2θ	Angle between incident and diffracted beams
Å	Ångstroem units (1Å=10^{-8}cm)
B	Atomic temperature factor
d	Days
F_o	Observed structure factor amplitude
h	Hours
I	Reflection intensity
MFID	Mean fractional isomorphous difference
min	Minutes
MIR	Multiple isomorphous replacement
$P(uvw)$	Patterson function
R	Crystallographic agreement residual index
s	Seconds
d	Interplanar spacing of a set of planes in a crystal
d_{min}	Minimum value of d *ie.* the resolution limit
α, β, γ	Real space unit cell angles
α_C	Calculated protein phase angle
α_H	Heavy atom phase angle
α_P	Protein phase angle
α_{PH}	Heavy atom derivative phase angle
$\mathbf{F_P}, \mathbf{F_{PH}}$	Structure factor for native protein (P) and heavy atom derivative (PH)
rms	Root mean square

$\mathbf{F}(hkl)$	Structure factor
F	Structure factor amplitude
λ	Wavelength of incident X-ray
ρ	Electron density
σ	Standard deviation
Ag	Antigen
CAMR	Centre for Applied Microbiological Research
CDR	Complimentarity determining region
Con A	Concanavalin A
EDTA	Ethylenediaminetetraacetic acid
ELISA	Enzyme linked immunosorbant assay
FPLC	Fast protein liquid chromatography
HEPES	4-(2-hydroxyethyl)-1-piperazineethanesulphonic acid
HLA	Human leukocyte antigen
IEF	Isoelectric focussing
IL	Interleukin
M_r	Relative molecular mass
MHC	Major histocompatibility complex
MRC	Medical Research Council
NCS	Non-crystallographic symmetry
NMR	Nuclear magnetic resonance
PAGE	Polyacrylamide-gel electrophoresis
PBS	Phosphate buffered saline
PEG	Polyethylene glycol
SAg	Superantigen
SDS	Sodium dodecyl sulphate

SEs	Staphylococcal enterotoxins (A-E)
SIDS	Sudden infant death syndrome
SRID	Single radial immunodiffusion
SRS	Synchrotron Radiation Source, Daresbury, UK.
TNF	Tumor necrosis factor
TRIS	Tris(hydroxymethyl)methylamine
TSS	Toxic shock syndrome
TSST-1	Toxic shock syndrome toxin-1
TcR	T cell receptor
Vβ	Variable β gene segment of the T cell receptor

CONTENTS

Chapter 2: Protein X-ray Crystallography

Reprints of Project Publications

TABLES AND FIGURES

Chapter 1

Chapter 2

Chapter 3

Chapter 4

Chapter 5

Chapter 1

Introduction

1.1 The Role of Staphylococcal Toxins in Disease

Staphylococcus aureus produces a wide variety of biologically active extracellular virulence factors, known to be the causative agents in the pathogenesis of a number of human diseases (Chesney *et al.*, 1984). These virulence factors include: hyaluronidase, leucocidin, lipase, protease, coagulase, haemolysins (A-D), exfoliative toxins, staphylococcal enterotoxins (SE) and toxic shock syndrome toxin-1 (TSST-1) (Tranter and Brehm, 1994). Some toxins produced by *Streptococcus pyogenes* (Group A), share cross-reactivity with SEB and SEC1 (Johnson and Schlievert, 1984; Bohach *et al.*, 1988; Abe *et al.*, 1991; Alouf *et al.*, 1991). These toxins have been described as 'superantigens' for their capacity to stimulate those T cells which possess a specific Vβ gene segment on the cell surface (Section 1.6).

1.2 Toxic Shock Syndrome Toxin-1 (TSST-1)

Toxic shock syndrome (TSS) was first described by Todd and coworkers in 1978 (Todd *et al.*, 1978) as an acute life-threatening multisystem disease (Table 1.1). The disease is caused by a toxin, toxic shock syndrome toxin-1 (TSST-1), produced by some but not all strains of *Staphylococcus aureus*. In menstrual cases the disease, which begins suddenly, was originally thought to be exclusively restricted to extended tampon use in young women (Davis *et al.*, 1980; Shands *et al.*, 1980), and caused by significant

colonization of the vagina by TSST-1-producing strains of *Staphylococcus aureus*.

Subsequent research has shown that TSS is not exclusively a menstrual event and can also occur after any surgical procedure in both men and women following post-operative wound infection (Schlievert, 1983). Between 15 - 30% of non-menstrual cases occur as a result of soft tissue infection and non-genital *Staphylococcus aureus* wounds (Schlievert, 1983; Blomster-Hautamaa and Schlievert, 1988). Toxic shock syndrome tends to occur if the infected person has none or very low levels of anti-TSST-1 antibodies present (Crass and Bergdoll, 1986). Indeed the presence of high levels of anti-TSST-1 antibodies has been shown to reduce the incidence of the symptoms of TSS (Staneck and Bonventre, 1984). Fatality rates for menstrual toxic shock syndrome are currently approximately 10% (Alouf *et al.*, 1991). In non-menstrual cases, in addition to TSST-1 the staphylococcal enterotoxins, in particular SEB and SEC1, may also cause toxic shock syndrome (Schlievert, 1984; Garbe *et al.*, 1985; Schlievert, 1986; Kunstmann *et al.*, 1989; Bohach *et al.*, 1990). Indeed, the SE make up approximately 50% of all non-menstrual cases of TSS, such as infected burns, while the other 50% of cases are caused by TSST-1 (Lee *et al.*, 1992a). The SE have also been shown to cause the symptoms of TSS in a rabbit model (Sloane *et al.*, 1991). Case reports of those adults who do not make a complete clinical recovery have been shown to suffer numerous illnesses including a permanent loss of hearing and extensive tissue necroses requiring plastic surgery and this has been attributed to capillary leakage (Lee *et al.*, 1991).

1.3 Staphylococcal Enterotoxins

The SE have long been known to cause staphylococcal food poisoning. Dack and co-workers (1930) were the first to show that this illness was caused by toxins produced by *Staphylococcus aureus* by examining the uneaten portion of a three-layer cream cake. This cake was thought to be the source of food poisoning in eleven people resulting in cramping, vomiting and diarrhoea. Laboratory analysis of the cake revealed Staphylococci. Growth media, inoculated with the contaminated cake, was then centrifuged and the supernatant given to human volunteers. These volunteers became ill with the same signs and symptoms as the original eleven (Bergdoll, 1990). The toxic factors were named enterotoxins because of their effect on the gastro-intestinal tract. However, this is a misleading name because there is no fluid accumulation when the toxins are assayed using the standard ligated rabbit ileal loop, as is normally seen with true enterotoxins such as *Escherichia coli* heat-labile enterotoxin (Iandolo and Tweeten, 1988; Sixma *et al.*, 1991). Numerous foods have been implicated in this type of food poisoning such as: dairy products, especially cream and custard fillings, and cooked meats. The most important source and route of transmission of such contaminated foods by *Staphylococcus aureus* is by food handlers. Indeed 30 - 40% of healthy individuals carry this organism, which is found mainly in the nose, hands, throat and skin (Bergdoll, 1990).

The clinical symptoms of staphylococcal food poisoning are: salivation, profuse vomiting, nausea, abdominal cramps and diarrhoea. These symptoms usually occur within 1 to 6 hours after ingestion of contaminated food but full recovery is usually seen between 24 to 48 hours. The severity of the symptoms depends on the amount of toxin present and the quantity

of the contaminated food ingested as well as the absence of the necessary circulating antibodies. Fatalities are very rare and are only occasionally observed in the very young or the elderly.

1.4 General Toxin Characteristics

1.4.1 Toxic Shock Syndrome Toxin-1

TSST-1 is a single chain polypeptide which does not contain any nucleic acid, carbohydrate, lipid or cofactor moieties. It has a M_r of 22,049Da as deduced from its nucleic acid sequence, which translates into 194 amino acids (Blomster-Hautamaa *et al.*, 1986a). It can exist at two different *p*Is: 7.08 and 7.22, which may be a result of deamidation during the production and/or purification processes (Blomster-Hautamaa *et al.*, 1986b). TSST-1 does not contain any cysteine residues and shares about 24% sequence identity with the SE (Figure 1.1). The toxin is trypsin resistant but can be degraded by exposure to papain or pepsin (Reiser *et al.*, 1983; Edwin and Kass, 1989).

TSST-1 was independently isolated and purified by two groups in 1981. Bergdoll and co-workers (Bergdoll *et al.*, 1981) called their toxin SEF, whilst Schlievert and his colleagues referred to it as pyrogenic exotoxin C (PEC; Schlievert *et al.*, 1981). Further detailed biochemical and immunological studies showed that SEF and PEC were in fact identical and the toxin was renamed toxic shock syndrome toxin-1 (TSST-1) (Bonventre *et al.*, 1983; Bergdoll and Schlievert, 1984). An ovine-derived form of TSST-1 has been isolated from mastitis-infected animals (Lee *et al.*, 1992b). Of the 194 residues, only nine are different compared with 'human' TSST-1.

1.4.2 Staphylococcal Enterotoxins

The structurally related SE can be classified into five serologically distinct groups: SEA (Casman, 1960), SEB (Bergdoll *et al.*, 1959), SEC (Bergdoll *et al.*, 1965), SED (Casman *et al.*, 1967) and SEE (Bergdoll *et al.*, 1971). SEC can be further subdivided into: SEC1 (Borja and Bergdoll, 1967), SEC2 (Avena and Bergdoll, 1967) and SEC3 (Reiser *et al.*, 1984) due to minor differences in their epitopes especially involving residues 20, 22 and 26 (Turner *et al.*, 1992). The SE range in size from 26 - 29 kDa, possess between 228 and 239 amino acids, and share 30-85% sequence homology. The gene sequences encoding all the SE have been elucidated (Betley *et al.*, 1990). The amino acid composition of the SE are similar with respect to the high content of aspartic acid, lysine and tyrosine residues, they all have one centrally located disulphide loop which varies in length from 10 to 20 residues. The only sequence (Figure 1.1) where there is up to five sequential amino acid residues identical amongst all the SE, follows the second cysteine residue of : SEA, SEB, SEC1-3, SED and SEE. This sequence is close to a conserved histidine residue thought to be involved in the emetic properties of SEA (Stelma and Bergdoll, 1982). All SE exist with multiple isoelectric points which may be attributed to deamidation caused during the culture or purification processes.

The SE can be split into two groups based on their sequence identity (Marrack and Kappler, 1990). One group consists of SEA, SED and SEE, with SEA and SEE sharing 85% primary sequence similarity (Huang *et al.*, 1987; Couch *et al.*, 1988; Bayles and Iandolo, 1989). The other group comprises SEB and the SECs which share 63% similarity (Huang and Bergdoll, 1970; Schmidt and Spero, 1983; Couch and Betley, 1989). All the toxins

are very soluble in water and salt solutions, are heat and protease resistant, and can withstand extremes of *p*H.

1.4.3 Animal Models

Many species of animals including rabbits, rats, kittens and primates (monkeys) have been tested in attempts to provide a suitable model for studying the biological activities of these toxins. Rabbits have been used to study shock induced by both TSST-1 and SE. Multi-organ damage at autopsy was shown to occur after administration of toxins to rabbits (Reeves *et al.*, 1986). Rats have been used for SE work but they do not possess a vomiting response and so cannot be compared directly. Their capacity to tolerate higher doses of SE, which are fatal to rabbits, has also been noted (Schlievert, 1982). The results of work carried out on the kitten model has been considered unreliable and therefore discredited (Bergdoll, 1983). In contrast humans and primates do react in a similar manner to challenge with SE. For this reason monkeys have been the animal of choice for experimental work (Bergdoll, 1988). In contrast with other toxins such as cholera, which induce diarrhoea via the activation of the adenylate cyclase pathway, the SE do not. The basis of the emetic response to SE, once they have passed through the gut wall, is still unclear. It may result from binding to local receptors in the digestive tract which transmit signals via the sympathetic and vagus nerves to the subcortical vomiting centre of the brain. Alternatively the SE may activate the release of leukotrienes from mast cells (Alber *et al.*, 1990). Controlled experiments in monkeys in which these nerves were severed, showed no signs of emesis when administered with SE (Alouf *et al.*, 1991).

1.5 Detection of Staphylococcal Toxins

Biological assays for the SE such as the monkey feeding test and kitten test are expensive and cannot be used for routine detection of these toxins. Furthermore, animals may eventually develop tolerance to the toxins (Bergdoll, 1988). Although they do not detect the biological activity of the SE, immunological assays have been developed which can rapidly determine the concentration of toxins in numerous samples. Indeed, there are now many methods available for the identification and quantification of TSST-1 and SE (Tranter and Brehm, 1994), which differ according to the level of sensitivity required (Table 1.2). Due to the fact that these toxins can bring about a response at nanomolar concentrations, only the ELISA, radioimmunoassay and reverse passive haemagglutination methods are suitable for screening purposes.

1.6 Conventional Antigens and Superantigens

Conventional peptide antigens are the degradation products of a much larger invading pathogen or protein. These immunogenic peptide fragments are recognised as a linear epitope by the T cell receptor (TcR) when complexed in the cleft of a major histocompatibility complex class I or class II (MHC I or II) glycoprotein molecule on the surface of an antigen presenting cell (Figure 1.2a; Germain and Margulies, 1993). Crystal structures of the peptide fragments bound to either the MHC I or II show how they become incorporated into the binding site cleft (Brown *et al.*, 1993; Madden *et al.*, 1993). There are two types of TcR, the most common is a heterodimer of α and β chains (Marrack and Kappler, 1987), the other being γ and δ chains; the δ is equivalent to the α chain and the γ equivalent

to the β chain. The $\gamma\delta$ TcR are found in the peripheral blood and tissues (Brenner *et al.*, 1986; Ferrick *et al.*, 1989).

All five germline encoded variable elements of the TcR α and β heterodimer: Vα, Jα, Vβ, Dβ and Jβ make a contribution to recognizing conventional antigens in this complex (Marrack and Kappler, 1987). Non-germline encoded amino acid residues between these different elements may also be involved thus increasing the number of possible antigens recognised. Figure 1.2a shows that the complementarity determining regions (CDR) CDR1 and CDR2 lie directly above the two α helices of the MHC II molecule. The CDR3 region, generated by the V-D-J junctional residues, is located above the peptide fragment. As a consequence of this variation, there are over a million possible arrangements of these elements which allow only a very small proportion of all T cells to be activated by a conventional antigen. It has been estimated that these conventional antigens stimulate between 0.0001% and 0.01% of resting T cells (Kotb, 1992).

It is generally accepted (White *et al.*, 1989; Cazenave *et al.*, 1990; Choi *et al.*, 1990; Marrack and Kappler, 1990; Pullen *et al.*, 1991) that TSST-1 and the SE have an absolute requirement to bind first to the outside of the MHC II molecules (Dellabona *et al.*, 1990) expressed on antigen presenting cells (monocytes/macrophages, B cells or any cell line expressing MHC II molecules) before binding to the TcR Vβ gene segment, (Figure 1.2b). The MHC I molecules do not appear to interact with SE or TSST-1 and are therefore not necessary for T cell activation (Fraser, 1989). Unlike conventional antigens, these toxins do not need to be processed before binding to the MHC II molecule and the TcR (Carlsson *et al.*, 1988; Fleischer and Schrezenmeier, 1988; Norton *et al.*, 1990). The toxin-MHC II complex

is then recognised by the TcR, specifically those T cells expressing a particular receptor Vβ gene sequence, which is specific to the toxin (Choi *et al.*, 1989; Kappler *et al.*, 1989; White *et al.*, 1989). The Vα portion does not appear to be required for superantigenic activity (Gascoigne *et al.*, 1991). The different Vβ specificities for the SE and TSST-1 are shown in Table 1.3.

This trimolecular complex brings about the subsequent stimulation, proliferation and thymic deletion of large numbers of specific Vβ T cells. Due to their ability to induce polyclonal stimulation of T cells based solely on the TcR Vβ type, rather than on contributions from both α and β chains, these toxins have been called 'superantigens' (White *et al.*, 1989). Other superantigens include the mouse mammary tumour virus, *Clostridium perfringes* enterotoxin, and *Streptococcus pyrogenes* toxins A-C (Marrack *et al.*, 1993; Micusan and Thibodeau, 1994). Superantigens can stimulate between 5% and 20% of the resting T cell population even at nanomolar concentrations (Kotb, 1992). The clinical symptoms of illness caused by the SE and TSST-1 may be due to an increase in the transcription activation and subsequent circulatory levels of chemical messengers, or cytokines, such as interleukin-1 (IL-1) and tumour necrosis factor (TNF) following massive T cell proliferation (Ikejima *et al.*, 1984; Parsonnet *et al.*, 1985; Fast *et al.*, 1989; Marrack *et al.*, 1990; Miethke *et al.*, 1992). Superantigens can also enhance the hosts susceptibility to lethal shock by Gram-negative endotoxins such as lipopolysaccharide (Sugiyama *et al.*, 1964; Schlievert *et al.*, 1981). Although superantigens have been shown to be pyrogenic and induce B cell proliferation and immunoglobulin secretion (Schlievert *et al.*, 1981; Mourad *et al.*, 1989; Wood and Holsapple, 1993), TSST-1

has also been shown to suppress immunoglobulin secretion. This latter property may result in the growth of Gram-negative bacteria (Poindexter and Schlievert, 1986) which may in turn enhance the potency of these molecules. There are two major differences between superantigens and other non-specific mitogens such as concanavalin A (ConA). Firstly ConA binds directly to the TcR and does not depend on any specific variable gene segment; secondly, presentation of non-specific mitogens by the MHC II molecules is not necessary for stimulation. A summary of some of the common properties of the superantigens is shown in Table 1.4.

Studies of monoclonal antibodies to the Vβ gene segment of the TcR have shown that almost all T cells with a particular Vβ element are stimulated by a specific superantigen (Fleischer and Schrezenmeier, 1988; Choi *et al.,* 1989; Uchiyama *et al.,* 1991). The other variable genetic elements of the TcR: Vα, Jα, Dβ and Jβ do not appear to be involved in this binding. The superantigen does not bind in the groove of the MHC II like normal antigens but at other sites on the molecule. There appears to be confusion at present as to the requirement for other co-receptors, such as lymphocyte function associated antigen 1 and 3, in order to bring about superantigenic function. Some researchers suggest that they are not required for superantigenic activity (Gascoigne *et al.,* 1991), whereas others argue that they are required for differential involvement (Mitrücker *et al.,* 1992; Lagoo *et al.,* 1994).

Although the literature contains much information regarding proliferation of T cells expressing $\alpha\beta$ TcR there is little reference to proliferation of T cells bearing $\gamma\delta$. The latter do appear to proliferate in a similar MHC II restricted manner (Fleischer and Schrezenmeier, 1988; Fleischer *et al.,*

1989). Rust and co-workers (1990) showed that SEA had a specificity for the Vγ9 molecule.

The toxins may induce the development of numerous T cell mediated autoimmune diseases as a consequence of their superantigenic activity (Kotb, 1992). These include Kawasaki disease, psoriasis and rheumatoid arthritis (Palliard *et al.*, 1991; Kotzin *et al.*, 1993). If a dramatic increase in T cell numbers occurs, any 'loose' self-T cells which have not been deleted in the thymus may proliferate and attack the host. In a similar way superantigens may also be implicated in other diseases such as sudden infant death syndrome (SIDS) (Telford *et al.*, 1989; Malam *et al.*, 1992). Staphylococcal enterotoxins have been found in approximately 40% of SIDS cases at autopsy (Blackwell *et al.*, 1992; Malam *et al.*, 1992). Most SIDS cases occur at a mean age of three months which is a similar age at which there is maximal expression of the Lewis blood group antigen. The Lewis blood group antigen cells and HEp-2 cells infected with respiratory syncytial virus have an affinity for strains of *Staphylococcus aureus* which produce enterotoxins. This 'niche' binding may allow *Staphylococcus aureus* to proliferate and secrete toxins into the bloodstream. Clearance of staphylococcal enterotoxins has been shown to occur via the kidney which may explain their presence in this organ at autopsy (Malam *et al.* 1992). In such cases death may have been due to a combination of lack of suitable superantigen antibodies, renal immaturity and poor toxin clearance.

The mitogenicity of the SE has been appreciated for some time ever since SEB was demonstrated to be mitogenic for human cells *in vitro* (Peavy *et al.*, 1970). SEA is the most potent microbial superantigen invoking cytokine release at concentrations as low as 10^{-12}M (Carlsson *et al.*, 1988;

Uchiyama *et al.*, 1989). The *in vivo* effect of SEA and SEB, has been demonstrated when the toxins were given intravenously to primates, resulting in vomiting and diarrhoea within minutes (Zehavi-Willner *et al.*, 1984). This was followed by a dramatic decrease of around 65% in the circulating lymphocytes which lasted for 24 h. These peripheral lymphocytes were found to have normal or decreased [^{3}H]thymidine incorporating activity. This lymphopenia was followed within 48 hours by lymphocytosis and the resulting cells were found to incorporate [^{3}H]thymidine normally without the need for any external stimuli.

1.7 Major Histocompatibility Complex Class II Molecules

Numerous studies have been performed to show that superantigens need to bind specifically and with high affinity to MHC II molecules before they interact with the TcR (Fraser, 1989; Mollick *et al.*, 1989; Scholl *et al.*, 1989a; Karp *et al.*, 1990). For example, monoclonal antibodies to MHC II (HLA-DR) molecules which prevent whole superantigen-HLA-DR complex formation have as a result, prevented T cell stimulation (Carlsson *et al.*, 1988; Fleischer and Schrezenmer, 1988; Fraser, 1989; Janeway *et al.*, 1989; Yagi *et al.*, 1990). Furthermore, the use of mutant cell lines deficient in MHC II molecules, which are unable to stimulate T cells, have shown unequivocally the absolute requirement for each molecule to present superantigens to the TcR (Herman *et al.*, 1991a). Given this requirement for MHC II molecules it is perhaps not surprising that the superantigens have been shown to have a high affinity for human MHC II molecules, with TSST-1 having a k_d of 3×10^{-8}M (Mourad *et al.*, 1989).

Recent work on the *in vitro* binary and ternary complex formation

between soluble SEB, MHC II (as HLA-DR1) and the TcR molecules, has cast doubts as to the necessity of the trimolecular complex requirement (Seth *et al.*, 1994). These workers used native gel electrophoresis and plasmon resonance affinity measurements, to show that SEB could complex directly to the TcR without the need for MHC II. However the same workers were also able to demonstrate the binding of SEB simultaneously to both MHC II and the TcR.

Hewitt *et al.* (1992) have explored the possibility that the MHC II molecule may be redundant under certain circumstances. These workers made use of a TcR Vβ3 region of HA1.7, which is a human HLA-DR restricted T cell clone specific for influenza haemagglutinin. In competition experiments using SEB and SEC2, they demonstrated unresponsiveness in HA1.7 by SEB even in the presence of SEC2. To confirm that SEB bound directly to the TcR without the need for MHC II molecules, they used an MHC II negative T cell line. Although addition of SEB to the transfected cells caused an increase in intracellular calcium ions and subsequent lymphokine production, the cells also showed a down-regulation of the TcR expression. Further challenge of these cells with SEB indicated a decrease in responsiveness. From these results Hewitt *et al.* deduced that SEB could interact directly with the TcR without the need for any MHC II molecules and as a consequence induce a state of unresponsiveness in HA1.7.

Given that all of the SE and TSST-1 show this ability to form a non-covalent complex with HLA-DR, HLA-DQ and HLA-DP (Scholl *et al.*, 1989a; Scholl *et al.*, 1990), there is a marked difference in the capacity of the various MHC II isotypes to present superantigens with HLA-DR$\gg$ HLA-DQ$>$ HLA-DP (Scholl *et al.*, 1989a,b; Karp, 1990; Mollick *et al.*,

1991; Ramesh *et al.*, 1992). In contrast, other workers have suggested that SEA binds to HLA-DR only (Fischer *et al.*, 1989; Fraser, 1989), and SEC2 to HLA-DQ only (Hermann *et al.*, 1989).

The SE and TSST-1 appear to bind to different sites on the MHC II molecules. Kappler *et al.* (1992) have shown that there may be two quite separate binding sites on the MHC II molecule. Competitive binding experiments between TSST-1 and SEB have shown that these two toxins do not compete for binding on HLA-DR molecules (Scholl *et al.*, 1989b; Chintagumpala *et al.*, 1991; Herman *et al.*, 1991b; Pontzer *et al.*, 1991; Russell *et al.*, 1992). In contrast SEA, SED and SEE were shown to compete with both TSST-1 and SEB for HLA-DR molecules. This indicates that SEA might bind to a site on the HLA-DR molecule β chain which overlaps with the site(s) required for both SEB and TSST-1 (See *et al.*, 1990; Chintagumpala *et al.*, 1991). Fraser *et al.* (1992) demonstrated the need for zinc ions for SEA and SEE to bind to MHC II molecules but zinc or other ions were unnecessary for the proper functioning of TSST-1. Herman and co-workers (1991b), and Karp and Long (1992) determined those residues on the MHC II molecule responsible for binding to SEA and SEE. Thus residue 81 was mapped to an α helix of the β chain which pointed away from the nominal antigen binding cleft.

Work using chimeric α and β chains of the isotypes HLA-DR and -DP molecules, expressed on murine cells, indicated that the TSST-1 binding site was on the α 1 domain of HLA-DR molecules (Karp *et al.*, 1990). The TSST-1 molecule was found not to bind at all to the -DP fragment (Karp *et al.*, 1990). Residues on MHC II molecules that have been shown to be important for TSST-1 binding are located on the α helices of both the

α and β chains (Braunstein *et al.*, 1992; Panina-Bordignon *et al.*, 1992). Specifically those residues 36 and 39 which are thought to bind TSST-1 have been shown to point away from the α helices involved in the peptide binding cleft.

The observation that an antigenic peptide was still capable of binding to the HLA-DR cleft whilst at the same time binding TSST-1, suggested that the Vβ domain of the TCR could still make contact with the α 1 domain of the HLA-DR without any apparent interference from TSST-1 (Kotzin *et al.*, 1993).

1.8 Major Histocompatibility Complex Class II Signalling

Superantigens have recently been used to demonstrate that the transmembrane MHC II molecules act as signal-transducing elements (Scholl *et al.*, 1992; See and Chow, 1992; Palkama and Hurme, 1993; Morio *et al.*, 1994). The superantigen/MHC II complex differentially regulates a number of cellular signalling events starting with tyrosine phosphorylation, gene transcription and eventually secretion of numerous cytokines (Lagoo *et al.*, 1994). Enhancement of cytokine production using TSST-1 can occur when using biotin-avidin to cross-link TSST-1 with the MHC II molecules (Scholl *et al.*, 1992). Suppression of tumour necrosis factor (TNF) production by TSST-1 in monocytes was shown using known inhibitors of both tyrosine kinase and protein kinase C. Interleukin-1 production by TSST-1 was totally prevented using a combination of the two previously mentioned inhibitors in addition to both cyclic AMP and cyclic GMP-dependent kinase inhibitors.

1.9 Antigen Presenting Cells and T Cells

See *et al.* (1992) showed that both monocytes and T cells are required for TSST-1 -induced TNF and interleukin production. Using either highly purified monocytes or T cells alone in addition to TSST-1, did not induce cytokine release. However, when both cell types were present in a 1:1 ratio TSST-1 induced cytokine release. In the same study antibodies against interferon-γ (IFN-γ) were used to see if this cytokine had any influence on the interaction between the monocyte and T cell. Anti-IFN-γ antibodies did not appear to prevent TNF production in this system. See and Chow, (1992) demonstrated that direct contact between the monocyte and T cell was a prerequisite for cytokine release by using a twin compartmentalized culture well containing the highly purified individual cell types. Even after introduction of TSST-1, no cytokines were found in the surrounding culture media.

Recently Lagoo and co-workers (1994) demonstrated that in the absence of monocytes, T cells challenged with SE undergo induction of cytokine gene transcription although there is no subsequent formation and release of interleukins and interferon. Gene transcription and release of these cytokines occurred in the presence of monocytes which suggests that perhaps adhesion molecules present on the monocytes and/or T cell population are required to trigger formation and release of cytokines from T cells.

1.10 T Cell Requirement For Superantigenic Activity

White and co-workers (1989) injected neonatal mice with SEB only to find near total elimination of all the mature and some immature T cells

with specific Vβ types (8.1 - 8.3). They concluded that this clonal deletion resulted in tolerance to further SEB injections. Direct evidence to support this hypothesis that an established T cell repertoire is necessary to bring about the biological reactions in response to superantigens was revealed in the form of experiments with mice deficient in T cells (Miethke *et al.*, 1993). When these mice were injected with TSST-1 they showed no symptoms characteristic of the superantigen stimulation. However if these T cell deficient mice were provided with T cells and injected subsequently with TSST-1 they suffered from shock showing the typical increase in TNF and interleukin-2 (IL-2) levels associated with superantigen stimulation. The same series of experiments showed the importance of TNF in shock, because those mice injected with antibodies against TNF did not demonstrate any of the symptoms normally associated with shock.

Further evidence for a T cell requirement has come from studies involving the drug cyclosporin A, an active inhibitor of T cell proliferation, which has been used in organ transplantation work. Cyclosporin A has been used not only to suppress cytokine mRNA expression but also to prevent shock (Bette *et al.*, 1993; Holbrook *et al.*, 1993; Miethke *et al.*, 1993). This drug has also been used to suppress arthritis induced by TSST-1 (Schwab *et al.*, 1993) which is thought to be linked to the prevention of cytokine production in T cells.

Although SEA and SEE are approximately 83% identical, they activate quite different Vβs on the TcR (Table 1.3). For example, SEA binds to Vβ3 but SEE does not; Vβ11 binds SEE but not SEA. Binding assays have been performed on a number of SEA/SEE hybrids in order to map those amino acids responsible for discriminating between the two different

Vβs (Irwin *et al.*, 1992; Hudson *et al.*, 1993). The results indicated that only two amino acid residues 206 and 207, located toward the C terminus, were responsible for this discrimination and as a consequence may directly interact with the TcR Vβ at this region.

1.11 B Cell Proliferation

TSST-1 has been shown to bind with high affinity to MHC II molecules on B cells isolated from tonsils (Mourad *et al.*, 1989) although T cells were found to be necessary for proliferation to occur. As a result of this the B cells changed into immunoglobulin-secreting plasma cells involving both the MHC/TSST-1 and TcR/CD3 complexes from the T/B cell interaction. Immunoglobulin secretion was found to be highly dependent on the ratio of T to B cells; secretion of immunoglobulins decreased with an increase in the total number of T cells which may partly explain the suppression of immunoglobulin production in patients exposed to superantigens.

1.12 Cytokine Production

In 1970 Peavy *et al.* described massive T cell proliferation using SEB with the concomitant production of the cytokine interferon-γ (IFN-γ) from human lymphocytes. This activity has subsequently been found in TSST-1 and all the known SE.

Cytokines are a group of low molecular weight glycosylated proteins (M_r 10 - 24 kDa) and are normally involved in the immunological response to conventional antigens. The complexity of the interactions between different species of cytokines makes analysis of their individual roles difficult.

The pathogenic effects attributed to both TSST-1 and SE may be related to the massive release of cytokines produced by both T cells and antigen presenting cells, over and above normal physiological levels. Cytokines such as INF-γ, IL-1, TNF-α and TNF-β are known to be produced in response to the presence of both TSST-1 and SE whereas: IL-2, IL-3 and IL-6 are produced on exposure to TSST-1 alone. In addition to the increase in cytokine production in response to superantigens there is also an increase in the expression of MHC II molecules and also cell adhesion molecules (Kotb, 1992).

One of the symptoms of toxic shock syndrome, hypotension, may be caused by an increase in capillary leakage and decreased vasomotor tone. This is thought to be directly related to the secretion of IL-1 and TNF-α. Studies on patients suffering from toxic shock syndrome have shown elevated levels of T cells expressing Vβ2 and TNF-α (Panina-Bordignon *et al.*, 1992).

1.13 Immunotherapy

Two compounds, caffeine and pentoxifylline, both from the family of chemicals known as methylxanthines, have been used in studies as possible therapeutic agents in connection with their ability to prevent T cell proliferation (Rosenthal *et al.*, 1992). Such immunotherapy could potentially be directed against autoimmune and inflammatory diseases. An anti-idiotypic antibody coupled to SEB has been used as a form of immunotherapy against tumours in mice (Ochi *et al.*, 1993). The results showed that this toxin-antibody conjugate resulted in a significant extension of the life of the mice and also prevented tumour growth.

Activation of cytotoxic T cells by superantigens including the SEs is attracting great interest as a means of lysing tumour cells containing MHC II molecules (Dohlsten *et al.*, 1991; Hansson *et al.*, 1992). Indeed these experiments showed that MHC II negative tumour cells in rats did not lyse in the presence of SEA or SEB unless IFN-γ was used to induce MHC II expression in the tumour cells. Such observations suggest that in the future SEs could be used to combat colonic and ovarian cancers in humans.

In an alternative form of cancer immunotherapy (Kalland *et al.*, 1993) a hybrid molecule, consisting of a colon carcinoma monoclonal antibody (C215) linked to SEA, bound to and lysed tumour cells. This preparation prevented any further growth of the tumour by secreting TNF and INF-γ *in vitro*.

Table 1.1 *Current medical criteria used to confirm TSS:*

Feature
Fever (> 39°C)
Hypotension (> 90mm Hg)
Diffuse erythematous rash
Abnormal: liver, heart, kidney and lung function
Central nervous system abnormalities
Subsequent desquamation on the palms of the hands and soles of the feet on recovery.

Table 1.2 *Immunological Detection Methods for Staphylococcal Toxins.*

Detection Method	Detectable Concentration Toxin Concentration (ng/ml)†
Single Gel Immunodiffusion	300-1000
Electro-immunodiffusion	500
Optimum Sensitivity Plate	500
Microslide Technique	100
Reverse Passive Haemagglutination	0.4
Radioimmunoassay	0.3
ELISA	0.1

† Data from Tranter and Brehm, (1994)

Table 1.3 *General characteristics of SE and TSST-1.*

Toxin	Mol. wt. (Da)†	Number of Amino Acids†	Major *p*I †	Human Vβ Specificity ‡
SEA	27,078	233	7.3	1.1, 3, 5, 6's, 7.3, 7.4, 9.1
SEB	28,336	239	8.6	3, 12, 14, 15, 17, 20
SEC1	27,496	239	8.6	3, 6.4, 6.9, 12, 15
SEC2	27,589	239	7.0	3, 5, 12, 13.2, 14, 15, 17, 20
SEC3	27,563	239	8.1	3, 5, 12, 13.2
SED	26,360	228	7.4	5, 12
SEE	26,425	230	7.0	5.1, 6's, 8, 11, 18
TSST-1	22,049	194	7.08-7.22	2

† Data from Alouf *et al.*, 1991; ‡ Data from Marrack and Kappler, 1990; Choi *et al.*, 1989; Kotzin *et al.*, 1993.

Table 1.4 *Properties of bacterial superantigens*

Feature
Polyclonal mitogen of T cells
Bind to MHC II molecules
Specificity of particular Vβ gene segment on T cell receptor
Induce cytokine production
Enhance host susceptibility to endotoxic shock
Enhancement and/or suppression of immunoglobulin synthesis.

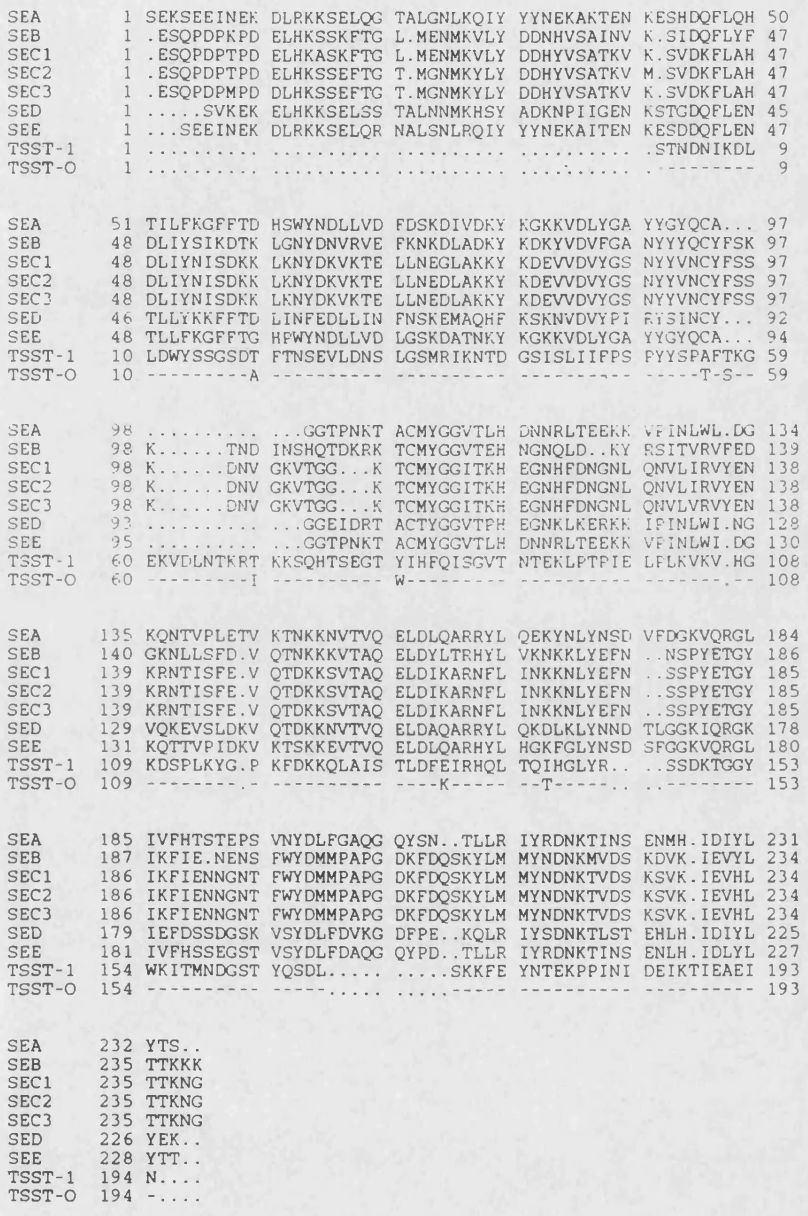

Figure 1.1 Amino acid sequence alignment of SEs A-E, wild type TSST-1 and TSST-O, produced by BESTFIT (GCG; Devereux *et al.*, 1984). Numbers are residue numbers. Hyphens in TSST-O indicate identical residues to TSST-1

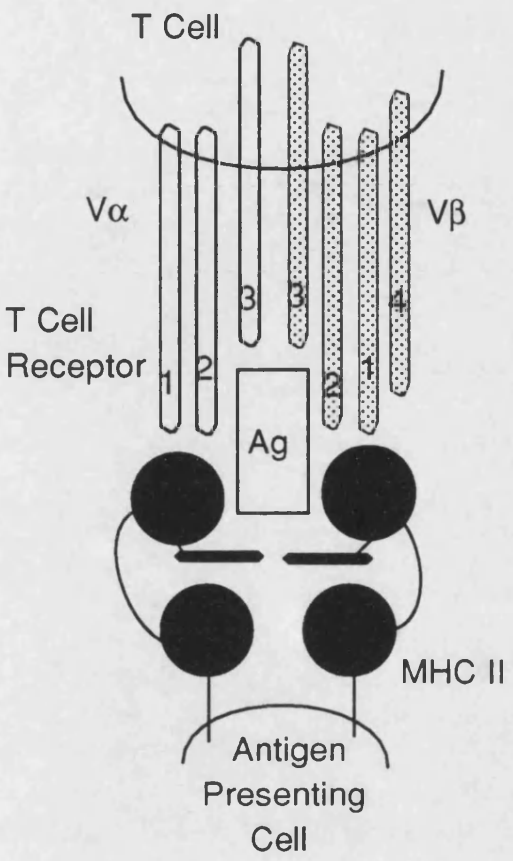

Figure 1.2a

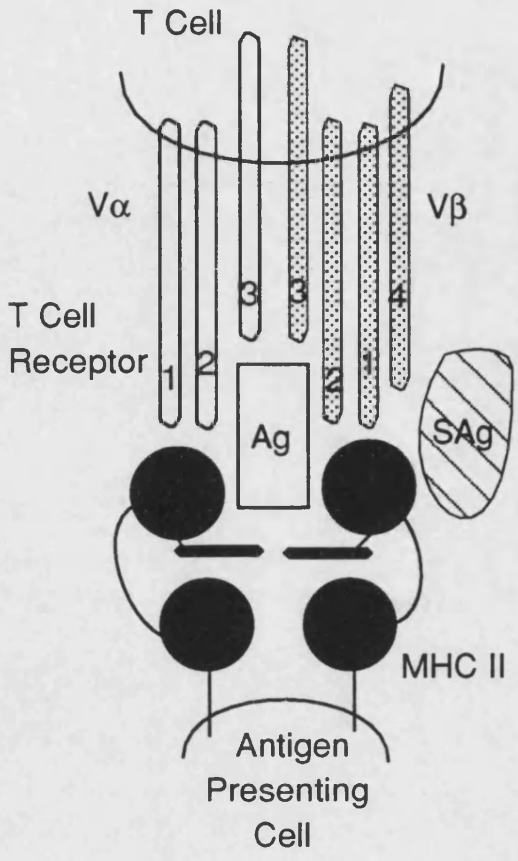

Figure 1.2b

Figure 1.2a Represents the interaction of a conventional peptide fragment with both the full MHC II molecule and the T cell receptor (TcR). The peptide fragment lies in the cleft formed between two α helices, one each from the α chain and the β chain, of the MHC II molecule. The T cell recognizes the peptide-MHC II complex involving numerous components within the α and β chain. The numbers within the TcR indicate the individual complementarity determining regions (CDR) involved in Ag-MHC II recognition. The most important CDR for peptide recognition is CDR3 from both the TcR α and β chains. CDR3 is made up of variations in the junctional regions from Vα-Jα and the Vβ-Dβ-Jβ.

Figure 1.2b Represents the interaction between the superantigen and the peptide fragment-MHC II-TcR complex. As can be seen from this diagram, the superantigen does not bind within the cleft of the MHC II molecule as does the peptide fragment. The superantigen makes contact with the outer α helical region of the MHC II molecule and the solvent exposed face of the TcR Vβ region.

Chapter 2

Protein X-ray Crystallography

2.1 Introduction

The molecular structure of a protein by single-crystal X-ray diffraction consists of a time-averaged molecule, which best fits the scattered X-ray intensities. This average structure consists of contributions from many different conformational intermediate states which arise from the temperature derived fluctuations and collective movements of the protein molecule during data collection. The final static model with its 'ideal' bond lengths and angles is at best only one conformation from the many possible and it must be borne in mind that proteins are not static even at their physiological temperature.

Although biological macromolecules function in aqueous solution, the final refined structure of proteins in the crystal form is still a reasonable representation of the protein in solution as demonstrated by the crystallization studies of several enzymes which were still fully active even after crystallization (Rossi, 1992). Protein molecules in a crystal pack together in such a way as to form a complex network of solvent channels throughout the crystal. This solvent, comprising of the mother liquor, bathes the protein molecules and permits the inward diffusion of any reactants to the active sites, and the movement of products out. As protein crystals can contain anywhere between 30% and 80% solvent, it is thought that the structure deduced from the crystalline form is similar to that in aqueous solution. This has also been demonstrated when comparing small protein

structures determined using both X-ray crystallography and nuclear magnetic resonance (NMR) techniques, and also from crystal structures derived from different space groups.

At present, there are only two major experimental methods capable of providing a three dimensional structure of a biological macromolecule, namely X-ray crystallography (Blundell and Johnson, 1976; *Methods in Enzymology* Vol 114 and 115) and NMR. Although NMR provides the 3D structure of the biomolecule in solution it can only yield detailed information for lower molecular mass proteins consisting of up to one hundred and fifty amino acids residues in size. The classical technique of single crystal X-ray crystallography can provide a wealth of information on macromolecules of a wide variety of sizes and also viruses. However, it can only be used if suitable crystals can be grown in the first instance.

Chemical reactions involve direct interactions between participating molecules, all of which must possess a particular conformation to enable the reaction to proceed. Hence, information on their three dimensional structure could help to explain how these molecules interact and bring about a chemical change, as in the case of enzymes and their substrates. The atomic structure of proteins derived from X-ray diffraction patterns has led to a wealth of information about patterns in protein folding and protein-protein interactions that lead to the formation of large stable biological structures.

2.2 Basic Theory and Practice of X-ray Crystallography

Protein structure can be inferred from a crystal by the way it diffracts a collimated beam of monochromatic X-rays. A protein crystal consists of a periodically repeated assembly of molecules in three dimensions. This

means the protein molecules in a well ordered crystal all possess the same orientation and local environment. The intervening spaces between the protein molecules are occupied mostly by disordered solvent molecules in equilibrium with the crystal supernatant. In this way the crystal diffracts the X-rays as a single molecule. If the protein molecules were orientated randomly, as in a powder sample, the resulting diffraction pattern would be impossible to interpret. X-rays are used to achieve high resolution, or extent of detail, that can be recovered from the crystals which obey the laws of diffraction. In order to 'visualize' the atoms in a protein molecule, the wavelength of the radiation used must be similar to the interatomic separations, for example the C-C single bond length is 1.5Å (1Å = 0.1nm). X-rays have wavelengths in the range 0.6 to 2.0Å and are therefore suitable for work of this nature.

An incident beam of X-rays will interact with the atoms (or more precisely their electrons) present in a crystal resulting in scattered radiation, as a result of reflections from the many planes of atoms. This takes the form of discrete spots which form a diffraction pattern. The periodic nature of the crystals enable it to act as a three dimensional diffraction grating and the resulting diffraction pattern is characteristic of the crystal lattice type and unit cell parameters. The reflected X-rays can reinforce one another in certain directions and are characterised by a location on a 3-D grid or reciprocal lattice. This relates the orientation of the crystal and the angle that the diffracting plane makes with the incident X-ray beam. This reflection can be labeled by three integers (*hkl*), or Miller indices, which relates the position of the reflection in the reciprocal lattice using a common origin.

Bragg (1913) showed that this reinforcement would only occur when the rays diffracted from parallel planes have a path difference of an integral number of wavelengths ie. when they are in phase with one another (Figure 2.1). This can be expressed mathematically as:

$$2d_{hkl}sin\theta = n\lambda \qquad [1]$$

where:

d_{hkl} is the perpendicular spacing between successive planes,

θ is the Bragg angle,

n is the order of diffraction (taken by convention to be 1),

λ is the wavelength of the incident radiation (in Å)

Equation 1 predicts the angular position of a diffracted ray. It also illustrates the inverse relationship between the crystal, in real space, and in diffraction space. If the resolution is given as d Å, data have been collected to a Bragg angle θ corresponding to $d = \lambda/2sin\theta$. The intensities of the reflections relate to the electron density of the atoms located on the Bragg plane. The low angle reflections, *ie.* those which deviate only slightly from the main X-ray beam, contribute to the broad features of the electron density map such as the gross shape of the protein molecule and the solvent; the high angle ones contribute to the fine detail or sharpness of the final electron density map.

2.3 Ewald Sphere

The reciprocal lattice and the Ewald sphere construction (Sphere of Reflection) are simple ideas to show the relationship between the planes

in a crystal exposed to an X-ray beam and their potential to satisfy the conditions of diffraction. The reciprocal lattice is fixed with respect to the real crystal lattice. Figure 2.2 describes the diametral plane passing through the Ewald sphere. The crystal is located at the centre of the sphere of reflection, C, at a radius of $\frac{1}{\lambda}$. The point O is the point at which the direct beam leaves the sphere after first passing through the crystal. O is the origin of the reciprocal lattice of the crystal and this point is fixed. Bragg's law is satisfied *ie.* a reflection will occur whenever a reciprocal lattice point is normal to the (hkl) plane.

2.4 The Electron Density Equation

X-ray crystallography ultimately describes the electron density within a unit cell. Each reflection, which is periodic in nature, can be approximated by sine and cosine functions. A Fourier synthesis describes such a periodic function and can be used to compute the electron density map from waves with known amplitude and phase. A reciprocal lattice point (hkl) corresponds to one wave passing through the unit cell. The contribution of the (hkl) reflection to the electron density is given by equation 2, otherwise known as the electron density equation:

$$\rho_{hkl}(xyz) = \frac{1}{V} F(hkl) e^{i\alpha(hkl)} e^{-2\pi i(hx+ky+lz)} \qquad [2]$$

where:

V is the volume of the unit cell

$F(hkl)$ is the amplitude of the diffracted wave.

$\alpha(hkl)$ is the phase angle of the wave relative to the origin of the cell,

hkl are the indices of the diffracted wave arising from planes d_{hkl}

In order to calculate the electron density both the amplitude and the phase of each reflection must be known. The amplitude is calculated from the experimentally determined intensities using:

$$I(hkl) \propto F(hkl)^2 \qquad [3]$$

Due to the technical limitations of data collection equipment routinely used, the phase of the reflections cannot be recorded, and constitutes the 'phase problem'. Unlike the light microscope, the image cannot be focussed using X-rays therefore the 'phase' of structure factor vector has to be determined using other techniques, namely isomorphous replacement or molecular replacement. These two techniques are discussed in more detail in Sections 2.9.1 and 2.10.

The wave scattered by the contents of the unit cell in the direction of the hkl reflection is described by the structure factor $\mathbf{F}$ (hkl):

$$\mathbf{F}(hkl) = F(hkl)e^{i\alpha(hkl)} \qquad [4]$$

The electron density equation can also be rewritten to involve contributions of the single atom j within the unit cell giving reflection (hkl):

$$\mathbf{F}(hkl) = \sum_{j=1}^{N} f_j(hkl) e^{2\pi i(hx_j + ky_j + lz_j)} \qquad [5]$$

where:

N summed over all atoms in the unit cell

j is the jth atom with coordinates (x_j, y_j, z_j)

f_j is the atomic scattering factor of the jth atom.

This equation indicates that the diffraction pattern can be calculated given that the coordinates of all the contributing atoms within the unit cell are known.

2.5 Steps in X-Ray Structure Determination

There are many stages involved in the X-ray structure determination of a new protein including:

- Protein preparation,
- Crystallization,
- Data collection,
- Data processing,
- Preparation of heavy atom derivative,
- Calculation of phases,
- Interpretation of the electron density maps,
- Refinement of the structure,
- Analysis of the final structure.

Figure 2.3 is a flow chart describing the different stages in the elucidation of a protein structure. The rest of this chapter deals with the basic stages involved in structure determination.

2.6 Crystallization

In order to determine the structure of a homogenous purified protein it is necessary to produce diffraction-quality crystals of the protein. Crystallization consists of those precise conditions under which the weak intermolecular forces between molecules of the protein produce a highly ordered packing as a crystal rather than as an amorphous precipitate. This stage is perhaps the rate-limiting step in the structure determination of any protein.

There are no standardised procedures for obtaining good quality crystals suitable for X-ray diffraction because of the large number of factors that can be varied *eg.* temperature, protein concentration and buffer *p*H *etc.* The classical vapour diffusion hanging drop and sitting drop techniques have been frequently used to produce crystals of the required quality (McPherson, 1990). This procedure requires the supersaturation of a crystallization drop which produces few subsequent nucleation sites for crystal formation and gives steady sustained growth. The advantage of this method is that it requires only small amounts of material and is suitable to screen large numbers of conditions. Recently a sparse matrix sampling system such as the 'Magic 50' (Jancarik and Kim, 1991) and crystal screen I and II (Hampton Research, USA.) have been devised to screen many of the factors involved in crystal formation. It involves producing 50 reservoir stock solutions containing various salts, precipitants and buffers.

The hanging drop method usually consists of mixing small amounts of the reservoir solution with equal volumes of the protein stock solution at a concentration of 15-20mg/ml on a plastic or siliconized coverslip. This is then inverted and sealed over a greased well of a Linbro plate (Flow Labs) containing 0.7ml of the reservoir solution. The drop is allowed to equilibrate with the reservoir at different temperatures. Visual inspection of the drop is performed using a microscope at least once every three or four days. For exposing to X-rays, the crystal is then carefully drawn up into a quartz capillary tube and the ends sealed with beeswax.

2.7 Data Collection and Processing

The first stage in solving the X-ray structure of a protein molecule is data collection and processing in order to characterise the unit cell parameters (lengths a, b, c and angles α, β, γ), determine the internal symmetry and find out to what spacing the crystal will diffract on an X-ray detector. The second stage is to systematically record as many reflections in as short a time as possible because of the sensitivity of biological macromolecules to the destructive free radicals produced by X-rays (Helliwell, 1992). In any data collection run, many thousands of reflections will be generated and each must be indexed (hkl) and its intensity determined.

The crystal is mounted on a goniometer which is then mounted onto the stepper motor of the diffraction apparatus. The distance between the crystal and detector face has to be altered to produce a clear and unambiguous separation of the adjacent diffraction spots on the diffraction image. If the unit cell parameters are unknown, this distance has to be determined by trial and error but once the preliminary parameters have been deduced

the empirical formula used for setting this distance is to divide the largest unit cell parameter by eight and then give it units of mm.

Once the unit cell parameters are known it is necessary to determine the swing angle (2θ) of the area detector with respect to the incident X-ray beam. Using a steady incremental increase in 2θ the maximum resolution can be determined. The exposure time per oscillation range given for each frame of data must also be determined. Using too short an exposure may prevent accurate detection of any reflections; too long an exposure will inevitably lower the lifetime of the crystal by the formation of free radicals. Normally the crystal tends to be oscillated a number of times within each oscillation range, to smooth out any fluctuations caused by variations in the X-ray beam.

Once the reflection positions and intensities have been recorded, operations such as statistical corrections for absorption, scaling and merging of the data have to be performed. The ability to collect and process data is directly related to the increase in sophistication in not only the software and algorithms but also in computing capacity available to the crystallographer.

2.8 Photon-Detection Equipment

2.8.1 Area Detector

The area detector is an electronic device used to detect photons diffracted by a crystal. The monochromatic X-ray beam is generated by a rotating anode emitting CuK_α radiation with a wavelength of 1.5418Å. The selected wavelength is obtained by use of a graphite monochromator. The diffracted X-rays cause ionization of the high pressure (4 atm) xenon gas

contained within the unit. This ionization event occurs once the diffracted rays have passed through the beryllium window. The electrons thus produced are then accelerated to the anode wires found within the chamber, thereby causing secondary ionization and hence amplification of the signal. The precise 2 D position of the ionization event is determined by a set of mutually perpendicular wires within the chamber. The photon position is then determined on a 512 $\times$ 512 grid and stored in the computer.

2.8.2 Image Plate

The MAR Research image plate is a fully automatic high performance electronic device which temporarily stores the X-ray reflections on a fixed phosphorescence screen, in the form of colour centres. The screen is then 'read' by a scanner (MAR Research Manual; Helliwell, 1992) consisting of a He/Ne laser light which then converts the reflections into a digital signal in the form of a 1200 $\times$ 1200 pixel matrix. The intensity of the luminescence is proportional to the number of absorbed X-ray photons. This read-out system is highly efficient, with a high signal to noise ratio, and takes only $\sim$90s between successive images to read and then erase the image. Compared to film, the image plate is free from chemical fog and spatial distortion and is reusable. This detecting device has an extremely low intrinsic noise level and coupled with its high spatial resolution is useful when processing data. As a result of improvements in the materials used, the exposure times have been reduced by at least a factor of 10 when compared to film (Helliwell, 1992).

2.9 Phase Determination

2.9.1 Isomorphous Replacement

Isomorphous replacement is an *ab initio* method to obtain initial estimates of phases for a novel protein *ie.* the first protein in a family (Green *et al.*, 1954; Bailey *et al.*, 1988; Wolf *et al.*, 1991). All atoms within a protein contribute to the diffraction pattern, and this technique relies on the fact that the introduction of one or two heavy metal ions at identical sites throughout the crystal will subtly change the resultant diffraction pattern. From these slight changes in the diffraction pattern the heavy atom positions can be calculated using a Patterson function from which initial estimates of the phases can be determined.

This process involves soaking native protein crystals with a heavy metal, such as Hg, U or Pt (Petsko, 1985). It is generally accepted that mercury ions bind to disulphide bonds in proteins. Data collection similar to that for the native protein must then be performed for the heavy atom derivative to verify that the heavy atoms do not alter the unit cell parameters determined for the native crystal, *ie.* they remain isomorphous.

2.9.2 Heavy Atom Derivative Preparation

Native crystals surrounded by a minimum amount of mother liquor are placed on a glass plate inside a humid chamber to prevent dessication of the crystals. This process is usually visualized by use of a light microscope. Next, the crystal plus the 'derivitized' artificial mother liquor are transferred to a microbridge (Harlos, 1992), which is then placed in a well containing 0.7ml of the artificial mother liquor, sealed with a coverslip

and stored at 16°C. Inspection of the derivitized crystals can be performed after one hour and then for regular intervals thereafter. Any potential heavy atom derivative crystals thought suitable for continued isomorphous replacement must then be carefully transferred to a quartz capillary tube, sealed and mounted on a detector/image plate for data collection.

2.9.3 Calculation of Phases From Derivative Data

The first stage in calculating the phases is to determine the structure factor contribution for a particular reflection from the native data, heavy atom derivative and the heavy atom, which are $\mathbf{F}_P$ $\mathbf{F}_{PH}$, $\mathbf{F}_H$ respectively. Assuming 'ideal' isomorphism they are related by the equation:

$$\mathbf{F}_{PH} = \mathbf{F}_P + \mathbf{F}_H \qquad [6]$$

This shows that they are additive vectors and can be represented graphically by Figure 2.4. $\mathbf{F}_H$ cannot be directly measured but it comprises of only a few atoms in the unit cell and can be calculated providing that its refined coordinate positions are known.

2.9.4 Heavy Atom Positions in the Unit Cell

To determine the positions of the heavy atom within the unit cell use is made of the Patterson function $P(uvw)$, a variant on the electron density equation using structure factors:

$$P(uvw) = \frac{1}{V}\sum_h\sum_k\sum_l \mathbf{F}^2_{hkl} e^{-2\pi i(hu+kv+lw)} \qquad [7]$$

The coordinates (uvw) locate the heavy atom positions in a Patterson

map. It uses as coefficients the squares of the measured structure factor amplitudes only *ie.* it does not require any phase information. The positions of the maxima represent the vector end points between the particular atoms referring to a common origin. In this instance a difference Patterson function is calculated *ie.* $(F_{PH} - F_P)^2$. The result of this is a contour map with peaks at positions of the vectors between atoms.

2.9.5 Multiple Isomorphous Replacement

This classical method is still widely used to solve the phase problem. It requires a second isomorphous heavy atom derivative with the heavy atoms binding at different sites to the first derivative. The phase problem can be solved by collecting two heavy atom derivative data sets with structure factor amplitudes F_{PH1} and F_{PH2} (where PH1 is from the first derivative and PH2 from the second) and determining the contributions of the separate heavy atoms within their refined positions $\mathbf{F}_{H1}$ and $\mathbf{F}_{H2}$ (Figure 2.5). This construction with the origin at O has a circle of radius F_P drawn around it. Two vectors $-\mathbf{F}_{H1}$ $-\mathbf{F}_{H2}$ are drawn from O and form the origin of two other circles with radii F_{PH1} and F_{PH2} respectively. Assuming the two derivative crystals are perfectly isomorphous with the native crystal, the three circles drawn in Figure 2.5 should intercept exactly at one point, X. The vector OX will therefore coincide with the structure factor of the protein. From this the initial phase angle can be estimated.

2.9.6 Estimation of the Isomorphous Differences

The next stage of data processing is to scale the derivative data to that of the native data using the Wilson scaling equation:

$$(F^{PH}_{scaled})^2 = k(F^{PH}_{obs})^2 e^{(-B sin^2\theta/\lambda^2)} \quad [8]$$

where the factor k is chosen to minimize the sum of the squares of the differences between the native and scales derivative intensities and B is the temperature factor.

Error estimates for the rms isomorphous error E may first be determined using the equation:

$$E^2 = \sum(|F_{PH} \pm F_H|)^2/N \quad [9]$$

using the centric refinement on all the sites. The occupancies for the heavy atoms can be estimated using the parameters of centric refinement. Using small intervals, the phase probabilities can be calculated and any measurements deemed improbable rejected. The E values can be reassessed during refinement using the equation:

$$E^2 = \sum(F_{PH(obs)} - F_{PH(calc)})^2/N \quad [10]$$

2.9.7 Interpretation of the Difference Patterson Maps

When the positions of the heavy atom sites in a crystal have been accurately located protein phase information can be determined by the

method of isomorphous replacement. The Patterson function is based on the squares of the differences in the amplitudes between two sets of data. The difference Patterson map consists of the peaks corresponding to vectors between heavy atom sites given both the native and heavy atom derivative data. A significant mean fractional isomorphous difference (MFID) value with one or two heavy atom sites per asymmetric unit should result in a few strong peaks which are visible on the Harker sections of the difference map. From these peaks, the heavy atom positions can be interpreted. If more than this number of heavy atom sites were present per asymmetric unit then inspection of the peaks found at the general positions in the difference Patterson map would correspond to the cross vectors between the non crystallographically related sites.

2.9.8 Heavy Atom Parameter Refinement

If the heavy atom structure factors $\mathbf{F}_H$ are known, then the protein phase angles α_P can be estimated from the magnitudes of both the native and derivative structure factors $\mathbf{F}_P$ and $\mathbf{F}_{PH}$. In order to calculate these heavy atom structure factors, their positions, degrees of substitution and thermal parameters should be accurately known for all the bound heavy atoms.

2.9.9 Phase Refinement

The initial multiple isomorphous replacement protein phases can be calculated from a trial set of heavy atom parameters. Error estimates for the rms isomorphous error E can be determined using the equation:

$$E^2 = \sum(|F_{PH} \pm F_H|)^2/N \qquad [11]$$

using the centric refinement on all sites. The occupancies for the heavy atoms can be estimated using the parameters of the centric refinement. The E values are reassessed during the refinement using the equation:

$$E^2 = \sum(F_{PH(obs)} - F_{PH(calc)})^2/N \qquad [12]$$

2.9.10 Phase Improvement

The initial phases derived from multiple or single isomorphous replacement are usually not of sufficient quality to produce an interpretable map. This is due in part to errors present in the phase estimates. Therefore, techniques such as solvent flattening and molecular averaging are used to improve and extend the low resolution multiple isomorphous replacement phases, to give an interpretable map.

2.9.11 Molecular Averaging

Many proteins crystallize in such a way that the asymmetric unit contains more than one molecule. In this instance there is a redundancy of data which can be processed using a method known as molecular averaging

(Bricogne, 1976). This technique requires a matrix to rotate one copy of the molecule onto the others within the asymmetric unit. Using the unphased data requires analysis of the interatomic vectors of the Patterson map. Although this technique is very useful in reducing the phase errors when there are multiple copies of the molecule available it does often result in a rather high noise level complicated by the intermolecular vectors.

If the data is of sufficient quality, phases can be extended to a resolution beyond those used to determine the initial electron density map. This involves using phases derived from a small band of structure factors just beyond the resolution limit used in the previous cycle of refinement. They are then combined with their corresponding experimentally determined amplitudes during the next cycle in the procedure.

2.9.12 The Solvent Flattening Procedure

In order to improve the molecular averaging technique, a solvent envelope or mask is required (Wang, 1985). This envelope, surrounds the protein molecule around the molecular boundary between the ordered protein molecule and the disordered solvent. The envelope is exploited to reduce the noise by averaging out, amongst the other molecules in the asymmetric unit, and thereby smoothing the map for a low resolution image of the protein. This technique assumes that even if noise is present, the density of the protein molecule will be much higher than that found within the solvent region. This region outside the protein density can then be set to zero and any negative density truncated. Each point within the protein envelope, as designated by the density in a sphere of known radius is averaged and the actual value for that point is then replaced by the av-

eraged value. This results in the generation of a new electron density map where the density at each point is now proportional to the sum of the high density level in the sphere surrounding it. The molecular boundary of the molecule can be determined by setting a density level which is based on the experimentally estimated solvent content of the protein crystal.

This method, which works best for high solvent content crystals (>55%), entails generating a molecular boundary or envelope around each molecules' electron density within the asymmetric unit of the initial multiple isomorphous replacement map, *ie.* the 'protein' region. Next the electron density outside this boundary, the solvent region, is set to a constant value *ie.* solvent flattening (Wang, 1985). This newly modified electron density map is then inverse transformed to generate a modified set of intensities and phases. The original multiple isomorphous replacement phases are then combined with those of the modified map in order to generate a new 'improved' electron density map. Making the solvent region 'redundant' can reduce some of the spurious noise and discontinuous regions generated from the original multiple isomorphous replacement map thus improving the quality of the electron density map. This procedure would then be repeated a number of times in combination with the molecular averaging procedure to produce a good quality electron density map which could be used for map interpretation.

2.10 Molecular Replacement

Molecular replacement can also be used to determine the initial phases of an unknown structure (Rossmann, 1972; Machin, 1985; Dodson *et al.*, 1992; Navaza, 1994). This knowledge-based technique requires

a well refined search model which is similar to the unknown. Molecular replacement depends on optimizing both the orientation (rotation function) and position (translation function) of the search model in the unit cell of the unknown to provide the best correlation between the observed and calculated diffraction data. This is performed using a Patterson search technique. In the case of the rotation function the search model orientation is altered until its calculated Patterson function is 'identical' to that of the unknown. The translation function is similarly determined and when this is complete a rigid body refinement is performed on these positional parameters. There are many problems with this technique, such as obtaining a sufficiently similar or homologous search model to that of the unknown. This will eventually lead to a list of possible peak solutions, and requires a significant amount of interpretation to obtain the correct solution.

It is imperative to obtain a good search model based not necessarily in terms of amino acid sequence but on the structural identity between two molecules. It is necessary to use a refined protein structure at the highest resolution possible because the method of molecular replacement constantly makes comparisons between observed experimental data and predicted data calculated from the refined search model. If a protein structure is obtained using a poor search model then the subsequent phases will be poor estimates of the actual phase. These phases will be heavily biased towards the search model and therefore potentially difficult to refine. Apart from not using a sufficiently good search model, another reason for the failure of this technique may result from using poor quality data. This technique is powerful enough to use only a part of the search model in order to get initial phase estimates.

In order to correctly superimpose a known structure in the unit cell of the unknown and obtain a good match, the search model must undergo a six-dimensional search. This can be split into two parts. The first is a rotation function performed by use of three variables in order to correctly orientate the molecule. Secondly, a translation function is performed, using three other variables, the distances, in order to correctly position the search model in the unit cell of the unknown. Whichever direction the search model is rotated and translated it always requires these six variables to completely describe the operation in moving one set of coordinates over to the unknown. Simply stated, if $\mathbf{X}_{orig}$ represents the vectors describing the atoms of the search model and $\mathbf{X}$ the transformation:

$$\mathbf{X} = [C]\mathbf{X}_{orig} + T \qquad [13]$$

where:

[C] is the rotation matrix $\mathbf{X}_{orig}$ determined in the first stage of molecular replacement into its new orientation,

T is the translation vector determined in the second stage.

Equation 13 will therefore minimize the difference when a comparison is made between the F_o and F_c. At present this function cannot occur in one move and it must be split into two parts: the rotation function and the translation function. The action of splitting the transformation into two parts enables a potential solution to be determined whilst simultaneously being more frugal with computer time and can be achieved by use of the Patterson function. Only two functions are necessary to define the position of proteins because amino acids usually exist in the L-form and only by the

introduction of mirror planes would create the D-form. Once the search model has been optimally orientated and positioned in the unit cell, the initial phases can be calculated for subsequent crystallographic electron density map fitting.

2.10.1 The Rotation Function

The rotation function is used to locate common vectors within a crystal. The rotation search is performed over all possible rotations in order to highlight any overlap between the two functions:

$$\mathbf{R}(C) = \mathbf{P}(uvw)\mathbf{P}_x(uvw) \qquad [14]$$

where:

$\mathbf{P}(uvw)$ is the Patterson function to be examined,

$\mathbf{P}_x$ the Patterson function corresponding to the same Patterson function having been related by the necessary angles.

Patterson functions use experimentally derived data, in the form of intensities without the need for any phase information and as such represent the vectors between elements of the scattering density. The Patterson function consists of two parts. Firstly those vectors within one protein molecule *ie.* intramolecular vectors which are confined to a sphere centred on the origin of the Patterson map and secondly those vectors between identical molecules within the asymmetric unit *ie.* the intermolecular vectors.

By carefully choosing the Patterson radius, and thereby reducing the intermolecular vectors, the chances of obtaining a good rotation peak

search can be increased. One other variable to be considered is the choice of resolution ranges. High resolution (>3.5Å) reflections describe the actual conformation of the residues while low resolution reflections (10−3.5Å) describe the general relationship between secondary structure elements to be found within the molecule. The rotation function will have a maximum when all the self vectors of one Patterson exactly coincide with those of the second. The fast rotation function can also be considered as a summation of intensities and the strongest reflections contribute significantly when compared to the weak ones. It is therefore advantageous to include all the strong reflections and reduce or omit the weak ones. This will allow enough reflections to be used to represent the data set collected without the function being dominated by only a few strong terms.

2.10.2 The Translation Function

The quality of the rotation function heavily influences the quality of the translation function. Once the orientation of the search model has been established in the unknown unit cell, the next three variables to determine are the relative positions of the model coordinates. Once the search model has been correctly positioned, all the remaining symmetry related molecules can be generated. From this the calculated Patterson cross vectors can be compared with the observed Patterson vectors. Self vectors can be ignored due to the fact that they are insensitive to translation but do form part of the background.

The initial step in molecular replacement is to determine the centre of mass of the search model, place it at the origin of an artificial unit cell $P1$ and calculate its structure factors which will then be used for the

rotation function search. The search model is rotated in small increments so as to cover as much volume as possible about the space group of the unknown structure. After each small increment a systematic inspection is made of the match between the search model and the Patterson map of the unknown. A peak list is then provided which indicates the agreement relative to the origin. Evidence for a good agreement might consist of a single large peak above background.

A number of factors need to be taken into consideration when deciphering the output. If no obvious peaks are produced then the resolution range should be altered. Should this again fail, an attempt should be made on an alternative search model. Altering the original search model may hold the key in determining the correct rotation function solution. For instance, assuming the search model has its complete amino acid sequence may help. Reducing all the side chains to its Cβ atom may reduce any unwarranted bias providing more detail in emphasising similarities in the secondary structure elements.

2.11 Interpretation of the Electron Density Map

After the initial electron density map has been produced the protein main chain may be manually added to the available density with sufficient fit to produce an atomic model using a dedicated computer graphics system (Jones, 1985). The ease at which the model building can be achieved, to give reasonable stereochemistry, is determined by the accuracy with which the phase estimates have been generated by either isomorphous or molecular replacement. If the data are of sufficient quality and the resolution is high then features like α helices or β strands may be discernable. The

continuous nature of the electron density may allow a significant portion of the main chain to be built.

2.12 Refinement

The first atomic model obtained from an initial electron density map usually contains a number of errors which do not closely follow the experimentally determined structure factors and thus may not be sterically correct (Brünger and Nilges, 1993). This is because maximum resolution is not high enough to position individual non-hydrogen atoms but only the gross main and side chains. The purpose of refinement is to improve the overall chemistry of the molecule with respect to the agreement between the observed structure factors and those calculated for the model by minimizing the energy. (Brünger *et al.*, 1987).

The conventional refinement protocol of a proposed model made use of a method known as least squares. This technique required many cycles of refinement followed by an extensive manual rebuilding on a dedicated computer graphics system. One disadvantage with this method was that it required extensive reinterpretation of the model within its electron density map. Furthermore the small radius of convergence prevented good resolution of any residues lying at a distance >1Å from their correct positions. Such residues remained trapped in a local minima and required manual intervention.

In recent years, a technique known as simulated annealing (Kirkpatrick *et al.*, 1983) has superseded the least squares method of refining protein molecules, which only allows a downward descent in energy. This new technique simultaneously uses molecular dynamics and crystal-

lographic refinement to explore a greater conformational space than could ever be achieved using the old method (Brünger *et al.,* 1987; Karplus *et al.,* 1987; Goodfellow *et al.,* 1989; Brünger and Nilges, 1993). The main advantage lies in the fact that the local minima problem is overcome.

One such refinement program is XPLOR (Brünger, 1988; Version 2.1). This program performs least squares refinement in addition to the simulated annealing refinement via molecular dynamics which increases the radius of convergence. The surface potential energy of the protein can be expressed as a function of the atomic coordinates of the model (Karplus *et al.,* 1987). Refinement using molecular dynamics and simulated annealing are performed by solving Newton's equations of motion in order to determine the change in atomic position with respect to time.

Empirical energy functions are required in order to establish the global minima of the model using the following equation:

$$E_{total} = E_{empirical} + E_{xray} \qquad [15]$$

where:

$E_{empirical}$ includes empirical energy information on all chemical interactions of the model,

E_{xray} denotes the squared differences between all observed and calculated diffraction data using an appropriate weight.

This empirical energy function (or geometric term) can be further broken down into the atomic coordinates describing the covalent interactions as well as the non-bonded interactions (hydrogen bonds, electrostatic and

Van der Waals), in the form of Cartesian coordinates.

$$E_{empirical} = K_b(b - b_\phi)^2 + K_\theta(\theta - \theta_o) + K_\phi(1 + cos(n\phi - \delta)) + \left(\frac{A}{r^{12}} - \frac{C}{r^6} + \frac{q_1 q_2}{Dr}\right) \quad [16]$$

where:

b is the internal coordinates for the bonds,

A, C are Lennard-Jones parameters,

q the atomic charge,

D dielectric constant,

θ is the bond angle,

ϕ are the dihedral angles,

r is the interatomic distance for any given geometry R

The E_{xray} is the crystallographic residual which is formed from the squared differences between the observed F_o and calculated F_c structure factor amplitudes summed over all reflections:

$$E_{xray} = (F_o - kF_c)^2 \quad [17]$$

where:

k is a scale factor used to minimize the residual.

Having got the coordinates of the atoms, XPLOR assigns random velocities to each atom. The refinement then proceeds by using an energy minimization program which relieves bad contacts and stresses caused by any non-bonded contacts.

2.12.1 Simulated Annealing

Simulated annealing uses molecular dynamics and can prevent problems associated with local minima. It has been described as being similar to a process in which a protein, in a 'heat bath', can be heated to extreme conditions (around $4000K$) which allows all the constituent atoms to move randomly in the liquid phase. The next step is for a 'slow cooling' (or annealing) of the protein in the bath to prevent the model from remaining in an incorrect state. This allows all the atoms to rearrange themselves into the lowest energy state by having access to smaller regions of conformational space and have a lower global minima than before. This improvement over previous methods allows for a global exploration of conformations even in an 'upward' direction.

2.13 Analysis

The final stage in the structure determination of a protein molecule is to assess the quality of the final model. The model must be chemically, conformationally and stereochemically correct. The bond angles and lengths should contribute to a chemically acceptable model. The conformationally reasonable model must have planar peptide bonds and residues that (usually) exist in the *trans* conformation; the side chain torsional angles must be in the staggered conformation.

A number of techniques exist to judge the quality of a model, which include the Ramachandran plot (Ramachandran and Sasisekharan, 1968) and the crystallographic reliability index or R-factor. The Ramachandran plot demonstrates the allowed pairs of angles (ϕ, ψ), for each amino acid residue in the model. The plot then indicates whether the specific backbone

conformational angle exists in an 'allowed' or 'disallowed' region. By systematically determining those residues that lie outside the allowed region from the plot and then locating that residue on the model, subtle changes can be made to these residues in order to bring them back into the allowed region and hence improve the overall accuracy of the model.

The main system used to assess the accuracy of a model is the *R*-factor which can be calculated from the following equation:

$$R = \frac{\sum(\mid F_{obs} \mid - \mid F_{calc} \mid)}{\sum \mid F_{obs} \mid} \qquad [18]$$

where:

F_{obs} are derived from the experimentally measured reflection intensities,

F_{calc} are the amplitudes derived from the latest model.

The *R*-factors can have values ranging from 0 to 1 with a value of 0 indicating a perfect agreement between the observed and calculated amplitudes. A value of 0.5 suggests a rather poor model with little hope for improvement even with alterations made to the structure. In a well refined structure to 2.5Å one would expect an *R*-factor of ~20%. It has been shown that poor search models can in fact be refined with apparently good *R*-factors (Bränden and Jones, 1990). The root mean square deviation from the ideal for bond angles and bond length should be less than 4° and 0.02Å respectively. Another analysis parameter used is the temperature factor or *B*-factor for each atom. This is a measure of the 'movement' of the atom about a fixed point. Therefore side chains would be expected to have more freedom of movement than say a main chain atom. If there are

multiple copies of the molecule within the asymmetric unit, a comparison should be made between these molecules. In this instance, the differences in the atomic coordinates should be less than 0.2Å.

2.14 Aims of this Study

Toxic shock syndrome toxin-1 and the SE possess several properties that are of clinical interest both in causing disease and as potential therapeutics. The initial aim of this project was to produce enough pure toxin (TSST-1, SEA, SEB and SEC2) to initiate crystallization trials. Having produced good quality crystals, structure determination was carried out. The structural aspects of these molecules determined by X-ray crystallography are important in identifying regions on these molecules which are involved in binding to MHC II and TcR. Such a study might form a basis for detailed protein engineering experiments in an attempt to understand the biological activities of these toxins.

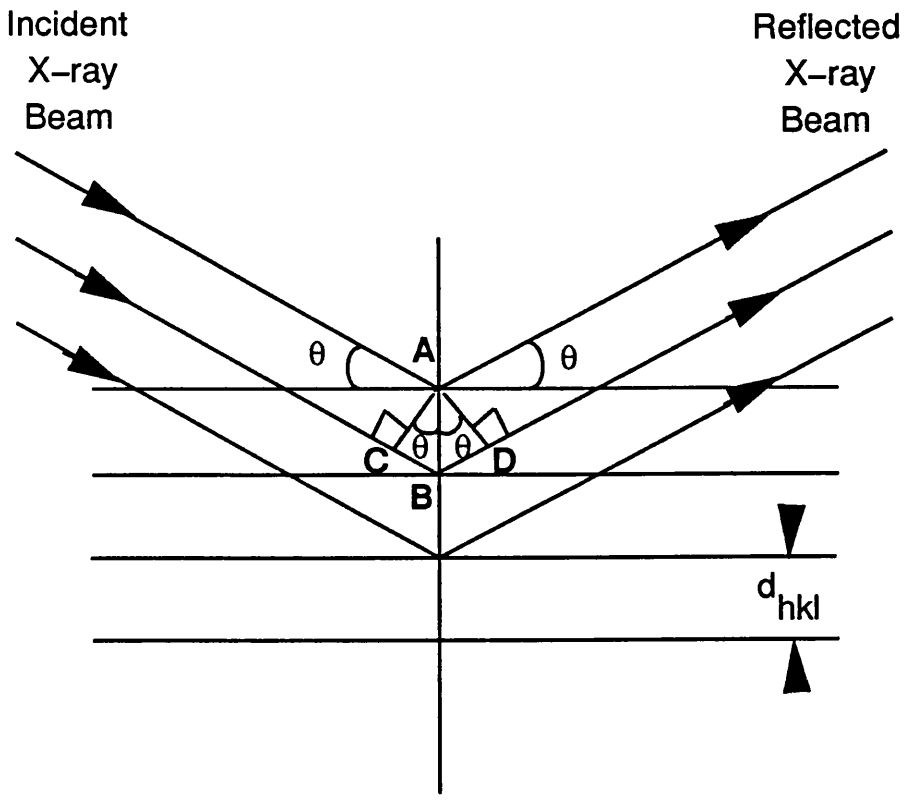

Figure 2.1 A diagram to illustrate the reflections from a Bragg plane.

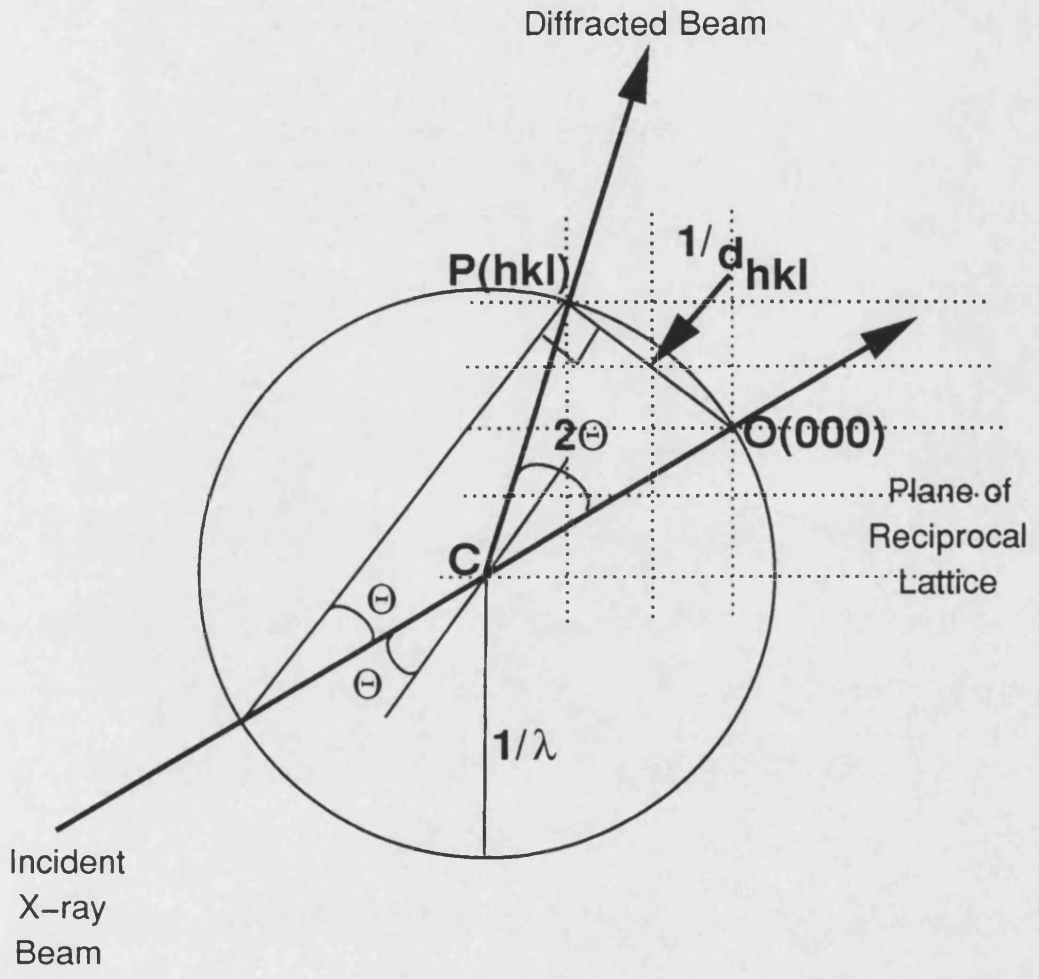

Figure 2.2 A diametral plane through an Ewald construction.

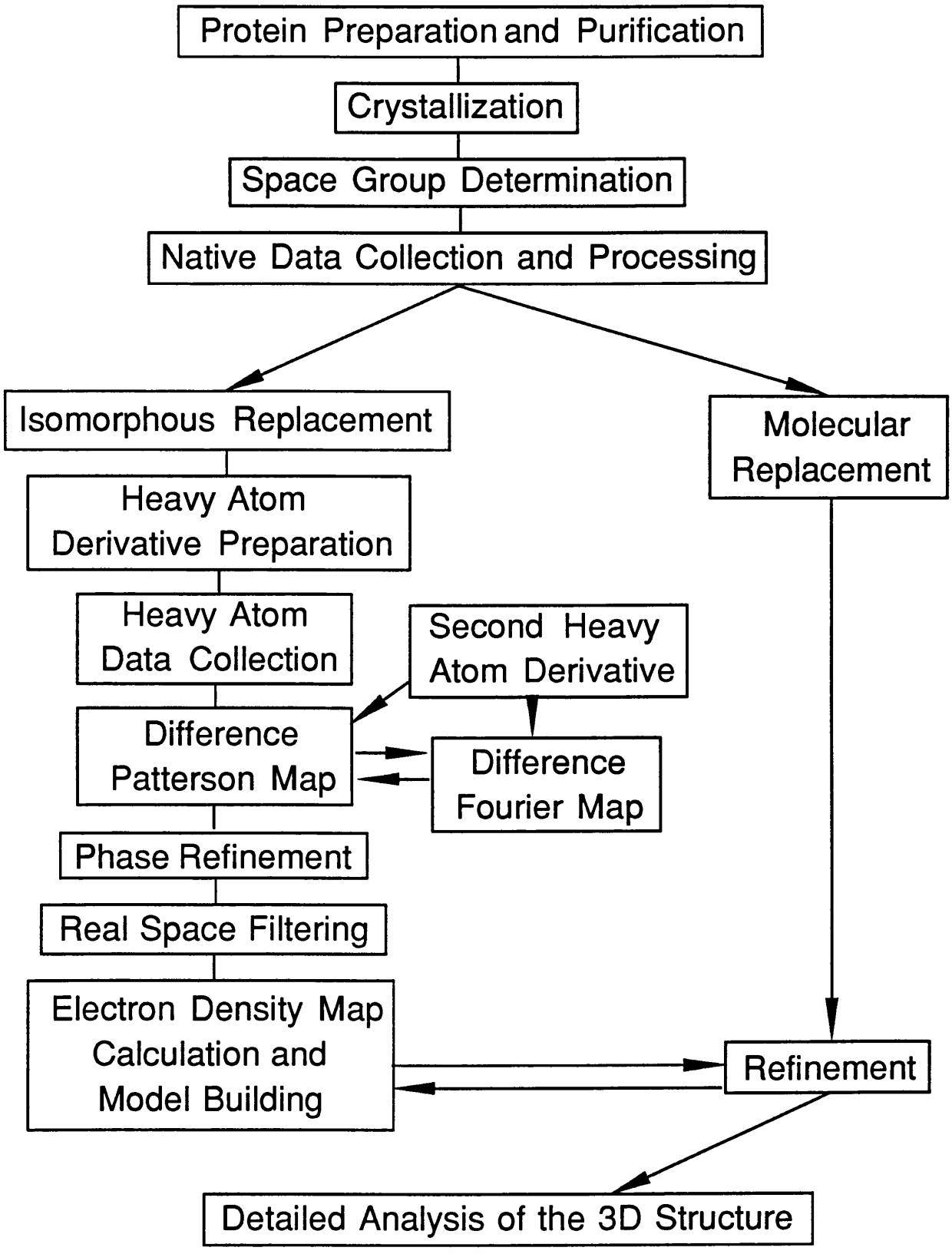

Figure 2.3 Steps in the X-ray analysis of protein crystals.

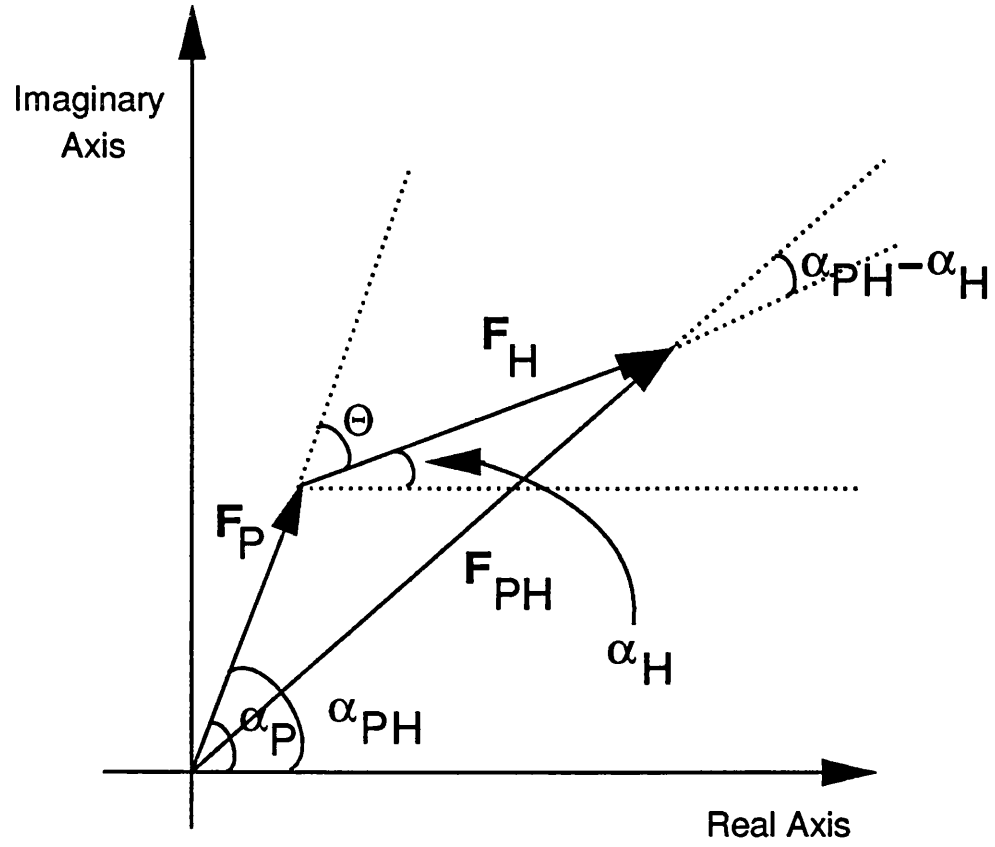

Figure 2.4 An idealised phase triangle used to relate both the native ($\mathbf{F}_P$) and heavy atom derivative ($\mathbf{F}_{PH}$) structure factors for each reflection, assuming perfect isomorphism between the two crystals.

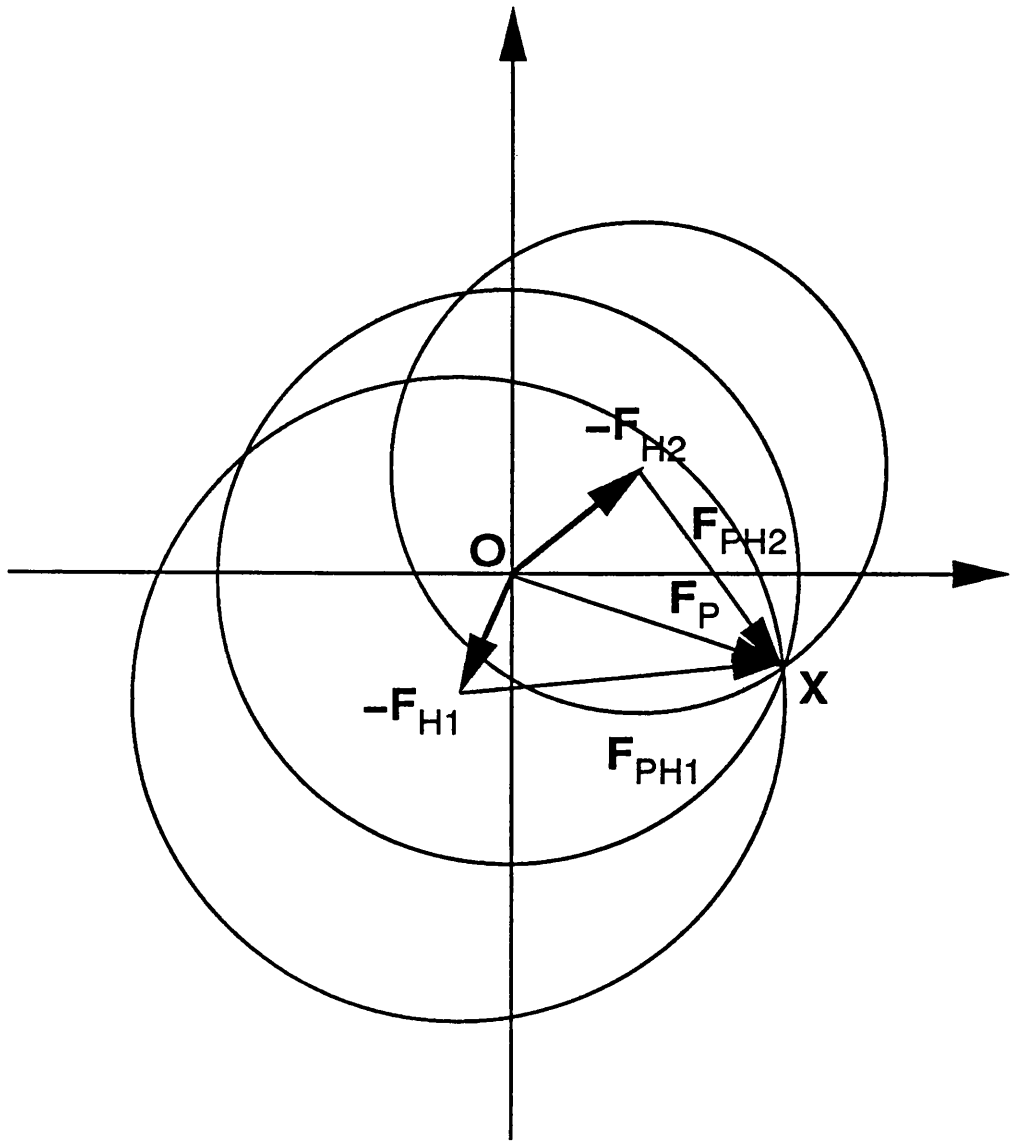

Figure 2.5 A construction for phase determination by the method of multiple isomorphous replacement. The heavy atom derivative contributions are given by -$\mathbf{F}_H$. The unequivocal phase $\mathbf{F}_P$ is given by **OX**.

Chapter 3

3.1 Purification, Crystallization and Structure Determination of Toxic Shock Syndrome Toxin-1

Toxic shock syndrome toxin-1 (TSST-1) and all of the staphylococcal enterotoxins (SEs) have been purified to homogeneity. Since the first enterotoxin (SEB) was purified (Bergdoll *et al.*, 1959) the protocols used have been simplified. Early procedures tended to contain many time consuming steps which add to the complexity of the purification routine and reduced the yields of toxin (Rosten *et al.*, 1989; Schlievert, 1989; Brehm *et al.*, 1990). More recently a simplified procedure for the purification of TSST-1 (Passalacqua *et al.*, 1992) and SE has been devised using dye-ligand chromatography (Reynolds *et al.*, 1988; Brehm *et al.*, 1990). To purify these toxins for X-ray crystallographic work a two-step purification procedure was used which was suitable for both small and large-scale production. This was based on dye-ligand chromatography using the triazine textile dye known as 'Red A' (Amicon Ltd.). Toxin prepared in this way was subsequently cleaned up by fast protein liquid chromatography (FPLC). The following section contains detail of the production and purification of TSST-1 and its subsequent crystallization and analysis.

3.2 Strains Used for Toxin Production

Staphylococcus aureus strain MN8 (kindly supplied by Professor M.S. Bergdoll, Food Research Institute, Department of Food Science and Industry, University of Wisconsin, Madison, USA.) was used for the production of TSST-1. Cultures producing TSST-1 were stored in growth medium

(see below) containing 50% v/v sterile glycerol (BDH; 121°C/ 15 min) and frozen in liquid nitrogen. When required stock cultures were thawed and subcultured through growth medium prior to being maintained on nutrient agar (Oxoid Ltd.) slopes at 4°C, for 1-2 days.

3.3 Growth Medium

Staphylococcus aureus strain MN8 was grown in culture medium, previously sterilized by autoclaving at 121°C for 20 minutes. The medium consisted of 20.0 g/l N-Z amine A (Sheffield Products) and 20.0 g/l protease peptone no.3 (Difco Laboratories) at a *p*H of 7.0. In addition, 50% (w/v) glucose, sterilized by autoclaving (121°C/ 15 min), was added to give a final concentration of 2 g/l in the medium.

3.4 Production of Toxic Shock Syndrome Toxin-1

To provide an initial inoculum, 1ml of sterile (121°C/15 min) phosphate buffered saline *p*H 7.4 (Appendix A) was washed over an agar slope culture of *S. aureus* and 0.7 ml of the resulting suspension used to inoculate 50ml of growth medium in a 300ml Ehrlenmeyer flask (Passalacqua *et al.*, 1992). The culture was shaken for 16 h - 20 h at 300 rpm in an orbital incubator (INR-200; Gallenkamp) at 37°C. After growth of this culture 10 ml was used to inoculate 500 ml of the same medium in a 2 l flask and shaken for 16 h - 20 h at 37°C. Finally, this seed culture (500 ml) was used to inoculate a 35 l bioreactor (Chemap AG) which contained 25 l of growth medium sterilized *in situ* (121°C/15 min), and 0.03% w/v (final concentration) polypropylene glycol 2000 antifoam (KW; Revai Chemicals Ltd.) previously sterilized by autoclaving (121°C/20 min) and added immedi-

ately prior to inoculation. To enhance production of TSST-1 an O_2/CO_2 (1:1) mixture (British Oxygen Co.) was filtered (Emflon; Pall) and sparged through the culture at 2 l/min. The stirrer speed of the fermenter vessel was set to 280 rpm and the culture grown for 16 h - 20 h at 37°C.

After growth the bacterial cells were removed from the culture medium using the Millipore Pellicon cassette system (Millipore UK Ltd.) containing ten 0.45 μm membranes (HVLP-OMP50) and the spent culture supernatant fluid concentrated to 1 l using the same Pellicon cross-flow filtration system fitted with two 10,000 molecular weight cut-off membrane cassettes (PLGC OMP05). To prevent growth and protease degradation of toxin during the remaining downstream processing, 0.5M EDTA (BDH) was added to the concentrated culture medium to give a final concentration of 0.2 mM. The concentrated culture supernatant fluid was placed in dialysis sacs (Scientific Instruments Ltd.) and dialysed overnight at 4°C against 20 mM potassium phosphate buffer at *p*H 6.5 and a final concentration of 0.2 mM EDTA.

3.5 Purification of Toxic Shock Syndrome Toxin-1

3.5.1 Dye Ligand Affinity Chromatography

Five hundred millilitres of Red A gel (Amicon Ltd) was placed in a large Buchner funnel, washed with 3 l of 8M urea (BDH) solution containing 0.5M NaOH (BDH) and loaded into a 4.5 cm × 31 cm column (Wright-Amicon Ltd.). The gel was allowed to settle and then washed with 8 volumes of 20mM potassium phosphate equilibration buffer, *p*H 6.5. The toxin was eluted from the Red A column using a stepwise increase in molarity of the phosphate buffer. Ten ml fractions were collected (Super-

perFract 2211; Pharmacia) at a flow rate of 40 ml/h during binding and 80 ml/h during elution. The protein content of the fractions was estimated by measuring the A_{280} using a Pye-Unicam PU 8600 UV/VIS spectrophotometer while the presence and concentration of toxin was measured using the single radial immunodiffusion assay (Section 3.6).

3.5.2 Fast Protein Liquid Chromatography

The Red A column fractions containing toxin were pooled and purified further using fast protein liquid chromatography (FPLC; Pharmacia Ltd.) to produce toxin for crystallization. Toxin samples were placed in dialysis sacs (Scientific Instruments Ltd.), dialysed overnight in 50mM sodium acetate buffer *p*H 5.0 at 4°C and loaded in batches of approximately 20 ml onto a FPLC HiLoad S Sepharose high performance 16/10 column (Pharmacia) previously equilibrated with dialysis buffer. The column was eluted at room temperature using a 150ml linear gradient (0-250 mM) of NaCl at a flow rate of 2 ml/min. Fractions were collected using a Pharmacia fraction collector (SuperFract 2211) and the toxin usually eluted as a single peak. All fractions which gave an A_{280} of greater than 0.2 units were collected and tested by single radial immunodiffusion for the presence of toxin. After elution both the Red A and the S Sepharose columns were regenerated according to the manufacturers instructions. Finally, the purified toxin was dialysed at 4°C for 16 h - 20 h against MilliQ (Millipore Ltd.) or ElgaStat (ElgaStat Ltd., High Wycombe) water (conductivities: >18 mΩ and >15 mΩ respectively). The concentration of the purified TSST-1 was determined using the extinction coefficient of 0.95 at 280 nm (Reiser *et al.*, 1983). The equivalent of 1 mg amounts of the freshly purified

toxin solution were added to small freeze-drying vials and lyophilized. The freeze-dried toxin was stored at 4°C until required.

3.6 Toxin Assay

Toxin concentrations were determined using a single radial immunodiffusion assay (Meyer & Palmieri, 1980). This was performed by mixing 4ml of 1% (w/v) agarose (BDH) in barbitone buffer *p*H 7.4 (Appendix A) that had been previously melted by steaming and incubated at 60°C with 4 ml of barbitone buffer containing 80 μl of rabbit anti-toxin antiserum. The solution was poured into a Merrid single radial immunodiffusion (SRID) plate (Mercia Brocades Ltd.), cooled to room temperature and 5mm diameter wells cut into the gel using a gel punch (LKB Ltd.). Ten microlitre samples containing toxin were placed in the well and the SRID plates incubated overnight in a moist chamber at 37°C. Toxin concentrations in the unknown samples were determined by measuring the diameters of the precipitin rings formed and comparing them to standards 10 μg/ml to 100 μg/ml of purified toxin solutions which were present on the same plate.

3.7 Criteria of Purity

The purity of toxin preparations was determined using sodium dodecyl sulphate-polyacrylamide gel electrophoresis (SDS-PAGE) on gradient gels (PAA 4/30; Pharmacia Fine Chemicals). After electrophoresis the gels were stained for 1 h in ethanol/acetic acid (3:1, v/v) containing 0.1% coomassie blue R250 (Pharmacia) and destained by diffusion overnight in accordance with the manufacturers instructions (Instruction Manual; Pharmacia). The toxin preparations were also loaded, in accordance with the

manufacturers instructions (Instruction Manual; Pharmacia), onto an isoelectric focussing gel (Pharmacia). Isoelectric focussing was performed on an Ampholine PAG plate gel (*p*H 3.5 to 9.5; LKB Instruments Ltd.) using an LKB Multiphor II system (Pharmacia LKB Biotechnology). The anode solution comprised 1M H_3PO_4 and the cathode 1M NaOH. Sample volumes (15 μl) containing 1.0 to 2.0 mg/ml of protein were applied to the gel and electrophoresis performed at 1500 V and 50 mA for 1.5 h. The *p*H gradient across the gel surface was determined after electrophoresis using a surface electrode (Pye Ingold). The staining and destaining procedures were performed as with the SDS-PAGE described above.

3.8 Gel Filtration Studies on Toxic Shock Syndrome Toxin-1

Gel filtration studies on TSST-1 was carried out at 4°C using two different buffer systems on a column (1.5 cm × 75 cm) containing 120 ml of Bio-Gel P-100 gel beads (Bio-Rad). In an initial experiment 0.1M acetate buffer *p*H 4.6 was used to simulate crystallization conditions. In a separate experiment 0.1M Tris-HCl buffer *p*H 7.2 was used to simulate physiological conditions. For each experiment, the column was initially washed with the appropriate buffer until the A_{280} read zero and the eluant *p*H was equal to that of the reservoir buffer used.

The column was calibrated for each buffer separately using blue dextran (M_r 2,000kDa) followed by low molecular weight calibration proteins (Pharmacia) in accordance with the manufacturers instructions (Pharmacia). After the molecular weight markers were loaded onto the top of the gel under gravity, the buffer reservoir was connected and 1.2 ml fractions collected, at a flow rate of 5 ml/h, using a Pharmacia fraction collector

(SuperFrac 2211). The A_{280} for each fraction was recorded using a CECIL CE6600 Multimode Computing UV Spectrophotometer. Fractions were collected until the A_{280} reached the baseline and the *p*H reached that of the reservoir buffer. After calibration, 1 mg of lyophilized TSST-1 was dissolved using 950 μl of the appropriate buffer and loaded onto the column. The column was eluted with the suspension buffer and 1.2 ml fractions were collected. The protein in the fractions was estimated by measuring the A_{280}.

3.9 Crystallization Studies

3.9.1 Native Toxic Shock Syndrome Toxin-1

For crystallization toxin stock solutions (20 mg/ml) were prepared by dissolving the lyophilized toxin preparations in 50 μl of MilliQ or ElgaStat water. Unless otherwise stated all the chemicals used in crystallizations trials were of analytical grade and obtained from Sigma Ltd. All of the stock solutions contained a final concentration of 0.02% sodium azide as a bactericide. The initial crystallization trials for TSST-1 were performed at room temperature by the hanging drop method (McPherson, 1982) using the sparse matrix sampling protocol of Jancarik & Kim (1991). The individual drops (approximately 6 μl) consisted of equal volumes of reservoir stock solution and toxin stock solution. The drops were mixed on either plastic (Thermanox) or siliconized glass coverslips, 22 mm diameter (Chance Propper Ltd.), which were then inverted over individual wells in a 24 well tissue culture plate (Linbro, Flow Labs) and sealed with high vacuum silicone grease (Dow Corning). Later crystallization trials were performed using the sitting drop technique in microbridges (Harlos, 1992) at 16°C. Over 1000

crystallization trials were performed to obtain good quality crystals suitable for crystallographic work. For diffraction analysis, the crystals were carefully mounted, by conventional methods (Ducruix and Geige, 1992), in fine quartz capillary tubes 0.7-1.0 mm diameter (Quartzkapillaren; Glas) along with a small amount of mother liquor to prevent crystal dessication.

3.9.2 Mutant Toxic Shock Syndrome Toxin-1 (K105E)

Two mutant TSST-1 toxins were used during this project. The first, K105E, in which the lysine residue at position 105 had been mutated to a glutamate was purified by Dr.C.P.Quinn and Mrs.R.Brehm from the Centre for Applied Microbiology and Research (CAMR), Salisbury. The second H135A, in which the histidine residue had been converted to alanine, was supplied in the form of a crude *E.coli* shockate by Professor P. Bonventre (Department of Microbiology and Molecular Genetics, University of Cincinnati Medical Centre, Cincinnati, Ohio, USA.). H135A was subsequently purified by Dr.D.Beer, CAMR. Crystallization trials for both of these mutant toxins were carried out using the same set of conditions which were used for the wild type protein.

3.10 Heavy Atom Derivatives

With no obvious structures similar to TSST-1 available in the Brookhaven Data Bank, molecular replacement method could not be used to determine the structure of this toxin. Instead, isomorphous replacement method by preparing heavy atom derivatives (Petsko, 1985) of TSST-1 was performed at the Laboratory of Molecular Biophysics, Oxford University.

Using a light microscope, small amounts of heavy atom solutions was

carefully added to the native crystals suspended in a minimum amount of mother liquor inside a humid chamber to prevent dessication. Native TSST-1 crystals were transferred to an artificial mother liquor containing a range of heavy atoms (Table 3.5; Results Section). The artificial mother liquor was prepared to stabilize the crystals and to prevent them from dissolving on introduction of the heavy atom salt. This liquor was similar in composition to that used for crystallization except for the polyethylene glycol 3350 concentration, which was increased to 30%, prior to addition of the heavy atom compound. The 'derivitized' crystal and the new artificial mother liquor were transferred to a microbridge (Harlos, 1992), placed in a well containing 0.7 ml of the artificial mother liquor and sealed with a coverslip before storage at 16°C. The derivitized crystals were inspected after one hour using a light microscope and then daily thereafter. Any heavy atom derivative crystals which looked suitable for diffraction (by initial inspection under the microscope) were carefully transferred to a quartz capillary tube, sealed and mounted on the imaging plate for data collection.

During these trials careful consideration was given to the *p*H employed during the native crystallizations to decrease the probability of heavy atom derivatives failing due to precipitation in the artificial mother liquor (Petsko, 1985), Wolf *et al.*, 1991 and Blundell and Johnson 1976). As TSST-1 does not possess any cysteine residues, mercury compounds were not used for a potential derivative search.

3.11 Toxic Shock Syndrome Toxin-1 Data Collection

3.11.1 Wild Type Toxic Shock Syndrome Toxin-1

Diffraction data were collected from native TSST-1 crystals at 3.5Å and 2.5Å resolution and from numerous heavy atom derivatives at 3.5Å. Heavy atom derivative data were collected at 3.5Å because the phase errors obtained at higher resolution may be quite high due to non-isomorphism. Data were collected using a MAR Research image plate system (Fuji Photo Film Co. Ltd.) with Cu_α X-rays (λ=1.5418Å) generated by a Rigaku RU200 rotating anode with a graphite monochromator operating at 60 kV and 70 mA. The 3.5Å data were collected at 1.5° oscillation at 30 min/image, and the 2.5Å data at 1.0° oscillation at 60 min/image. To achieve a complete native data set to medium resolution, the most effective method was to collect approximately ten images and then to skip 7°. During data collection the crystals were translated to minimize radiation damage and to record the best diffraction data (Figure 3.1).

The native and heavy atom imaging plate data were processed separately (Figure 3.2; Appendix B) including the MOSFLM computer package (A.Leslie, MRC Cambridge.). The data were scaled and merged using the programs ROTOVATA and AGROVATA (Love, 1993). The unit cell parameters were monitored during data collection. If the unit cell parameters of the heavy atom derivative remained very close, *ie.* ~5% (isomorphous), to that of the native crystal dimensions after a preliminary analysis, data collection was continued. Otherwise data collection was abandoned and the whole exercise repeated for a different derivative.

3.11.2 Mutant Toxic Shock Syndrome Toxin-1 (K105E)

Initial data collection was performed at ambient temperature on a Siemens area detector mounted on a Siemens rotating anode X-ray source using CuK_α radiation (λ=1.5418Å) and operating between 44-50 kV and 76-80 mA. Two crystals of mutant TSST-1 K105E were found to be suitable for diffraction studies but they were poorly ordered with high mosaicity. The crystal to detector distance was 17.0 cm with a 2θ angle of 20°. Oscillation range was 0.25°/frame and 150 s/frame. Further crystallization trials are required to improve the quality of these crystals. All data from the initial diffraction studies were processed on a VAX workstation using the XDS package of programs (Kabsch, 1988; Figure 3.3 and Appendix B). Further characterization of these crystals at the Synchrotron Radiation Source, Daresbury showed possible diffraction to 2.5Å.

3.12 Estimation of the Isomorphous Differences

The first stage in the elucidation of the structure of TSST-1 was the processing and scaling of the derivative data to that of the 3.5Å native data. This was performed using the program DIFFER (Stuart *et al.*, 1979; Appendix B). An important feature of the DIFFER analysis is the mean fractional isomorphous difference value which is expressed as a percentage and describes the difference in scattering between the native and heavy atom derivative amplitudes resulting from introduction of the heavy atom. A value between 15% and 30% suggests a good derivative assuming all other unit cell parameters remain isomorphous with the native.

3.13 Interpretation of the Difference Patterson Maps

After accurate location of the heavy atom sites in a derivative crystal protein phase angles for each reflection can be estimated. However, it may be necessary to have more than one derivative in order to estimate the phase angles with minimum errors. The Patterson function is based on the squares of the differences in the amplitudes between two sets of data. Quite often the heavy atoms do not bind at the same sites on the protein. The binding will depend on the heavy metal and the nature of the protein. The difference Patterson map consists of peaks corresponding to vectors between heavy atom sites given both the native and heavy atom derivative data. Given a significant mean fractional isomorphous difference value with one or two heavy atom sites per molecule in the asymmetric unit, the heavy atom positions can be interpreted from a few strong peaks which can be located on the Harker sections of the difference map. Difference maps are needed to identify additional sites if there is more than one derivative.

3.14 Heavy Atom Phasing

Using the heavy atom structure factors (Section 2.9.3) $\mathbf{F}_H$ can be calculated and the protein phase angles α_P can then be estimated from the size of both the native and derivative structure factors $\mathbf{F}_P$ and $\mathbf{F}_{PH}$. Lower resolution (6.0Å) studies of TSST-1 gave approximate parameters for the uranyl fluoride derivative. The binding sites for the uranyl acetate derivatives were obtained by difference Fourier analysis.

Phase refinement was initiated within the resolution range 10Å to 6Å for 8 heavy atom sites after their coordinate positions were determined from the difference Patterson maps. The initial multiple isomorphous replace-

ment protein phases were calculated from a trial set of heavy atom parameters using the program PHASE (P.Shaw, unpublished; Appendix B). These heavy atom parameters were refined in turn using the least squares phased refinement based on the program REFINE for each derivative (P.Shaw, unpublished; Appendix B).

Results and Discussion

3.15 Production and Purification of Wild Type Toxic Shock Syndrome Toxin-1

After fermentation of *S.aureus* MN8 for 16 to 20 h at 37°, TSST-1 was purified from concentrated culture supernatant fluid to >99% purity by chromatography on Red A (Figure 3.4) and FPLC (Figure 3.5). The concentration of toxin in the final fermenter culture was estimated to be 0.044 mg/ml. Table 3.1 indicates the recovery of TSST-1 during the Red A and FPLC stage of purification. Although the purified TSST-1 preparations migrated as a single band on an SDS-PAGE gel (Figure 3.6), the purified toxin preparation did not give a single band when assessed by isoelectric focussing (Figure 3.7). This phenomenon has been noted from previous purification protocols used (Alouf *et al.*, 1991). Although the *p*I values for the major bands may be attributed to the different systems used to determine the *p*I, an explanation for the multiple forms is more difficult to ascribe. It may be due to deamidation during the purification protocol (Alouf *et al.*, 1991).

3.16 Crystallization of Toxic Shock Syndrome Toxin-1

3.16.1 Native Toxic Shock Syndrome Toxin-1

In general, single parallelepiped crystals of TSST-1 formed within one week, using either hanging or sitting drop methods under the conditions described in Table 3.2. However, subsequent crystals grown at 16°C were both larger and of superior quality when compared to those grown at room temperature (Figure 3.8). They appeared to have a hexagonal cross-section

of 0.3 to 0.4 mm with a length of up to 1.0 mm.

3.16.2 Mutant Toxic Shock Syndrome Toxin-1 (K105E)

Crystals of recombinant TSST-1 (rTSST-1) mutant K105E but not H135A were obtained using similar conditions to wild-type TSST-1 (Table 3.2). Small crystals of rTSST-1 H135A were obtained at 16°C when the buffer was changed to HEPES *p*H7.5 (Table 3.2). These crystals had a different morphology compared to that of the native TSST-1 crystals indicating that they may have a different packing arrangement within the crystal lattice. Due to time constraints, further analysis of these H135A crystals was not performed.

3.17 Preliminary Characterization of Crystals

3.17.1 Wild Type Toxic Shock Syndrome Toxin-1

These crystals belonged to the orthorhombic space group $C222_1$ (a = 108.6Å, b = 177.6Å, c = 97.5Å; Table 3.3) and, assuming that there were three molecules in the asymmetric unit, the specific volume of the protein was 3.55Å^3/Da which falls within the range normally observed for protein crystals, in accordance with Matthews (1968), and corresponds to a 65% (v/v) solvent content. Initial investigations at the SRS Daresbury (Beam line 7.2) showed that they diffracted to a maximum resolution of 1.9Å.

The TSST-1 crystals also appeared to possess pseudo-hexagonal symmetry with space group $P6_322$ and cell dimensions of $a = b$ = 104.1Å and c = 97.5Å, $\gamma = 117°$ containing one molecule in the asymmetric unit. Even though the y angle was close to 120°, 'forcing' these pseudo-hexagonal val-

ues during data processing failed to fit a hexagonal space group. However, an equivalent orthorhombic space group $C222_1$, in a lower symmetry, could account for all the systematic absences and was found to be the alternative space group which gave good merging statistics (Table 3.4). This pseudo-hexagonal symmetry was later confirmed by careful observation of the packing of molecules in the asymmetric units during isomorphous replacement method structure determination. These units contained one half of a crystallographic dimer and one non-crystallographic dimer arranged on a pseudo-hexagonal net.

3.17.2 Mutant Toxic Shock Syndrome Toxin-1 (K105E)

Preliminary data processing of two crystals of TSST-1 K105E using XDS (Kabsch, 1988) indicated that it had identical space group and unit cell parameters as the wild type (Table 3.3). These data gave an R_{merge} of 14.6%. This high R-factor suggested underlying high mosaicity and poor internal order. These data gave 19,834 unique reflections to 2.5Å with a total completeness of 53.2%. These data were used for subsequent refinement using XPLOR (Brünger, 1988).

3.18 Determination of the Multimeric State of Wild Type Toxic Shock Syndrome Toxin-1

It has been reported in the literature that TSST-1 exists in the monomeric state in solution (Naidu *et al.*, 1989). However, in the crystal form of TSST-1 reported here, there were three molecules in the asymmetric unit. In order to address this question, purified preparations of TSST-1 were applied to a gel-filtration chromatography column of Bio-gel P-100 in

an attempt to separate any multimeric forms under gravity (Section 3.8). In each case TSST-1 eluted as a single sharp peak with both TRIS-HCl and acetate buffer (Figures 3.9 and 3.10 respectively). From the plot of k_{av} vs. log M_r (Figure 3.11), in accordance with the manufacturers instructions, it was estimated that the M_r of TSST-1 was 25.9 kDa in acetate buffer, and 28.5 kDa in Tris-HCl buffer. These results suggest that within experimental error, at these two *p*H values, TSST-1 exists as a monomer. The M_r of TSST-1 from the nucleotide sequence is 22,049 Da (Blomster-Hautamaa and Schlievert, 1988). Therefore, the three molecules in the asymmetric unit of the crystallized toxin are probably an artefact of protein packing within the crystal and as such are not expected to fulfil any physiological function.

3.19 Heavy Atom Derivative Trials

Twenty seven heavy atom solutions at concentrations ranging from 1 mM to 10 mM were used to soak native TSST-1 crystals for varying lengths of time (Table 3.5). Many of these compounds (Table 3.5) reacted with the native TSST-1 crystals and caused the cracking of the crystal. Other derivatives actively dissolved the crystals as seen by the obvious loss of the very sharp long edges characteristic of TSST-1 crystals. Despite this, many derivatized crystals maintained their morphology during heavy atom soaking (Table 3.5) and were mounted and placed on the MAR Research imaging plate and data collected at 3.5Å. Data from the native crystals and all the heavy atom data were processed using the programs illustrated in Figure 3.2.

Table 3.6 indicates that both the uranyl acetate and uranyl fluoride

gave a mean fractional isomorphous difference (MFID) value of 29.9% and 17.1% respectively. These two were therefore chosen as potential derivatives to estimate the preliminary phases for the TSST-1 structure. A summary of the MIR and solvent flattening statistics can be seen in Tables 3.7 and 3.8 respectively.

3.20 Interpretation of the Difference Patterson Maps

The uranyl acetate/native difference Patterson maps were performed in the resolution range 10Å to 6Å and calculated using the native data to 3.5Å. Phase extension to 2.5Å was performed using the technique of molecular averaging with the program GAP (D.Stuart and J.Grimes, unpublished), by a 3-fold real space averaging. This resulted in an R-factor and correlation of 0.31 and 0.91, respectively, between the observed data and data obtained by inversion of the averaged solvent flattened map.

3.21 Electron Density Map of Wild Type Toxic Shock Syndrome Toxin-1

The background noise in the initial ($2|F_o| - |F_c|$) electron density map produced at 3.5Å was generally low. A significant portion of β strands and the major α helix were identifiable in the 3.5Å electron density map. Although it was possible to follow the polypeptide chain some regions were unclear due to occasional breaks in electron density.

After the 2.5Å map was calculated there was a significant improvement in the electron density and the secondary structure elements were well defined with clearly visible side chains. Initially location of the N and C termini was difficult. However, after establishing the first and last

residues, the trace from the N to C termini was very clear with few breaks in connectivity in the map. When this was completed, segments of the polypeptide backbone were identified and fitted to the electron density map of one TSST-1 molecule. In order to complete the structure interpretation and to obtain the atomic coordinates for TSST-1, the β strands of the cell adhesion molecule CD2, refined to 2.8Å (Jones *et al.*, 1992), were imported into the computer for subsequent manipulation. These β strands were transposed over and into the TSST-1 density. Manipulation of these newly inserted strands fitted the density better and ensured the correct position for the residue side chains. The β turns were then added and linked with the β strands already in place. Fitting the α helices was easier than that for the β strands due to the ordered nature all α helices display. Finally the loops between the secondary structure elements were then carefully added.

Almost all of the amino acid side chains had well defined density and were clearly visible. The sequence for the more obvious large side chains like Trp, Phe and His residues were identified and positioned in the map from knowledge of their general shape. It was easy to identify prominent features such as the location of tyrosines Tyr 51 and Tyr 52 and Lys 121 and Lys 122. The amino acid sequence was then checked in the forward and backward direction for fitting into the electron density available. Throughout manual rebuilding, local least squares energy minimization for the segments of the structure were performed using the program FRODO (Jones, 1985) and the side chain sequence was then incorporated using the program CALPHA (R.Esnouf, unpublished), and reordered from 1 through to 194 (Blomster-Hautamaa and Schlievert, 1988). In total 1559 protein atoms were fitted

into one molecule of TSST-1.

3.22 Refinement of Wild Type Toxic Shock Syndrome Toxin-1 Structure

The 2.5Å starting model was refined using the package XPLOR (Version 2.1; Brünger, 1988). Initially strict non crystallographic symmetry (NCS) restraints were employed as described in the XPLOR manual (Version 2.1; Brünger, 1988) for the refinement of the three TSST-1 molecules found within the asymmetric unit. XPLOR contains a facility which utilises the non-crystallographic symmetry found within the unit cell during simulated annealing refinement. It can also allow 'strict' or 'restrained' refinement. The former makes use of a designated monomer, which is assumed for the purposes of the refinement to be similar to the remaining molecules within the asymmetric unit, and that any alterations to this monomer are reflected in identical changes to the two remaining monomers. The non-crystallographic symmetry operators, which represent the rotation matrices and also the translation vectors, generate the remaining molecules of the asymmetric unit and are subsequently applied to the monomer. Indeed, the F_{calc} for the entire asymmetric unit is generated from this single molecule. The advantage of this strict refinement is that any noise present is reduced by averaging it over the whole asymmetric unit. The restrained refinement option allows for the contents of the asymmetric unit to be refined independently. The non-crystallographic symmetry related atoms within each molecule are restrained about their average position. A flow diagram of the programs used can be seen in Figure 3.12.

Round 1

With strict NCS restraints applied, a new electron density map was calculated and all 194 main and side chains were systematically adjusted as necessary using the program FRODO on an Evans and Sutherland graphics system (ESV 10), for one molecule only.

Round 2

Refinement continued as in round 1 using the same protocol, including strict NCS restraints. At the end of round 2, a detailed analysis was made of the molecule using a Ramachandran plot. This plot describes the ϕ,ψ angles found in the present model with the experimentally 'allowed' values (Ramachandran and Sasisekharan, 1968). These angles were monitored for each residue for any unacceptable geometry and adjustments to the model were made accordingly.

Round 3

After round 2 the strict NCS restraints were relaxed. By the end of round 3, refinement of all 3 molecules was checked individually.

Round 4

The final R-factor was 21.3% for all reflections in the range 8.0 to 2.5Å. A portion of the final $2|F_o| - |F_c|$ electron density map for TSST-1 is shown in Figure 3.13 contoured at 1σ.

The present 3-D model, refined to 2.5Å resolution, contains all 194 amino acid residues and includes 4677 non-hydrogen atoms for all three

molecules in the asymmetric unit. The overall structure has a crystallographic R-factor of 21.3% for all data to 2.5Å (15.6% for $F > 3\sigma$). It has good geometry as exemplified by rms deviations in bond lengths of 0.011Å and in bond angles of 2.64°. With the exception of Ser 86 all of the non-glycine residues, have ϕ,ψ angles which lie within the allowed zone of the Ramachandran plot (Ramachandran and Sasisekharan, 1968) with $\phi = 61°$, $\psi = -157°$ (Figure 3.14). The C_α coordinates for each molecule were superimposed in a pairwise manner with one another which gave an rms difference of 0.13Å, 0.15Å and 0.15Å for the molecules 1-2, 1-3 and 2-3 respectively, indicative of a high degree of similarity between the three molecules.

3.23 Description of Wild Type Toxic Shock Syndrome Toxin-1 Structure

The structure of a single TSST-1 molecule is illustrated in Figure 3.15 referred to as its 'standard' orientation. The molecule has approximate dimensions 45Å × 45Å × 58Å. It can be divided into two distinct structural domains both of which contain a significant number of β strands. The two domains are linked through a long α helix which is functionally important. Overall, 17% of the structure exists as α helices, 46% as β strands and the remaining 37% as β turns and loops. The secondary structure assignment was based on the program DSSP (Kabsch and Sander, 1988; Figure 3.16).

3.23.1 Domain 1

Domain 1 comprises of the N terminal residues 1 to 95 and includes five β strands (β1 to β5) and one α helix (α1; Figure 3.17). After a short

N terminal portion, which is sterically adjacent to domain 2 and includes the first α helix α1 (7 to 15), this domain is dominated by a distinctive antiparallel β barrel comprising of two β sheets (β1, β4 and β2 β3 β4 β5). The β strands are all connected by loops with no α helices. This β barrel is elliptical in cross-section (Figure 3.18) and has a criss cross pattern (Figure 3.19). The β barrel has a core of hydrophobic residues: Phe 20, Val 25, Met 33, Ile 35, Ile 45, Phe 47, Pro 54, Phe 56, Val 62, Leu 64, Ile 81 and Val 88. The concave region of domain 1 is delineated by strands β1 β2 and β3 and is noticeable for its clustering of hydrophobic solvent accessible residues.

This overall feature comprises five β strands forming a β barrel with the addition of a small α helix linking strands β 3 and β 4, is not unique having been observed in SEB (Swaminathan *et al.,* 1992) and other structures including two toxins, verotoxin-1 (Stein *et al.,* 1992) and heat labile enterotoxin (B subunit; Sixma *et al.,* 1992), and also staphylococcal nuclease (Hynes and Fox, 1991). None of these proteins share high sequence homology with one another, yet they all show very similar tertiary structure. All of these proteins apart from SEB have been shown to bind either oligosaccharides or oligonucleotides. The binding sites are located to one side of the β barrel called the 'OB fold' (Murzin, 1993).

3.23.2 Domain 2

The C terminal domain 2, consists of residues 96 to 194 which constitute seven β strands (β6 to β12), one major α helix (125 to 140) and two single turn 3_{10} helices (173 to 177 and 183 to 185). This domain is dominated by the major helix α2, which has five β strands cupped around it

forming a β barrel. This β barrel is slightly twisted with a less pronounced concave surface on one side. The upper part of the $\alpha 2$ helix interacts with $\alpha 1$ helix from domain 1; the lower part of the $\alpha 2$ helix interacts with a 3_{10} helix. Unlike domain 1, the distribution of amino acid residue types within this domain shows no distinctive features.

The C terminal domain of TSST-1 appears to be unique amongst the bacterial superantigens but could nevertheless be considered a variation of the 'β grasp' motif (Murzin, 1992; Overington, 1992). This has been seen in a number of other proteins with an α helix tightly surrounded by 4 β strands. These proteins include chloroplast ferredoxins (Tsukihara *et al.*, 1981), immunoglobulin G-binding domain of streptococcal protein G (Achari *et al.*, 1992) and ubiquitin (Vijay-Kumar *et al.*, 1987).

3.23.3 Intermolecular Contacts

Wild type TSST-1 packs into the $C222_1$ unit cell with approximately 65% solvent. There are three molecules in the asymmetric unit which are governed by crystallographic and non-crystallographic (local) symmetry as shown in Figure 3.20. Molecules designated 1 and 3 constitute part of the dimer on the crystallographic 2-fold axis and molecule 2 forms one half of the non-crystallographic dimer.

These intermolecular interactions in TSST-1 involve residues from domain 1 on the 'top' surface of both molecules (with respect to its standard orientation), which seem to lie at 45° to one another. The main contributions are from $\alpha 1$ helix and strands $\beta 4$ and $\beta 5$ which participate in dimer interactions. There are only 16 unique hydrogen bond contacts between the three molecules in the asymmetric unit of less than 3.5Å, 15

of which lie at the interface between molecules 1 and 3 (Table 3.9).

3.24 Comparison of Toxic Shock Syndrome Toxin-1 and SEB Structure

The crystal structure of SEB has recently been determined (Swaminathan *et al.*, 1992). The overall topology of TSST-1 is clearly similar to that exhibited by SEB (Swaminathan *et al.*, 1992), with domain 1 of SEB consisting of a β barrel structure based on five β strands forming two β sheets (1, 4 and 5 and 2, 3, 4 and 5), and domain 2 of SE containing a major helix (α4) tightly covered by 5 β strands (6, 7, 9, 10 and 12). Despite the lack of any significant sequence similarity (approximately 24%) between these two toxins (Figure 1.1), they possess similar secondary structure features (Figure 3.21). A conservation of the global fold is perhaps not unexpected considering their similar biological properties and their interaction with both MHC II and TcR *in vivo*.

The evolutionary relationship of these enterotoxins is quite evident from the preservation of the distinct two-domain fold and it is possible that they diverged from a common ancestor. However when the structures are compared in more detail, they are not strictly conserved because the whole TSST-1 molecule is smaller than SEB by 45 amino acid residues (M_r 22 kDa and SEB 28 kDa respectively). As such, a number of differences must occur which can be attributed to secondary structure deletions in TSST-1. Domain 1 of TSST-1 comprises 96 amino acid residues compared with SEB which contains 120 residues.

There are three main regions in domain 1 where the structure of TSST-1 and SEB differ to a great extent, and two in domain 2. When the

TSST-1 domain 1 pattern is compared with that of SEB (Table 3.10), the equivalent α1 helix in SEB is replaced in TSST-1 by an extended region of six amino acid residues. The SEB α2 helix is equivalent to the TSST-1 α1 helix. The short α helix (α3) of SEB linking strands β3 and β4, has been replaced with a short loop of 12 residues (48 to 59) in TSST-1. The equivalent disulphide loop of SEB is not present in TSST-1 *per se* but is replaced by a much shorter loop of three residues between β strands 4 and 5 (residues 75 to 78), In the reported structure of SEB (Swaminathan *et al.*, 1992) residues 99 to 105, were missing. This was attributed to the increase in flexibility of these residues beyond the disulphide. In all the loop regions between the β strands in TSST-1 there are variations to be found in the number of residues when compared with SEB (Table 3.10). For example there are only two residues between β1 and β2 and three residues between β2 and β3 in TSST-1 but there are 8 and 12 residues respectively between similar strands in SEB.

3.25 Refinement of Mutant Toxic Shock Syndrome Toxin-1 (K105E) Structure

As the mutant TSST-1 K105E unit cell parameters were isomorphous with the wild type (Table 3.3). It was decided to use the wild-type TSST-1 model for refinement against the mutant data. Table 3.11 illustrates the in-house data collection. The refinement consisted of several steps using the XPLOR (Brünger, 1988) computer package (Figure 3.22). For refinement purposes the original residue Lys 105 in the wild type TSST-1 was replaced with an alanine. This was done to prevent any side chain bias from the original lysine in the electron density for this region. After one round of

refinement the final R-factor for the model was 21.3% (Table 3.12) for 15389 reflections ($F > 3\sigma(F)$) between 8.0 and 2.8Å. The final TSST-1 K105E model had an rms bond length 0.006Å and an rms bond angles of 1.454°. Figure 3.23 demonstrates the glutamate 105 modelled in the electron density. There were still a number of breaks in the electron density map along both the main chain and side chains. This may have been due in part to the lack of completeness of the data used in the refinement.

Table 3.1 *Purification of TSST-1 by 'Red A' and fast protein liquid chromatography (FPLC) from 25 litre fermenter culture.*

Stage	Total Toxin (mg)	% Yield (Stage)	% Yield (Overall)
Final Fermenter Culture	1100	100	100
Initial Dialysis	957	87	87
Red A Chromatography	880	92	80
Second Dialysis	825	94	75
FPLC	660	80	60

Table 3.2 *A comparison of the final crystallization conditions employed for native and recombinant TSST-1.*

Toxin	Toxin Stock Conc^n (mM)	Buffer	*p*H	Salt or Organic Solvent	PEG† 3350 (%)
TSST-1	20	0.1M Acetate	4.6	0.2M $(NH_4)_2SO_4$	23-27
TSST-1 K105E	20	0.1M Acetate	4.6	0.2M $(NH_4)_2SO_4$	23
TSST-1 H135A	20	0.1M HEPES*	7.5	10% 2-Propanol	20

† Polyethylene glycol; * HEPES, 4-(2-hydroxy ethyl)-1-piperazineethanesulphonic acid.

Table 3.3 *Crystal data for wild type and mutant TSST-1*

Feature	TSST-1	K105E
Space Group	$C222_1$	$C222_1$
Unit Cell Parameters (Å)		
a	108.6	108.6
b	177.6	177.6
c	97.5	97.5
$\alpha=\beta=\gamma$	90°	90°
Solvent Content	65%	65%
No. Molecules in Asymmetric Unit	3	3
Oscillation Range (°)	0.25°	0.25°
Time (s) per Oscillation	200-300	150
No. of Crystals Used	8	2
d_{min} (Å)	2.5	2.8

Table 3.4. *Summary of TSST-1 Imaging Plate Diffraction Data.*

Feature	Native 1	Native 2	Native (1+2)	Uranyl Acetate	Uranyl Fluoride
d_{min} (Å)	3.5	2.5	2.5	3.5	3.5
No. of Crystals Used	1	2	3	1	1
Crystal to Detector Distance (mm)	189.1	124.2	124.1	189.1	189.1
No. of Reflections	20,717	49,530	70,247	11,104	13,938
No. of Unique Reflections	11,231	29,155	30,009	9,186	10,536
% Complete	94	87	89	77	88
R_{merge}	7.5	7.5	8.6	8.4	4.5
MFID	-	-	-	29.9	17.1

$R_{merge} = \sum(/\bar{I}_{obs} - \bar{I}/) \sum \bar{I}$. MFID- Mean fractional isomorphous difference.

Table 3.5. *Heavy atom derivative trials for TSST-1.*

Compound Number	Heavy Atom (mM)	Conc^n	Soak Time	Comments
D1	EMP	10	22h	Cracks
D2	Lead Acetate	10	46h	V.poor diffraction
D3	Mercury Iodide	5	6h	
D4	Bakers	9.3	5h	Ruined
D5	Bakers	9.3		Cracks (30 mins)
D6	Mercury Iodide	5		Crystal redissolves
D7	Bakers	0.93		Cracks (10mins)
D8	EMP	1	25h	Crystal redissolves
D9	EMP	5	3h	
D10	Platinum Cyanide	5	3h	
D11	Lead Acetate	5	21	Cracks
D12	Platinum Cyanide			
D13	Uranyl Acetate	10	16h	Yellow crystal
D14	Gold Chloride	5	16h	
D15	Platinum Chloride	5	16h	
D16	Samarium Acetate	5	20	
D17	EMP	5	24h	
D18	Lead Acetate	10	24	
D19	Platinum Cyanide	5	24h	

Table 3.5. *Heavy atom derivative trials for TSST-1, continued.*

Compound Number	Heavy Atom (mM)	Conc^n	Soak Time	Comments
D20	Uranyl Acetate	10	12	
D21	Gold Chloride	5	10	Poor diffraction
D22	Uranyl Acetate	10	12h	Small cracks
D23	Gold Chloride	5	10h	Poor diffraction
D24	Gold Cyanide	10	37h	
D25	Uranyl Fluoride	10	23h	
D26	Uranyl Acetate	10	13	
D27	Gold Chloride	5	3h	Yellow crystal

Table 3.6. *TSST-1 derivative data collection to 3.5Å.*

Number	No. of Images	% Complete	MFID†	R_{merge}
D1	ND			
D2	ND			
D3	21	57	15.34	10.3
D5	ND			
D13*	22	77	29.86	8.4
D14	60	76	34.47	8.8
D15	34	72	16.03	6.6
D16	35	74	16.05	6.6
D17	7	17	15.69	4.1
D18	5	15	13.0	10.5
D19	5	15	9.3	6.3
D21	ND			
D22+R13	52	90	30.43	7.2
D22	30	68	26.43	8.0
D23	ND			
D24	4	20	7.24	3.5
D25*	40	88	17.06	4.5
D27	9	39	33.4	16.3

† MFID, mean fractional isomorphous difference; ND, not determined.

Table 3.7. *A summary of MIR phasing.*

Feature	Uranyl Acetate	Uranyl Fluoride
No. Sites	5	3
R_C to 6.0Å (3.5Å)	0.55	0.49 (0.56)
Phasing Power to 6.0Å (3.5Å)	1.9	2.1 (1.7)

R_C:Cullis R-factor for centric reflections. Phasing power: mean value of the heavy atom structure factor amplitudes divided by the residual lack-of-closure error.

Table 3.8. *A summary of TSST-1 solvent flattening.*

d_{min} (Å)	Pre-Wang FM	% Solvent	Wang R-Factor	Phase Change	Wang FM
6.0	0.60	65	26.3	41.3°	0.78
3.5	-	65 (55)	22.6 (18.7)	50.5° (48.3)	0.77 (0.80)

Table 3.9. *Intermolecular hydrogen bond contacts in the TSST-1 asymmetric unit.* †

Molecules	Donor	Acceptor	Distance (Å) ‡
1-3	Ser 001 **N**	Thr 038 **O**	2.73
	Asn 003 **N**	Asp 039 **O**	3.11
	Asn 005 **ND2**	Gly 078 **O**	3.27
	Lys 007 **NZ**	Asp 039 **O**	3.02
	Arg 068 **NH2**	Thr 011 **O**	2.93
	Ser 072 **OG**	Asp 011 **OD2**	2.94
	Tyr 080 **OH**	Thr 008 **OD2**	3.31
	Ser 080 **OH**	Thr 011 **OD2**	3.37
3-1	Ser 001 **N**	Thr 038 **O**	2.71
	Asn 003 **N**	Asp 039 **O**	3.15
	Lys 007 **NZ**	Asp 039 **O**	2.90
	Arg 068 **NH2**	Thr 011 **O**	2.91
	Ser 072 **OG**	Asp 011 **OD2**	2.93
	Tyr 080 **OH**	Thr 008 **OD2**	3.43
	Ser 080 **OH**	Thr 011 **OD2**	3.21
1-2	Ser 034 **NH1**	Asp 160 **O**	3.17

† Data compiled using DSSP and HERA ‡ Residues listed make protein-protein contacts within a 3.5Å cut-off distance.

Table 3.10. *Secondary structure comparison between TSST-1 (this study) and SEB (Swaminathan et al., 1992).*

	TSST-1	SEB	
Secondary Structure	Residues	Secondary Structure	Residues
–	–	α1	12-17
α1	7-15	α2	21-29
β1	18-29	β1	33-39
β2	32-37	β2	48-52
β3	41-47	β3	63-68
–	–	α3	70-78
β4	60-75	β4	81-89
β5	79-89	β5	112-120
β6	101-106	β6	127-138
β7	109-111	β7	141-151
β8	119-124	β8	1154-156
α2	125-140	α4	157-172
β9	152-158	β9	182-190
β10	161-166	β10	195-200
3_{10}-1	173-177	α5	210-217
β11	181-182	β11	222-225
3_{10}-2	183-185	–	–
β12	186-193	β12	229-236

Table 3.11 *Recombinant TSST-1 K105E in-house data collection.*

Resol^{n} Range (Å)	No. of Poss. Reflect^{ns}	Cumu^{ve} No. of Poss. Reflect^{ns}	No. of Reflect^{ns}	Cumu^{ve} No. of Reflect^{ns}	% Poss.
∞-15.00	186	186	37	37	19.8
15.00-10.00	397	583	326	363	82.1
10.00-8.00	518	1101	439	802	84.7
8.00-6.00	1435	2536	1268	2070	88.3
6.00-5.00	1774	4310	1546	3616	87.1
5.00-4.50	1550	5860	1306	4922	84.2
4.50-4.00	2411	8271	2019	6941	83.7
4.00-3.50	3969	12240	3135	10076	78.9
3.50-3.20	3695	15935	2739	12815	74.1
3.20-3.00	3351	19286	2241	15056	66.2
3.00-2.80	4309	23595	2416	17472	56.1
2.80-2.70	2680	26275	1233	18705	46.0
2.70-2.60	3102	29377	1042	19747	33.5
2.60-2.50	3605	32982	87	19834	2.4
Total		32982		19834	53.2

Table 3.12. *R-factor changes during recombinant TSST-1 (K105E) refinement.*

	R-factor Start	*R*-factor End
Prepstage	32.4	27.3
Slowcool	27.3	26.8
Bref	26.2	21.9
Pos1	21.5	21.3

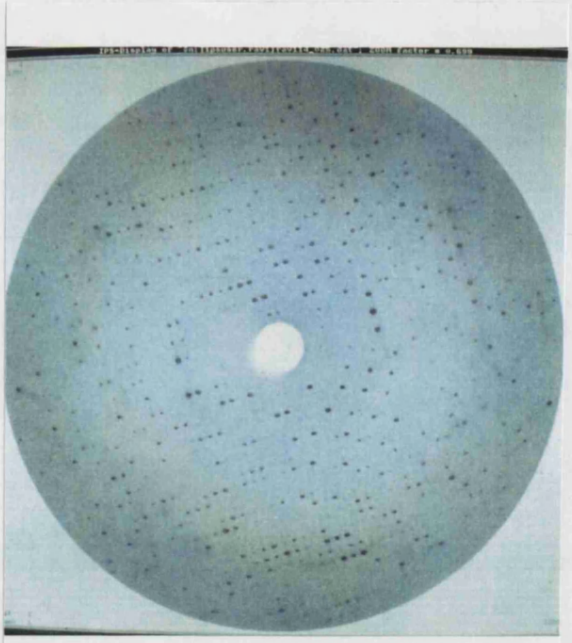

Figure 3.1 A typical diffraction pattern of TSST-1 to 2.5Å to show the quality of diffraction. Photo taken at SRS Daresbury PX 7.2.

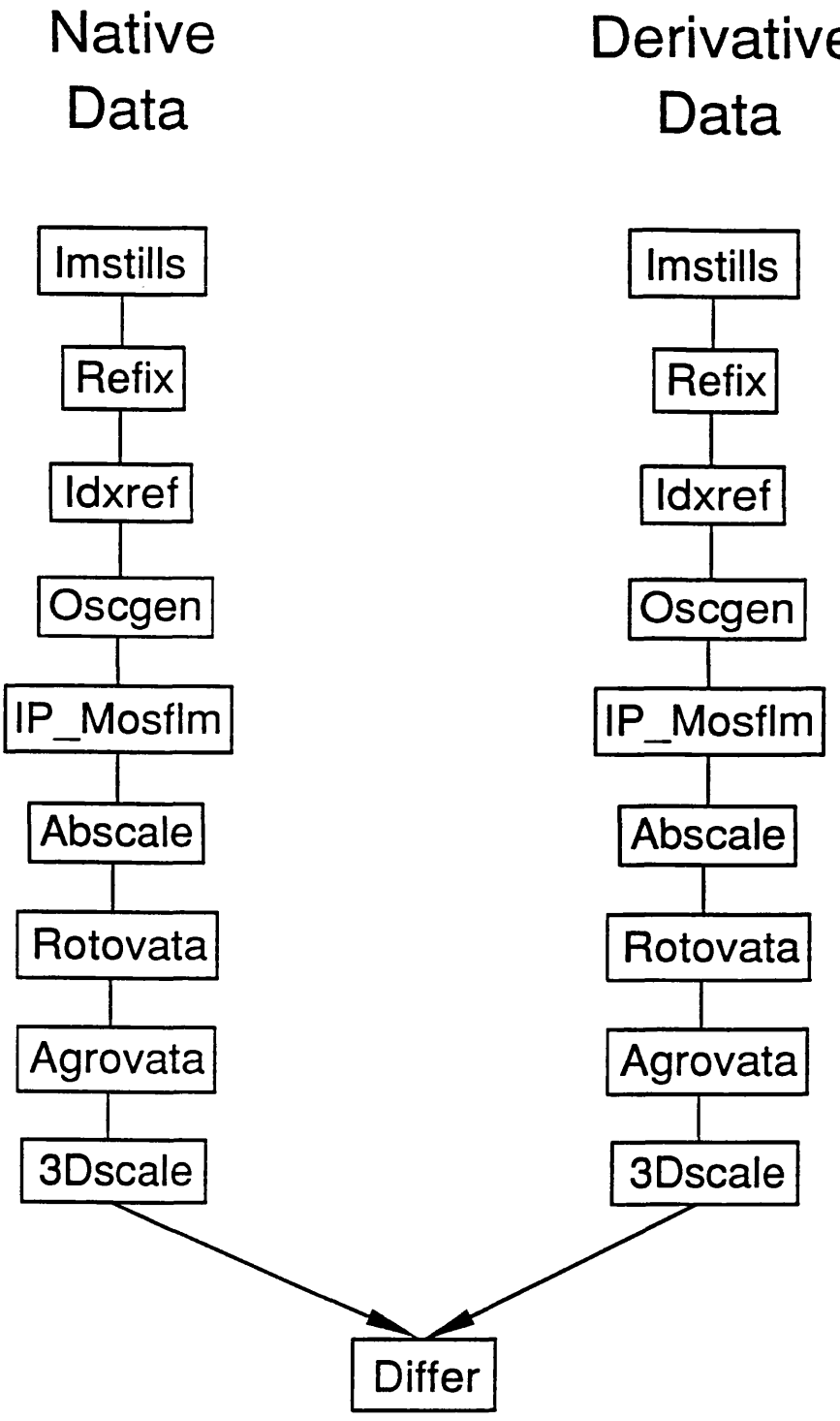

Figure 3.2 Flow diagram to show the programs used in data collection and processing of native and derivative TSST-1.

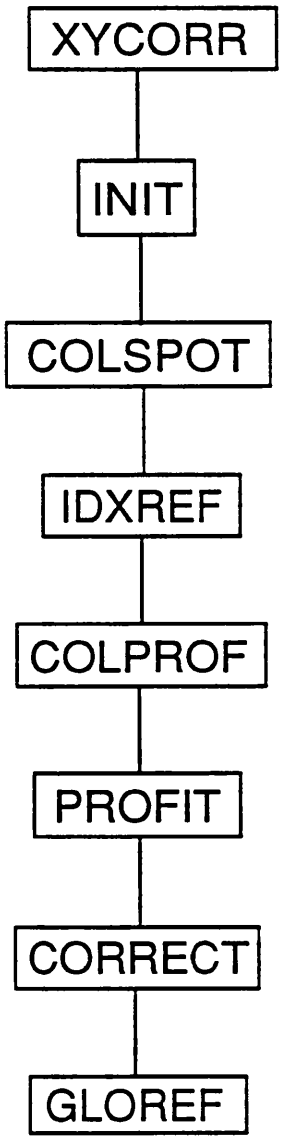

Figure 3.3 Flow diagram for XDS data processing (Kabsch, 1988).

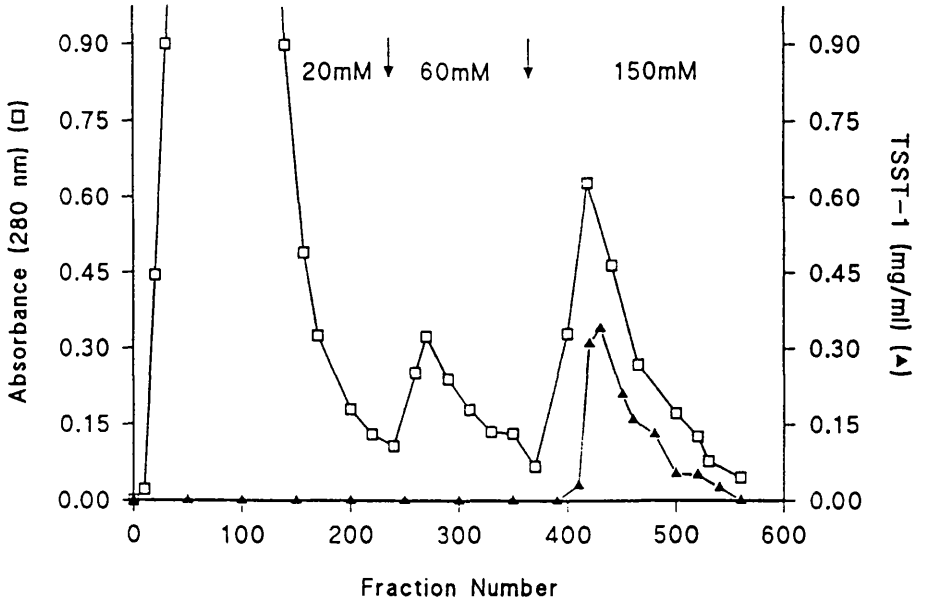

Figure 3.4 Dye ligand chromatography of TSST-1 from 25 l of culture supernatant using Red A. The column (4.5 × 31 cm) was equilibrated in 20 mM phosphate buffer, *p*H 6.5, and eluted with a stepwise increase in molarity of phosphate buffer *p*H 6.5, as indicated. Fractions (10 ml) were collected at a flow rate of 40 ml/h (during binding) and 80 ml/h (during elution) and their absorbance was measured at 280 nm.

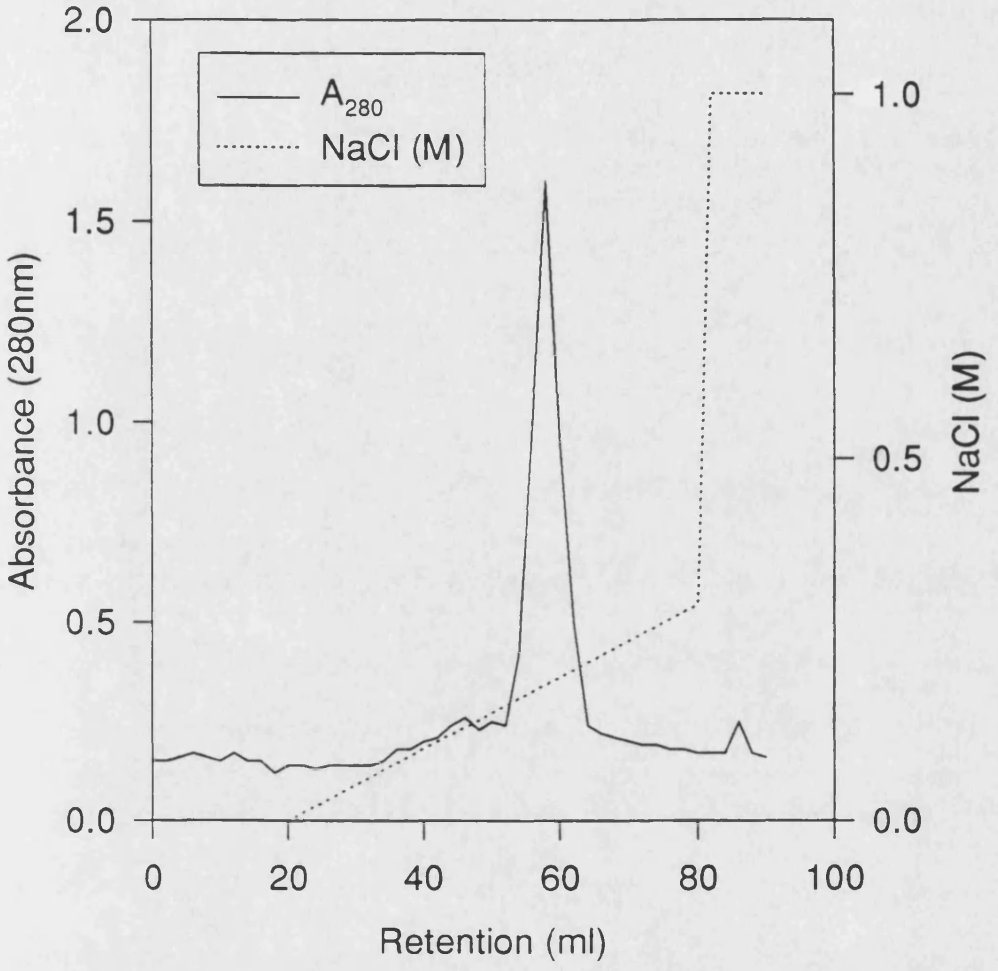

Figure 3.5 Final purification of TSST-1 by FPLC, after previous chromatography using Red A. The 20 ml HiLoad S Sepharose high performance 16/10 column (Pharmacia) was equilibriated with 50 mM sodium acetate buffer (*p*H 5.0). Toxin was eluted using 150 mM linear gradient of increasing NaCl concentration (up to 250 mM) at a flow rate of 2 ml/min.

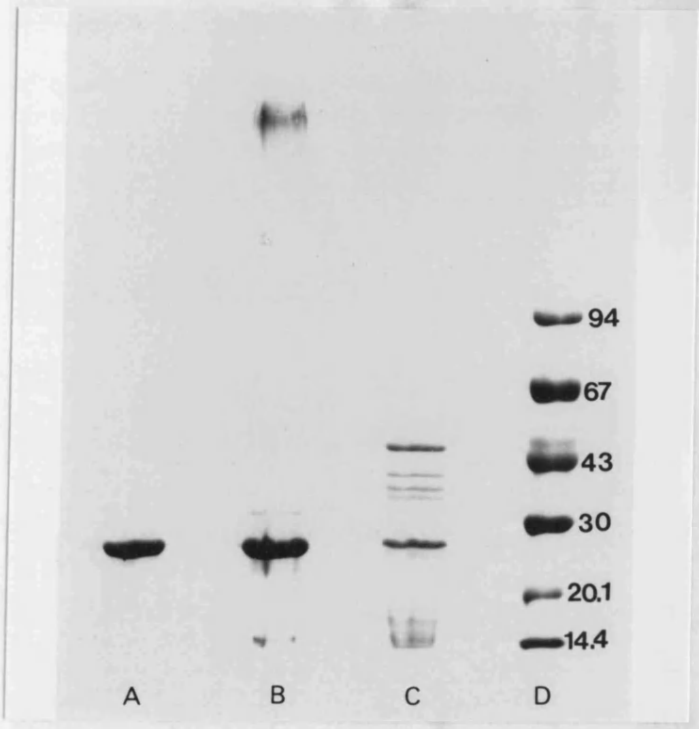

Figure 3.6 An SDS-polyacrylamide gradient (8 to 18%) precast gel (Pharmacia) analysis of stages in the purification of TSST-1. Lane A, pooled fractions from fast protein liquid chromatography. Lane B, pooled fractions eluted from Red A. Lane C, concentrated culture supernatant fluid. Lane D, molecular mass markers (Pharmacia; kDa): phosphorylase *b*, 94; albumin, 67; ovalbumin, 43; carbonic anhydrase, 30; trypsin inhibitor, 20.1 and α-lactalbumin, 14.4. Lanes A to C were loaded with 10 μl of sample containing 0.5 to 1.0 mg protein per ml.

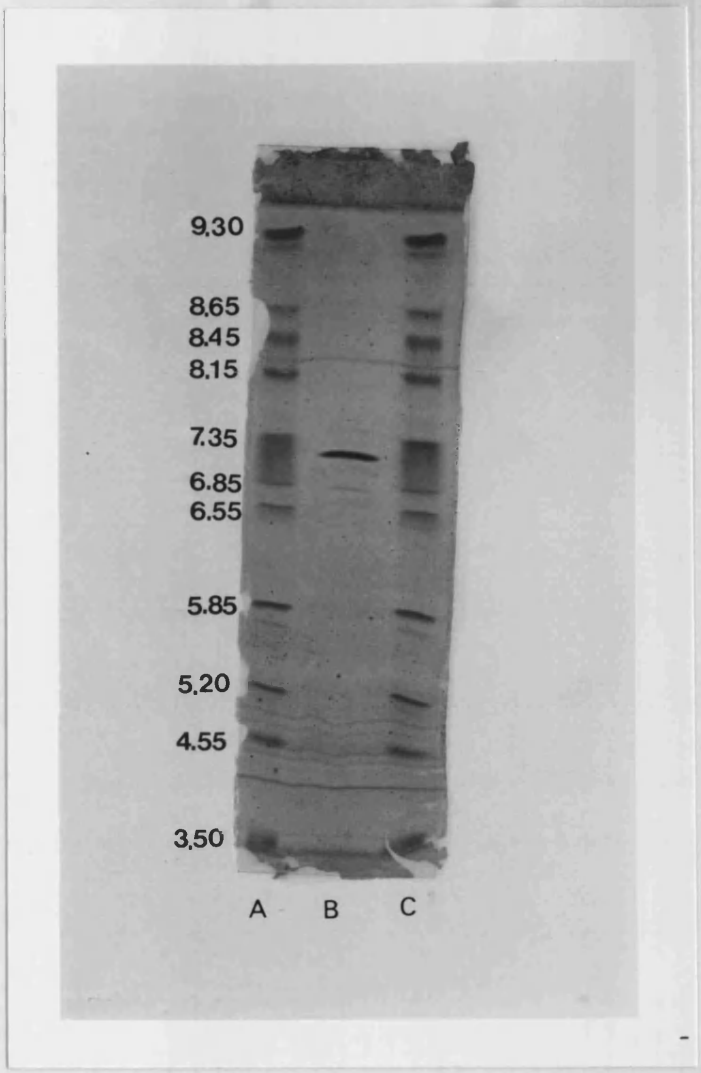

Figure 3.7 Isoelectric focusing of TSST-1 purified by FPLC. Lanes A and C, *p*I markers: trypsinogen, 9.30; lentil lectin (basic band), 8.65; lentil lectin (middle band), 8.45; lentil lectin (acidic band), 8.15; myoglobin (basic band), 7.35; myoglobin (acidic band), 6.85; human carbonic anhydrase B, 6.55; bovine carbonic anhydrase B, 5.85; β-lactalbumin A, 5.20; soybean trypsin inhibitor, 4.55 and amyloglucosidase, 3.50. Lane B, TSST-1.

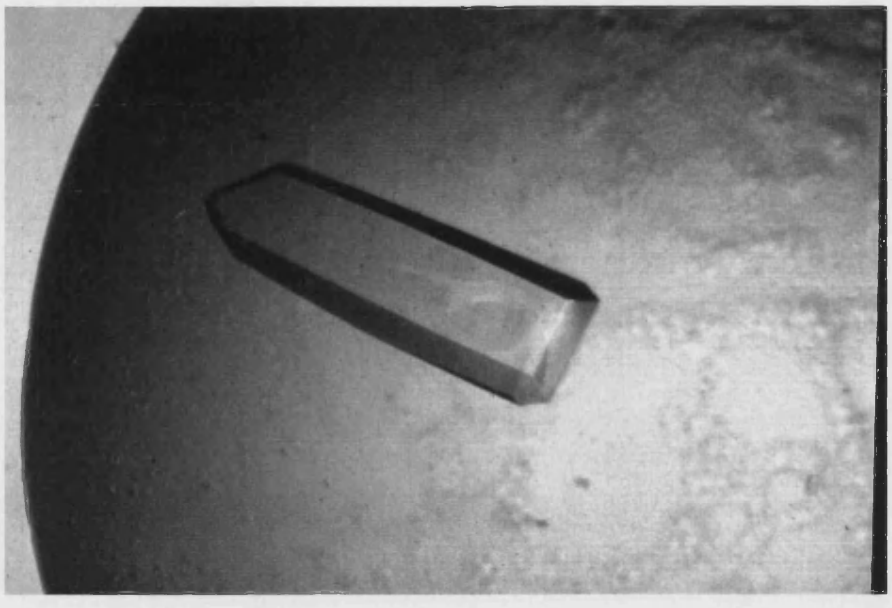

Figure 3.8 Orthorhombic crystal of native TSST-1. The crystal dimensions are 0.3 mm × 0.4 mm × 0.8 mm.

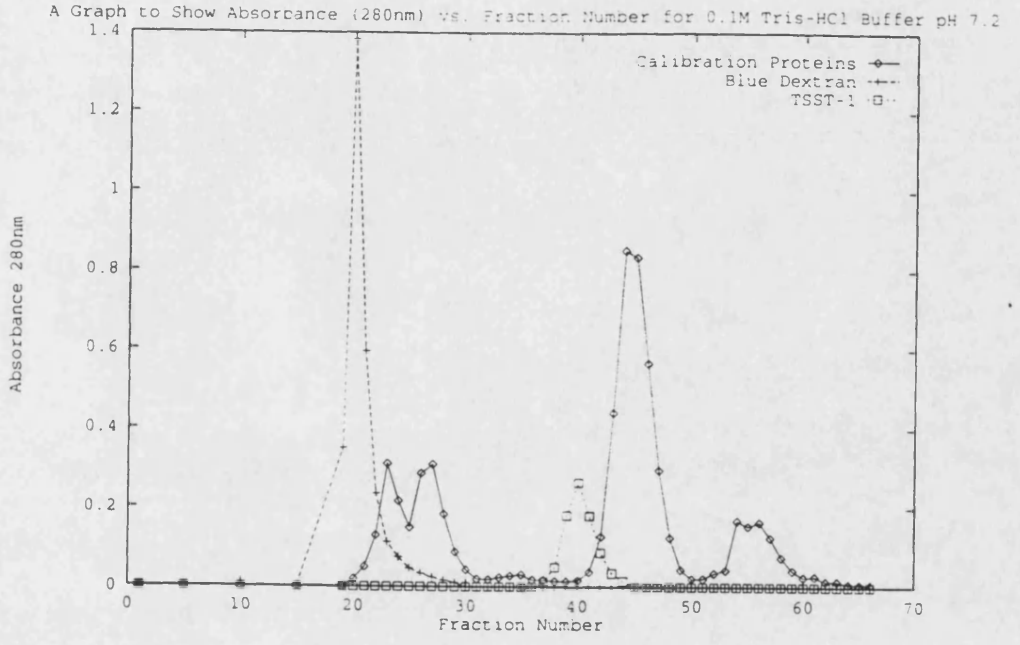

Figure 3.9 Gel filtration using 0.1M Tris-HCl buffer, *p*H 7.5, showing the separation of standard proteins superimposed with TSST-1 using P-100 gel (Bio-Rad) and column (1.5 × 75 cm) under gravity at a flow rate of 5 ml/h. The calibration proteins (Pharmacia) are (kDa): ribonuclease A, 13.7; chymotrypsinogen A, 25.0; ovalbumin, 43.0; bovine serum albumin, 67.0.

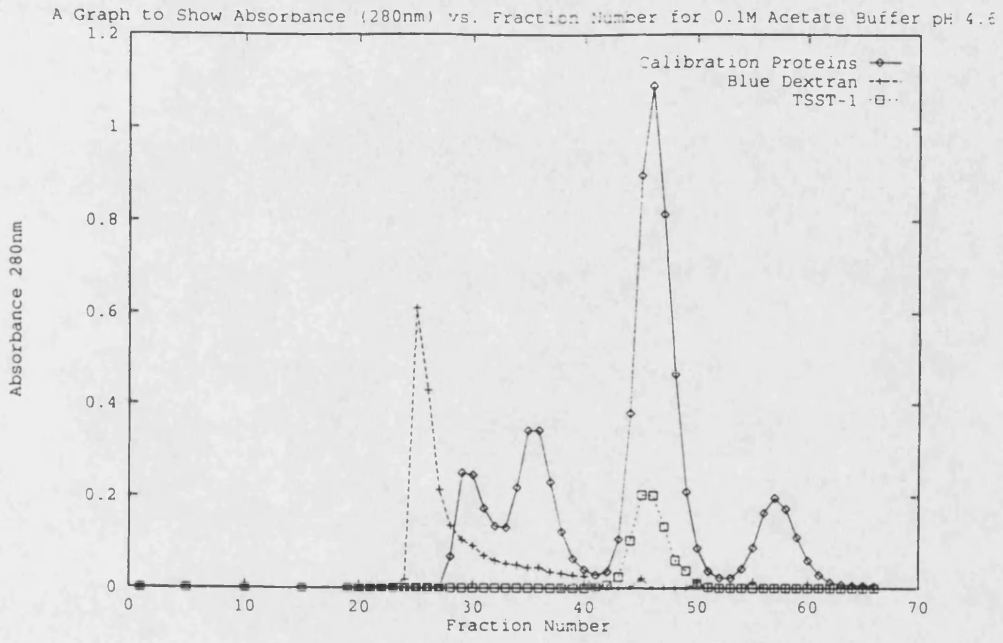

Figure 3.10 Gel filtration using 0.1M acetate buffer, *p*H 4.6, showing the separation of standard proteins superimposed with TSST-1 using P-100 gel (Bio-Rad) and column (1.5 × 75 cm) under gravity at a flow rate of 5 ml/h. The calibration proteins are (kDa): ribonuclease A, 13.7; chymotrypsinogen A, 25.0; ovalbumin, 43.0; and bovine serum albumin, 67.0.

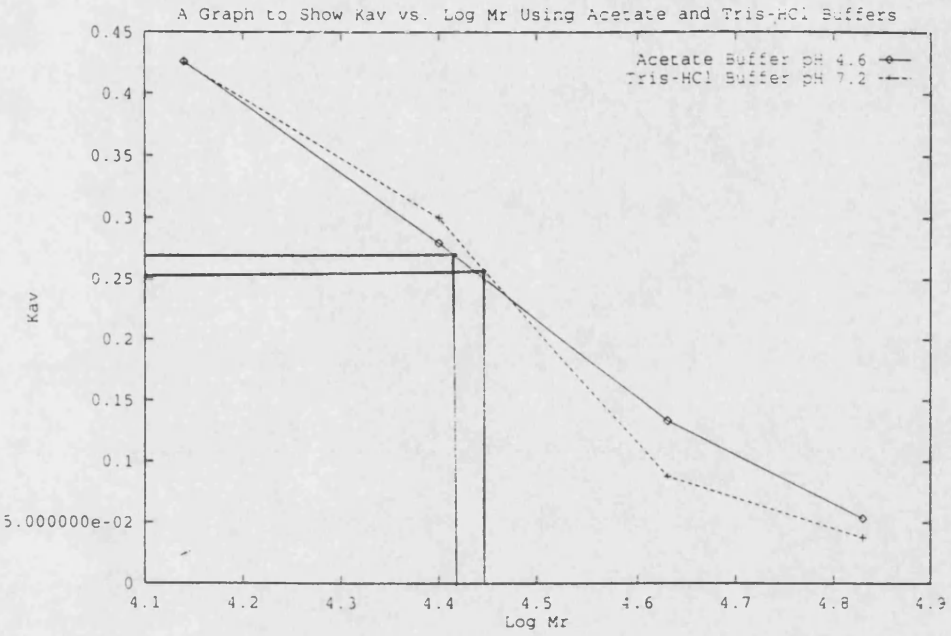

Figure 3.11 A graph to show K_{av} against log M_r for both the TRIS-HCl and acetate buffers in the determination of the multimeric state of TSST-1.

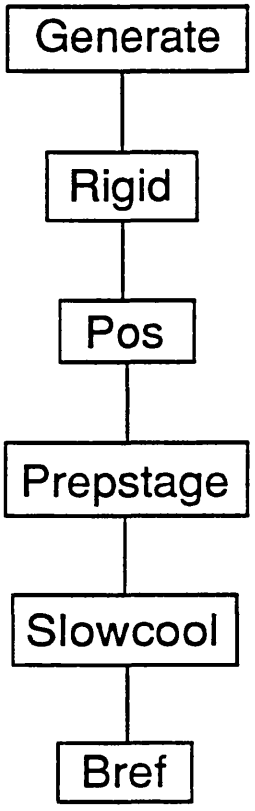

Figure 3.12 Flow diagram for wild type TSST-1 refinement through the XPLOR package of programs (Brünger, 1988).

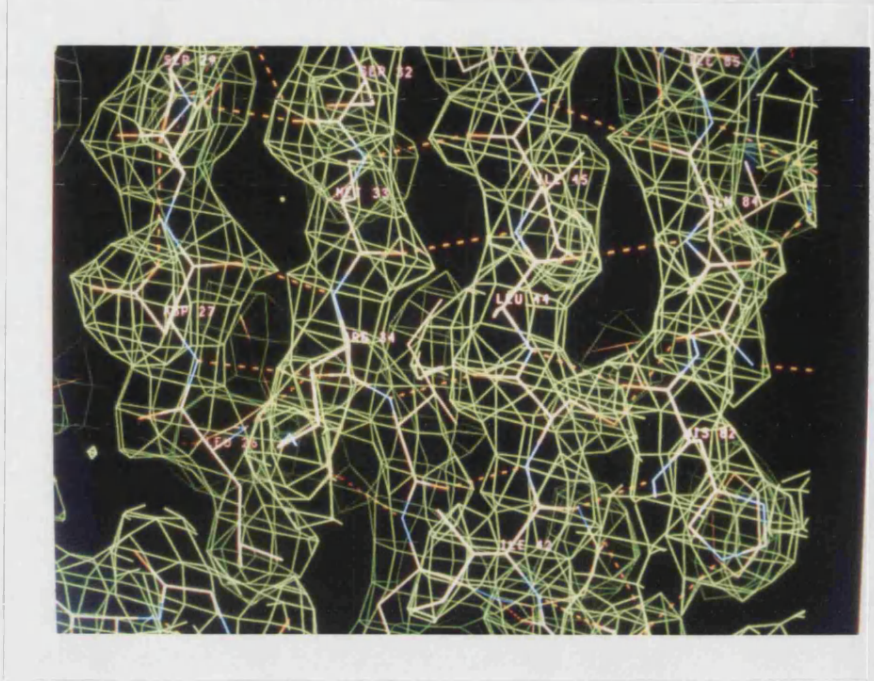

Figure 3.13 A $2F_o - F_c$ electron density map of a typical region in the fully refined structure of TSST-1. The map was contoured at 1.0σ and created in FRODO (Jones, 1985).

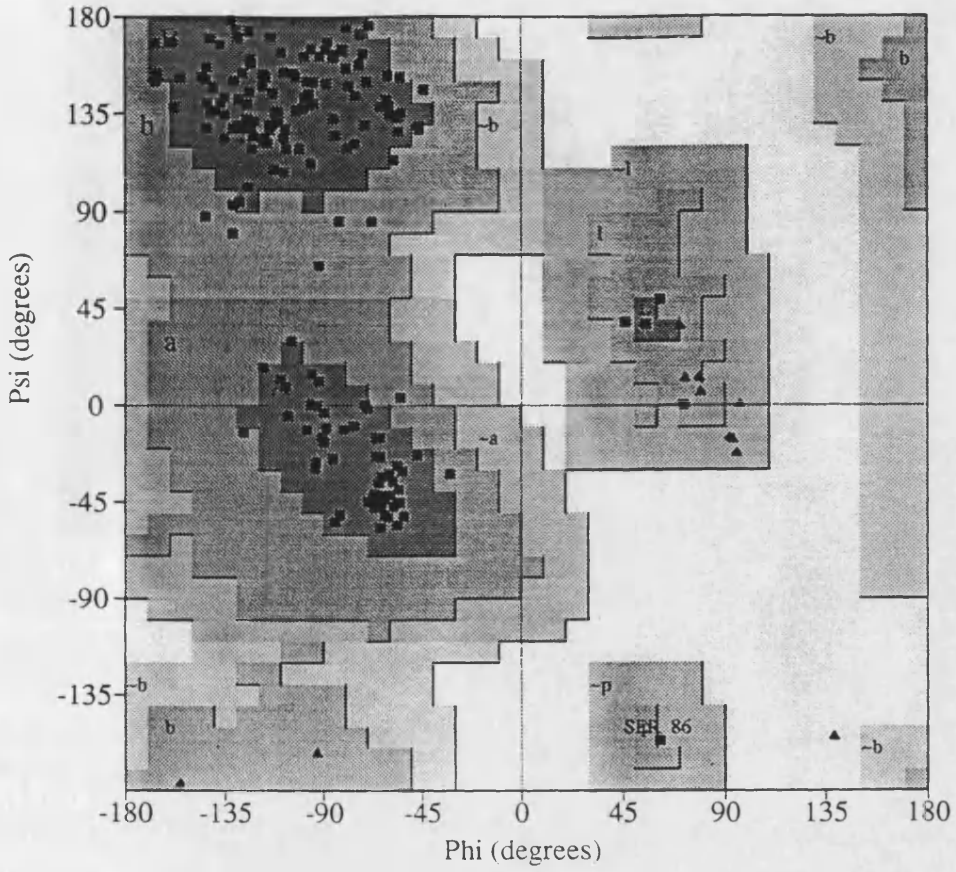

Figure 3.14 A Ramachandran plot of the fully refined TSST-1 structure using PROCHECK (Laskowski *et al.*, 1994). Glycine residues are indicated as triangles.

Figure 3.15 A ribbon diagram to illustrate the polypeptide fold of TSST-1 in its 'standard' orientation. Helices are coloured red (3_{10} helices are drawn more thinly than normal helices), the β strands are coloured green and loops yellow. The N and C termini are represented by blue and red balls respectively.

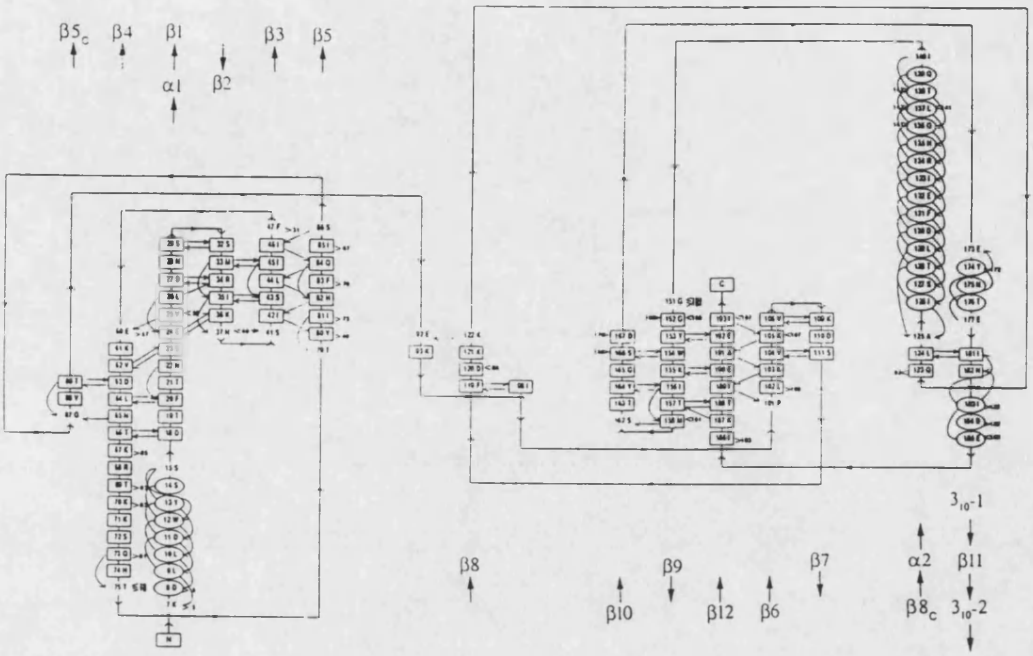

Figure 3.16 A secondary structure hydrogen-bonding diagram of toxic shock syndrome toxin-1. The secondary structure was defined using the program DSSP (Kabsch and Sander, 1993). All main chain hydrogen bonds are indicated as small arrows , from the donor to the acceptor. Residues involved in α helices are indicated as elipses and those contributing to the β sheets are boxed. The larger bold arrows indicate the direction of the β strands.

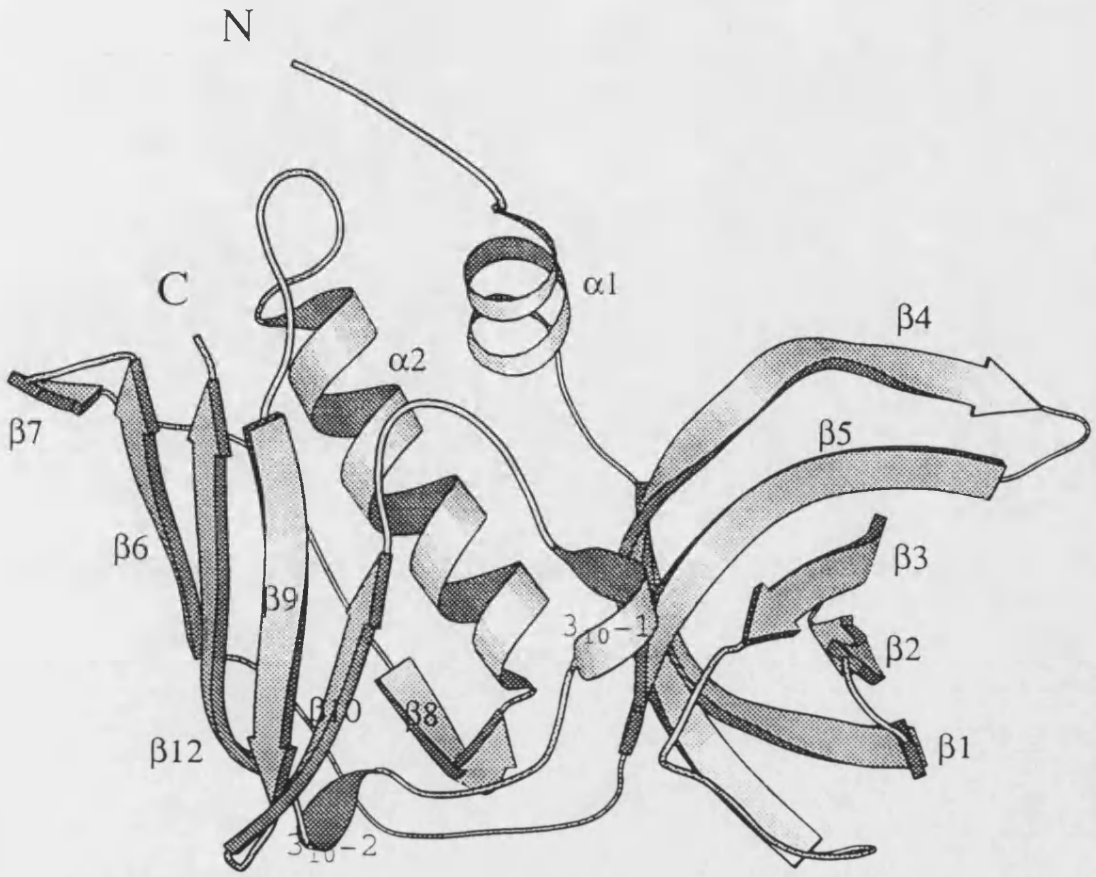

Figure 3.17 Identification of secondary elements of TSST-1 in its standard orientation. N and C termini are indicated. Figure produced with MOLSCRIPT (Kraulis, 1991).

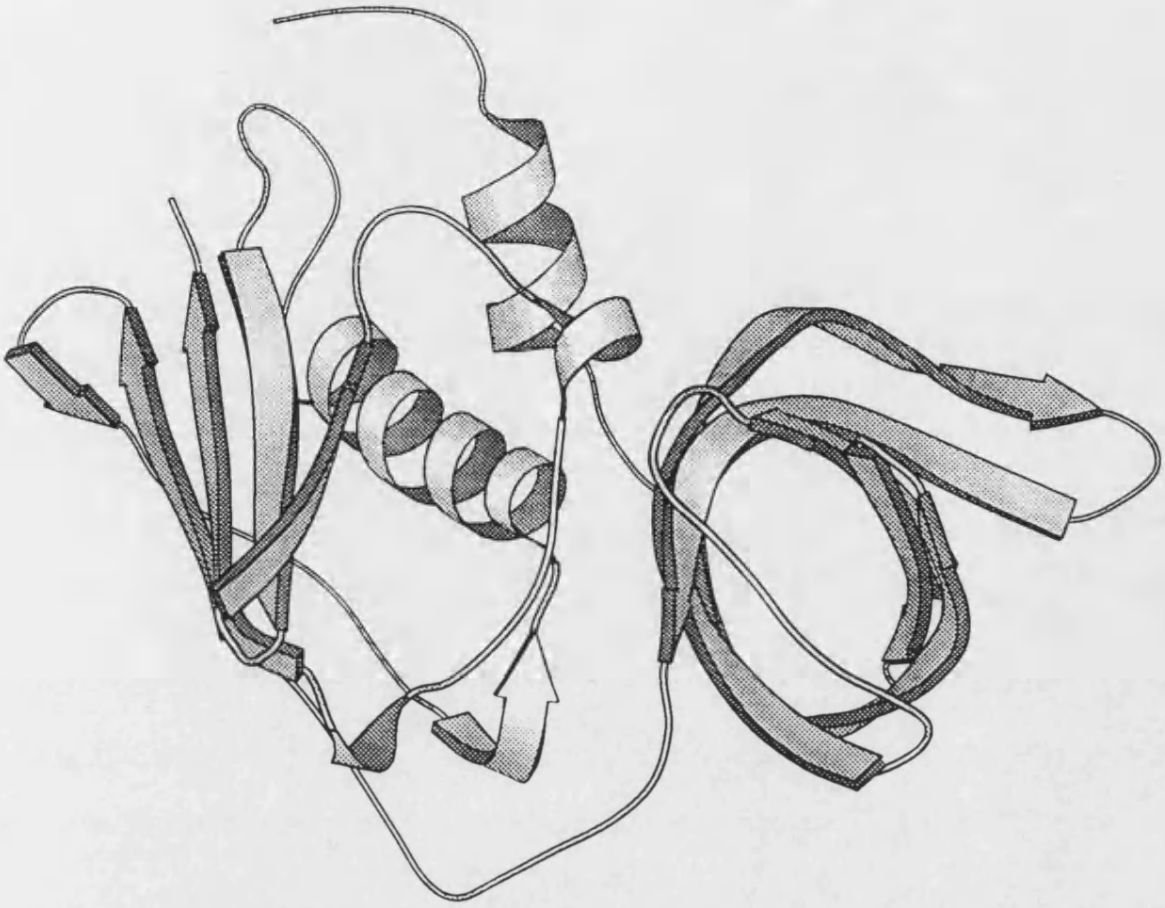

Figure 3.18 Diagram to illustrate the β barrel in domain 1 of TSST-1. This figure has been rotated approximately 100°, topside backward, about a horizontal axis running through the molecule in its standard orientation. Figure produced with MOLSCRIPT (Kraulis, 1991).

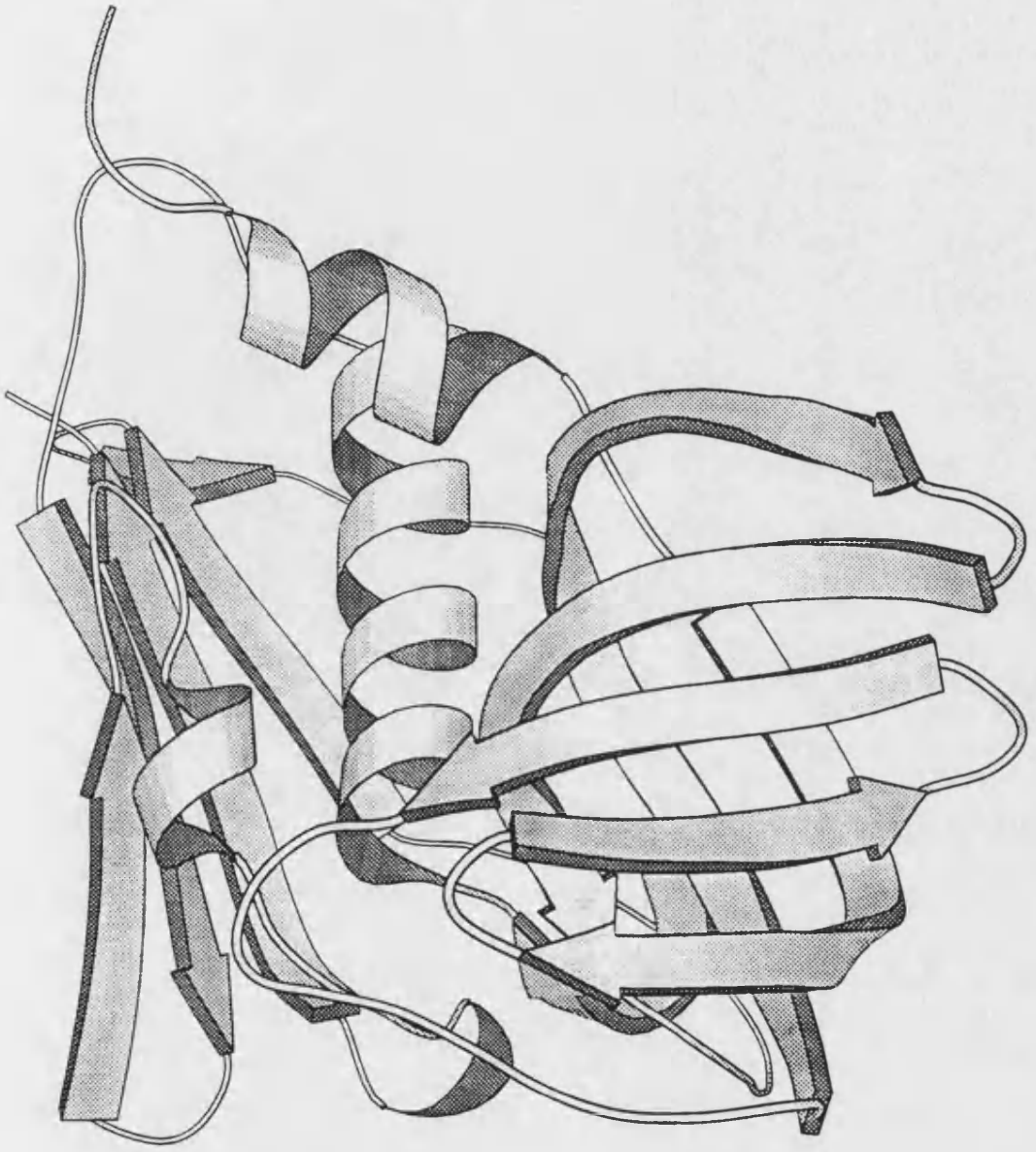

Figure 3.19 Diagram to illustrate the criss cross pattern of the β strands in domain 1 of TSST-1. This figure has been rotated approximately 35°, right side forward, about a vertical axis from its standard orientation. Figure produced with MOLSCRIPT (Kraulis, 1991).

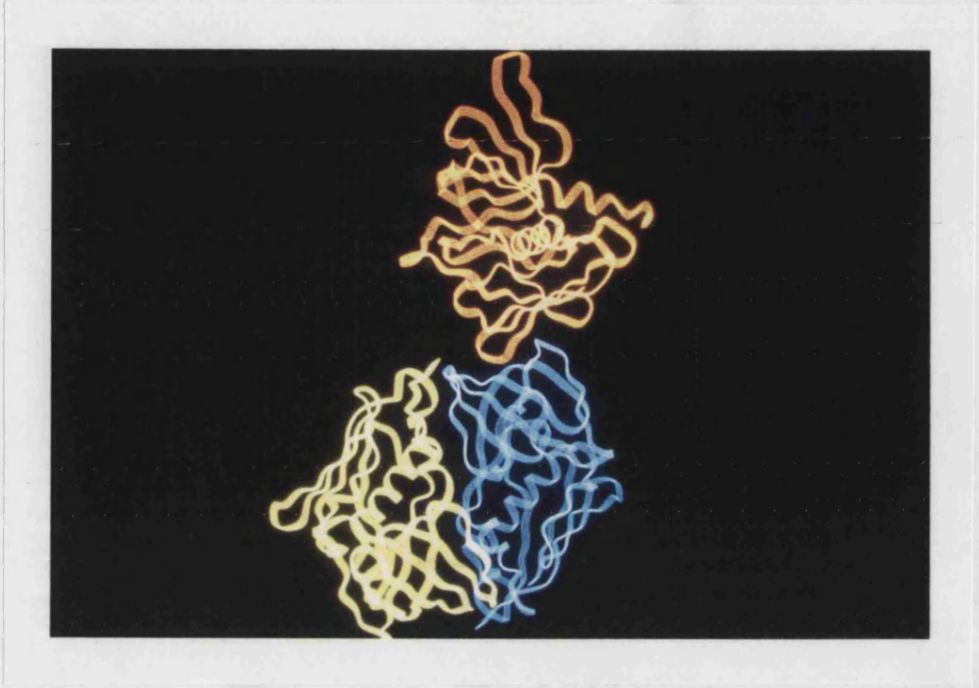

Figure 3.20 The packing of 3 TSST-1 molecues in the asymmetric unit. Molecule 1 is coloured blue, molecule 2 orange and molecule 3 in yellow. Figure produced with FRODO (Jones, 1985).

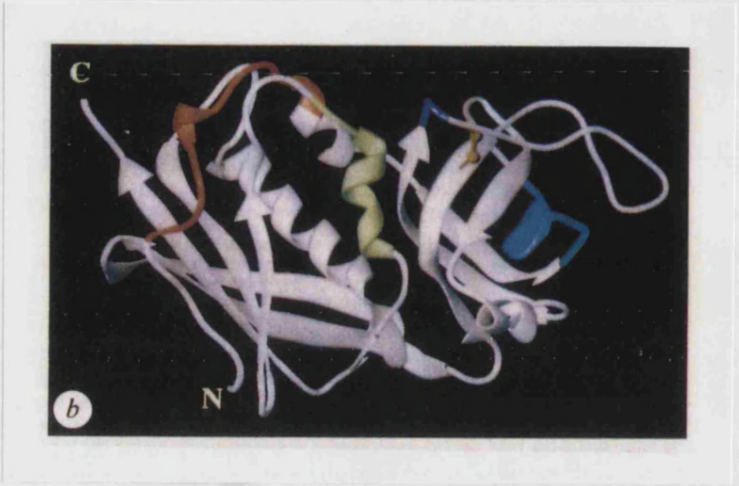

Figure 3.21 A ribbon diagram of SEB. Regions implicated in MHC II binding are identified. Region 1 (residues 9 to 23) in red, region 2 (residues 40 to 53) in blue and region 3 (residues 60 to 61) in white. Residues implicated in TcR binding: residues 90 to 92 in dark blue and residues 208 to 217 in light green. The disulphide loop is yellow. Figure produced from Swaminathan *et al.*, (1992).

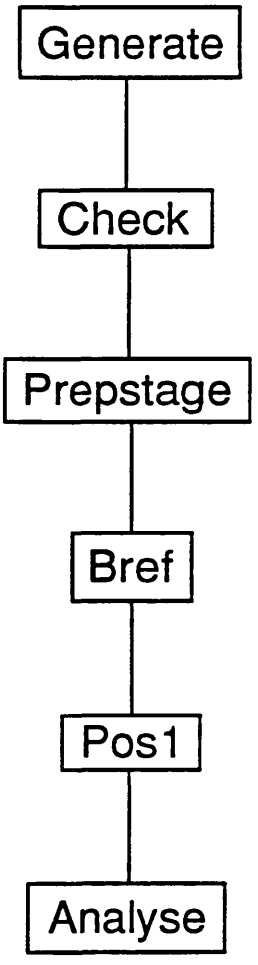

Figure 3.22 Flow diagram for refinement of mutant TSST-1 K105E using XPLOR package of programs (Brünger, 1988).

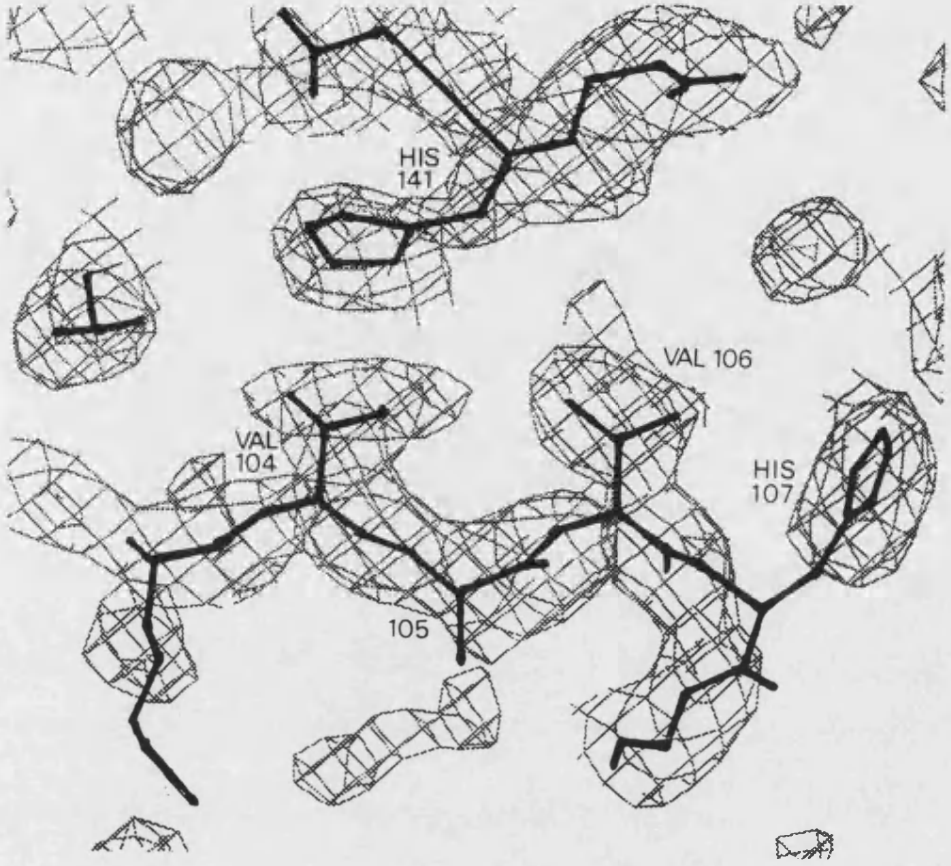

Figure 3.23 A $2F_o - F_c$ electron density map of the mutated residue 105 in the structure of mutant TSST-1 K105E after one round of refinement. During refinement residue 105 was modelled as alanine. The map was contoured at 1.0σ and created in FRODO (Jones, 1985).

Chapter 4

Purification of SEA and Crystallization of Staphylococcal Enterotoxins A, B and C2

4.1 Production and Purification of SEA, SEB and SEC2

Staphylococcal enterotoxins B and C2, purified by affinity chromatography on Red A (Brehm *et al.*, 1990), were a gift from Mrs. R.D.Brehm, Developmental Production Department, Centre for Applied Microbiological Research, Salisbury.

4.2 Strains Used for SEA Production

Staphylococcus aureus strain FRI-722 (kindly supplied by Professor M.S. Bergdoll, Food Research Institute, Department of Food Science and Industry, University of Wisconsin, Madison, USA) was used for the production of enterotoxin SEA. Stock cultures were stored frozen, in liquid nitrogen (BOC), in growth medium (see below) including 50% v/v glycerol. When required the stock cultures were thawed and subcultured through growth medium prior to being maintained on nutrient agar (Oxoid Ltd.) slopes at 4°C for up to 3 days.

4.3 Growth Medium

Staphylococcus aureus strain FRI-722 (SEA) was grown in culture medium, previously sterilized by autoclaving at 121°C for 20 minutes. The medium consisted of 20.0 g/l N-Z amine A (Sheffield Products) and 20.0 g/l proteose peptone no.3 (Difco Laboratories) and was adjusted to a *p*H

of 6.8. After the medium had cooled to room temperature, 0.5% (w/v) thiamine and 1% (w/v) niacin growth factors, previously sterilized by filtration using a 0.2 μm pore filter (Millex; Millipore Ltd.) were added to the growth medium. In addition, 50% (w/v) glucose, sterilized by autoclaving (115°C/15 mins), was added to give a final concentration of 2 g/l in the growth medium.

4.4 Production of SEA

To provide an initial inoculum, 1ml of sterile phosphate buffered saline (Appendix A) was washed over an agar slope culture of *S. aureus* FRI-722 and 0.7 ml of the suspension used to seed 50 ml of growth medium in a 300 ml Ehrlenmeyer flask. The culture was then shaken at 300 rpm in an orbital shaker (INR-200; Gallenkamp), for 16 h to 20 h at 37°C. After growth of this culture, 10 ml was used to inoculate 500 ml of the same medium in a 2 l flask, and shaken (300 rpm) overnight at 37°C. Finally this seed inoculum (500 ml) was used to inoculate a 15 l Biostat E bioreactor (B.Braun Medical Ltd.) which held 15 l of growth medium sterilized *in situ* (121°C/20 min), containing 0.03% (final concentration) sterile (121°C/15 min) polypropylene glycol 2000 antifoam (KW; Revai Chemicals Ltd.). The air into the fermenter vessel was filtered (Emflon; Pall), and the dissolved oxygen concentration set to 20% and controlled using both agitation and aeration (10 l/min). The stirrer speed was initially set to 280 rpm and the culture grown overnight at 37°C.

After growth the bacterial cells were removed from the culture medium using a Millipore Pellicon cassette system (Millipore UK Ltd.) containing 10 $\times$ 0.45 μm membranes (HVLP OMP50) and the culture fil-

trate concentrated down to 1 l using the same Pellicon cross-flow filtration system fitted with two 10,000 molecular weight cut-off membranes (PLGC OMP05). To prevent growth and degradation of toxin occurring during the remaining downstream processing, 0.5M EDTA (BDH) was added to the concentrated culture medium to give a final concentration of 0.2 mM. The concentrated culture supernatant fluid was dialysed overnight at 4°C in 20 mM potassium phosphate, buffer *p*H 6.8.

4.5 Purification of SEA

4.5.1 Dye Ligand Affinity Chromatography

Purification of SEA by dye-ligand chromatography was essentially the same as that used for the purification of TSST-1 as described in Section 3.5.1.

4.5.2 Fast Protein Liquid Chromatography

Those Red A column fractions containing SEA were pooled and purified further using fast protein liquid chromatography (FPLC; Pharmacia Ltd.). Also, samples of SEB and SEC2, previously purified by Red A chromatography and stored frozen in 60 mM potassium phosphate buffer (SEB) or 35 mM potassium phosphate buffer (SEC2) both at *p*H 6.5, were thawed and placed in dialysis tubing (Scientific Instruments Ltd.). All toxin samples were individually dialysed overnight in 50 mM sodium acetate buffer *p*H 5.0 at 4°C and loaded in separate batches of approximately 20 ml onto an FPLC HiLoad S Sepharose high performance 16/10 column (Pharmacia) which had previously been equilibrated with dialysis buffer. The column was eluted at room temperature using a 150 ml linear gradient

(0-250 mM) of NaCl at a flow rate of 2 ml/min. Fractions were collected using a Pharmacia fraction collector (SuperFrac 2211) and those giving an A_{280} >0.2 units were collected and tested for the presence of toxin using single radial immunodiffusion (Section 3.6). After elution both the Red A and the S Sepharose columns were regenerated according to the manufacturers instructions. Finally the purified toxins were all dialysed against MilliQ or ElgaStat water. The concentration of the purified toxin samples was determined using the relevant extinction coefficient at 280 nm (Table 4.1). The equivalent of 1 mg amounts of the freshly purified toxin solution were added to small vials and lyophilized before storage at 4°C until required.

4.6 Toxin Assay

Enterotoxin concentrations were estimated using single radial immunodiffusion (Meyer and Palmieri, 1980) as described in Section 3.6.

4.7 Criteria of Purity

The purity of the toxin samples was determined using sodium dodecyl sulphate -polyacrylamide gel electrophoresis (SDS-PAGE) on precast gradient gels (Mini-PROTEAN II, BioRad) at 150 V for 1.5 h. The gel was stained for 1 h on ethanol/acetic acid (3:1, v/v) containing 0.1% coomassie blue R250 (Pharmacia) and destained overnight by diffusion. Isoelectric focussing of the purified toxins was also carried out as described in Section 3.7

4.8 Crystallization

The toxin stock solution was prepared by resuspending the lyophilized toxin preparations in MilliQ or ElgaStat water. Unless otherwise stated all chemicals used were of analytical grade from Sigma. All of the stock solutions contained a final concentration of 0.02% sodium azide as a bactericide. The initial crystallization trials for SEA, SEB and SEC2 were performed at room temperature by the hanging drop method (McPherson, 1982) using the sparse matrix sampling protocol of Jancarik and Kim (1991). In the crystallization of SEA, a new sparse matrix protocol called Crystal Screen II (Hampton Research, USA.) was also used. The individual drops (6μl) consisted of equal volumes of reservoir stock solution and toxin. The drops were mixed on either plastic (Thermanox) or glass coverslips (Chance Propper Ltd.), which were then inverted over wells in a tissue culture plate (Linbro, Flow Labs) and sealed with high vacuum silicone grease (Dow Corning). The crystals were mounted in quartz capillaries as described in Section 3.9.1.

Results and Discussion

SEA, SEB and SEC2 were all purified using a combination of Red A (Figure 4.1) and FPLC (Figures 4.2, 4.3 and 4.4 respectively). The concentration of SEA in the culture media after large scale culture was estimated to be 0.028 mg/ml and after purification the overall yield for SEA (Table 4.2) was 34% from the fermenter culture. This yield was less than that previously reported to be 49% by Brehm *et al.* (1990). The difference in these yields can be explained by loss resulting from the final FPLC clean up step Despite these losses, the simplicity of the purification protocol enables it to be used to prepare large amounts of toxin for crystallography. SDS-PAGE gels of SEA, SEB and SEC2, purified to the FPLC stage were all shown to exist as a single band, with a purity >99% (Figure 4.5). However, these same samples on an IEF gel indicated that these toxins all existed in multiple isoelectric forms (Figure 4.6).

4.9 Crystallizations

4.9.1 SEA

Crystals of SEA were not obtained despite the extensive use of both the Magic 50 and Crystal Screen II (Hampton Research) protocols over a range of different temperatures (13°C to 25°C) and protein concentrations (2 mg/ml to 20 mg/ml).

4.9.2 SEB

SEB crystallized as 'rosette-like' plates when a 20 mg/ml protein stock solution was mixed with an equivalent volume of 0.1M TRIS buffer

*p*H8.5 containing 0.2M lithium sulphate and 28-32% polyethylene glycol 3350.

4.9.3 SEC2

Small crystals of SEC2 appeared after four weeks when a 2 mg/ml protein stock solution was mixed with an equivalent volume of 0.1M cacodylate buffer *p*H6.5 containing 0.15M ammonium sulphate and 26% polyethylene glycol 3350. These crystals reached a maximum size of 0.3 mm × 0.4 mm × 0.8 mm (Passalacqua *et al.*, 1993) after eight weeks (Figure 4.7).

4.10 Data Collection and Processing of SEC2

For diffraction analysis, crystals of SEB and SEC2 were carefully mounted as described in Section 3.9.1. Initial data collection for SEC2 were performed at ambient temperature on a Siemens area detector mounted on a Siemens rotating anode X-ray source using CuK_α radiation and operating between 44-50 kV and 76-80 mA with a wavelength of 1.518Å. Crystals of SEC2 were found to be well ordered and suitable for diffraction studies. However, crystals of SEB were highly disordered and even after extensive attempts to produce ordered crystals by varying crystallization conditions, they diffracted to only 5Å and were not considered for further analysis. All the data from these studies were processed on a VAX workstation using the XDS package of programs (Kabsch, 1988).

Two SEC2 crystals were used to collect this in-house data and gave an R_{merge} of 7.5% with a total completeness of 86.6%. The 2θ angle was 25° and the time per frame of 420 s. Table 4.3 illustrates the in-house data collection for SEC2. Initial results from XDS (Kabsch, 1988) indi-

cated that the SEC2 crystals belonged to the tetragonal space group $P_1 22$ with unit cell parameters of a=b=43.2Å and c=290.9Å (Passalacqua *et al.*, 1993). Assuming a monomer per asymmetric unit, the specific volume of the protein was 2.46Å^3/Da and corresponds to 50% (v/v) solvent content (Matthews, 1968). Preliminary data processing of the SEC2 crystals showed that the large c edge was 290Å which suggested that data collection would best be performed at the SRS. The crystal to detector distance on the in-house equipment was approaching its limit for data collection at 28.5 cm.

Native SEC2 data were also collected at the SRS Daresbury (PX 9.5) (λ=0.92Å) and processed to 3.4Å using the program DENZO (Otwinowski, 1993) which has the facility for interactive indexing of the diffraction spots. The crystal to detector distance was 325 mm, 60 s/°, 0.75°/ oscillation and 2 oscillations per image. Only one SEC2 crystal was required to collect this data (Table 4.4). The final R_{merge} was 5.5% but analysis of the number of reflections per shell indicated that 83.2% of the data was collected to 3.4Å. In the event it was decided to use the SRS Daresbury data with 3927 unique reflections for subsequent molecular replacement analysis.

4.12 Structure Solution of SEC2 Using Molecular Replacement

4.12.1 MERLOT Molecular Replacement

During this study the 3-D structure of TSST-1 was found to resemble that of SEB (Swaminathan *et al.*, 1992). The homology between SEB and SEC2 is reported to be 86% hence TSST-1 was initially regarded to be a good search model for the structure determination of SEC2 by molecular replacement.

Patterson functions of the complete TSST-1 structure were used in the initial rotation searches. These were based on the calculated structure factors for TSST-1 in an artificial unit cell of 80 × 80 × 80Å. The Crowther rotation search (Crowther, 1972) was carried out over the resolution range 8 to 4Å. Harmonic coefficients were calculated using a Patterson cut-off radius of 24Å to reduce the problem of intermolecular vectors. Figure 4.8 shows the programs used in MERLOT molecular replacement (Fitzgerald, 1988; Appendix B). Refinement of the β value given from ROTATION was carried out using ROTATION-FINE. The Lattman rotation function using the program LAT was used to refine this peak and from this the translation search was performed (Lattman and Love, 1970).

4.12.2 Structure Refinement of the MERLOT Solution

Initial R-factor refinement was carried out on the TSST-1 search model after it was first converted to a polyalanine structure. A polyalanine structure was used reduce any bias given by any incorrect side chains in TSST-1. It was then orientated and positioned in accordance with the MERLOT solution. The initial R-factor was 55% for data from 8 to 4Å. Refinement was performed using a combination of the molecular dynamics and simulated annealing from the XPLOR package of programs (Brünger, 1988), with manual rebuilding. An overview of the protocol is given in Figure 4.9. The final R-factor for this polyalanine model was 37%.

Using the polyalanine model a $(2 \mid F_o \mid - \mid F_c \mid)$ map was calculated which was assessed against the density using FRODO (Jones, 1985). The electron density map was initially very difficult to interpret with a significant amount of ambiguous density. This was due to the size differ-

ential between TSST-1, with 194 amino acids, and the much larger SEB molecule with 239 amino acids. Several attempts were made to manually alter certain main chain connectivity and to include any side chains whenever possible. From the secondary structure alignment of TSST-1 with SEB (Table 3.10), it was possible to add the entire SEC2 α2 helix in one attempt (Figure 1.1). When the α2 helix was added to the map more scattering matter was available for phase calculation. The polyalanine α1 and α3 helices were incorporated into the main chain ready for further refinement. From a visual inspection of the SEB structure, (Swaminathan *et al.* 1992), a polyalanine 'disulphide loop' was incorporated, in addition to the first 17 amino acid residues.

Three further rounds of refinement were performed on the model including addition of the other side chains to try and increase the scattering matter available to provide phases for the calculation of structure factor. It was obvious however by the end of round 4, that there were significant problems with the new TSST/SEC2 model (R-factor of 58.5%). These problems included significant numbers of bad side chain contacts which could not be relaxed during simulated annealing refinement. These side chain clashes were extremely difficult to remedy using manual rebuilding in an attempt to establish an improved agreement between the model and the available data. The final electron density map generated was poor.

A second attempt to determine a correct molecular replacement solution using the same sequence of programs resulted in the generation of a different potential rotation function peak. The top peak was used for the subsequent molecular replacement trial and the model was converted to its polyalanine equivalent and repositioned according to this potential solution

ready for refinement. After round 1, SEC2 side chains were added to the search model using FRODO. The major α helix was the first secondary structure element to be added which resulted in an improved R-factor of 39.6%. An inspection of the results from the second round of refinement after the symmetry operators were included however revealed several internal intramolecular clashes which prevented structure solution.

4.12.3 AMoRE Molecular Replacement

Due to the poor results of molecular replacement with the MERLOT package, a new package called AMoRE (Navaza, 1994) was used in a final attempt to solve the SEC2 structure using the refined TSST-1 structure as the search model. AMoRE is a new molecular replacement computer package which has been improved over previous methods by involving more powerful algorithms (Navaza, 1994). It is a much quicker automated package of programs which explores a great many potential solutions. AMoRE makes use of a correlation coefficient as its main selection criteria for peaks as well as an R-factor value. This improved algorithm is used to calculate the structure factors of the rotated and translated search model.

The TSST-1 monomer was used as the first search model and the data processed using the series of programs which make up this package, (Figure 4.10; Appendix B). The final correlation coefficient as defined in AMoRE (Navaza, 1994) was 24 with an associated R-factor of 54.2% (Table 4.5), suggesting that this first solution was not correct. When this procedure was repeated using a different resolution range, without changing the other values, the molecular replacement solution was still found to be incorrect. The difficulty associated with using this technique is that any correlation

coefficient value approaching 60% is in effect a random solution. Although the whole process was repeated after changing the sphere of radius there was still no sufficiently acceptable solution. Having used the whole TSST-1 molecule as a search model, molecular replacement was attempted using a polyalanine TSST-1 search model by converting the side-chains to their β carbons thus reducing any bias given by incorrect side chains.

The individual TSST-1 domains (1-96 and 97-194) were used in another attempt at molecular replacement. On the first run with domain 1 *ie.* residues 1 to 96, AMoRE failed. A comparison of the structures of TSST-1 with SEB showed that there were significant differences between the secondary structure elements at the very beginning of the two molecules. However, analysis of the molecular replacement output provided no genuine solution. Repeated attempts to vary the resolution range and the sphere of radius for domain 1 were unsuccessful. The same result was obtained during attempts to solve the SEC2 structure using the full TSST-1 sequence for domain 2, although there was no need in this case to remove any residues from the domain. Even conversion of the two individual domains to the polyalanine model and altering parameters such as the sphere of radius failed to provide any peaks; all the correlation coefficients were >50% (Table 4.5).

In a final attempt to solve the SEC2 structure the whole TSST-1 model was converted to a polyalanine structure replacing only those residues known to be in the secondary structure elements of SEC2 from the SEB data (Swaminathan *et al.*, 1992). The SEB data was extrapolated to the SEC2 sequence (both SEB and SEC2 have 239 amino acid residues; Table 1.1) and assuming that the secondary elements are identical, all

'known' residues of SEC2 were replaced (not inserted) into the TSST-1 search model. This resulted in 120 residues being replaced in the polyalanine TSST-1 model with SEC2 residues. Despite this the new search model in its entirety or even its individual domains failed once again to produce any noticeable peaks above background.

Having tried a number of different strategies to solve the structure of SEC2, none of them gave a solution. After all these efforts it was clear that it was rather difficult to obtain a clear solution for the SEC2 structure using molecular replacement and TSST-1 as the starting structure.

Table 4.1 *Extinction coefficients for staphylococcal enterotoxins A, B and C2.*

Toxin	Extinction Coefficient (A_{280})
SEA†	1.46
SEB‡	1.2
SEC2*	1.13

Data from †Schantz *et al.*, 1972; ‡Borja and Bergdoll, 1967; *Schantz *et al.*, 1965

Table 4.2 *Purification of SEA by 'Red A' and fast protein liquid chromatography (FPLC) from 15 litre fermenter culture.*

Stage	Total Toxin (mg)	% Yield (Stage)	% Yield (Overall)
Final Fermenter Culture	420	100	100
Initial Dialysis	327	78	78
Red A Chromatography	252	77	60
Second Dialysis	176	70	41
FPLC	143	81	34

Table 4.3. *SEC2 in-house data collection.*

Resol^{n} Range (Å)	No. of Poss. Reflex^{n}	Cumul^{ve} No. Poss. Reflex^{n}	No. of Reflex^{n}	Cumul^{ve} No. of Reflex^{n}	% Poss.
∞-15.00	71	71	41	41	57.7
15.00-10.00	149	220	129	170	86.5
10.00-8.00	185	405	172	342	92.9
8.00-6.00	478	883	447	789	93.5
6.00-5.00	588	1471	567	1356	96.4
5.00-4.50	508	1979	505	1861	85.5
4.50-4.00	759	2738	758	2619	99.8
4.00-3.50	1269	4007	1266	3885	99.7
3.50-3.40	334	4341	333	4218	99.7
3.40-3.30	386	4727	384	4602	99.4
3.30-3.20	437	5164	437	5039	100.0
3.20-3.10	461	5625	459	5498	99.5
3.10-3.00	585	6210	573	6071	97.9
3.00-2.90	609	6819	601	6672	98.6
2.90-2.80	735	7554	716	7388	97.4
2.80-2.70	809	8363	791	8179	97.7
2.70-2.60	980	9343	850	9029	86.7
2.60-2.50	1112	10455	26	9055	2.3
Total		10455		9055	86.6

Table 4.4. *SEC2 SRS Daresbury data collection.*

Resol^n Range (Å)	1	2	3	4	5
∞-15.00	71	71	44	44	61.9
15.00-10.00	149	220	124	168	83.2
10.00-8.00	185	405	163	331	88.1
8.00-6.00	478	883	414	745	86.6
6.00-5.00	588	1471	526	1271	89.4
5.00-4.50	508	1979	470	1741	92.5
4.50-4.00	759	2738	696	2437	91.6
4.00-3.90	201	2939	190	2627	94.5
3.90-3.80	230	3169	209	2836	90.8
3.80-3.70	252	3421	238	3074	94.4
3.70-3.60	253	3674	239	3313	94.4
3.60-3.50	333	4007	316	3629	94.8
3.50-3.40	334	4341	298	3927	89.2
Total		4341		3927	83.2

Column 1, number of possible reflections; 2, cumulative number of possible reflections; 3, number of reflections; 4, cumulative number of reflections; 4, percentage possible.

Table 4.5 *Summary for SEC2 AMoRE trials.*

Search Model Variation	Sphere of Radius (Å)	Resolution Shells	Corellation Coefficient	*R*-Factor
Whole TSST-1	28	15-4	24	54.2
	28	10-4	22	53.0
	24	15-4	25.9	55.2
Polyalanine TSST-1	24	10-4	34.2	54.3
Domain 1 TSST-1	24	10-4	19.7	54.6
Domain 2 TSST-1	24	10-4	28.4	56.1
	24	20-4	25.3	55.2
	24	15-4	26.1	55.8
Polyalanine Domain 1 TSST-1	24	10-4	26.1	53.8
	24	15-4	27.1	55.7
Polyalanine Domain 2 TSST-1	24	10-4	26.1	55.8
	24	15-4	25.9	56.4
TSST-1/SEC2 Hybrid	24	10-4	30.7	54.9

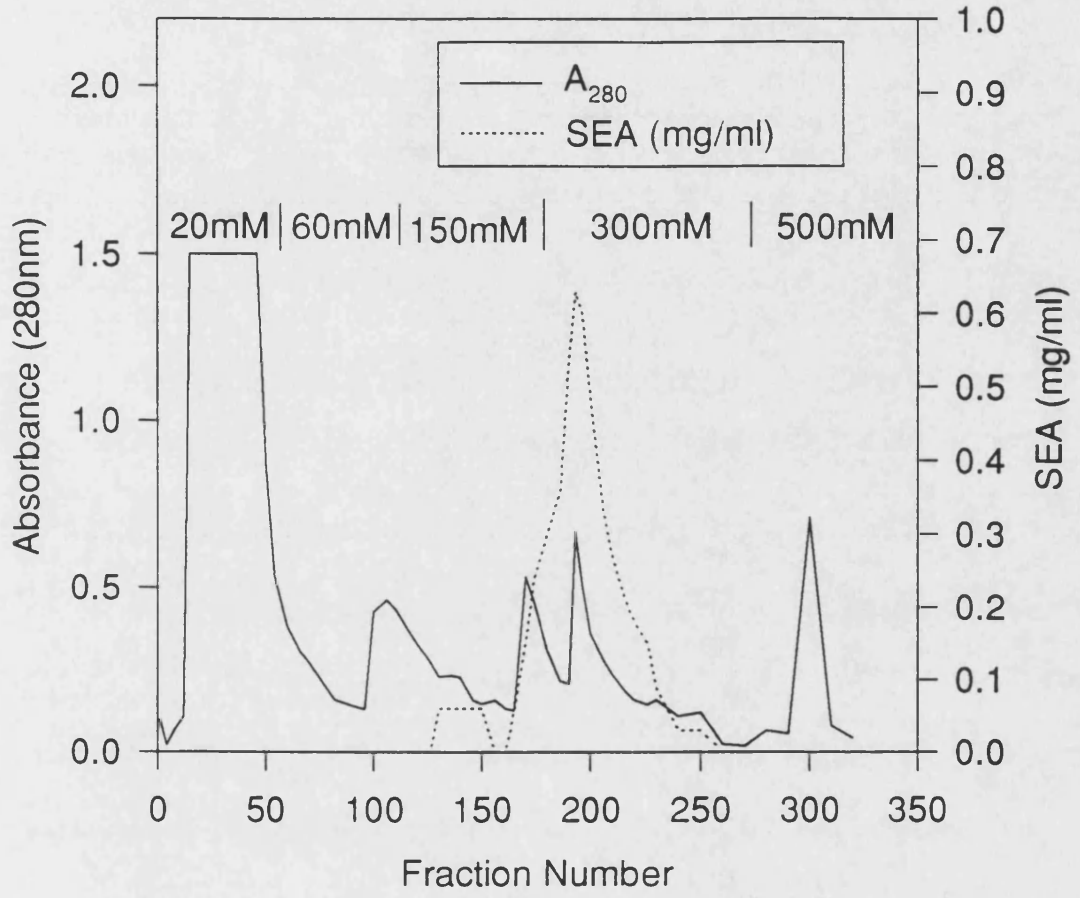

Figure 4.1 Dye ligand chromatography of SEA using Red A. The column (4.5 × 31 cm) was equilibrated in 20 mM phosphate buffer, *p*H 6.8, and eluted with a stepwise increase in molarity of phosphate buffer, *p*H 6.8. Fractions (10 ml) were collected at a flow rate of 40 ml/h (during binding) and 200 ml/h (during elution) and their absorbances measured at 280 nm.

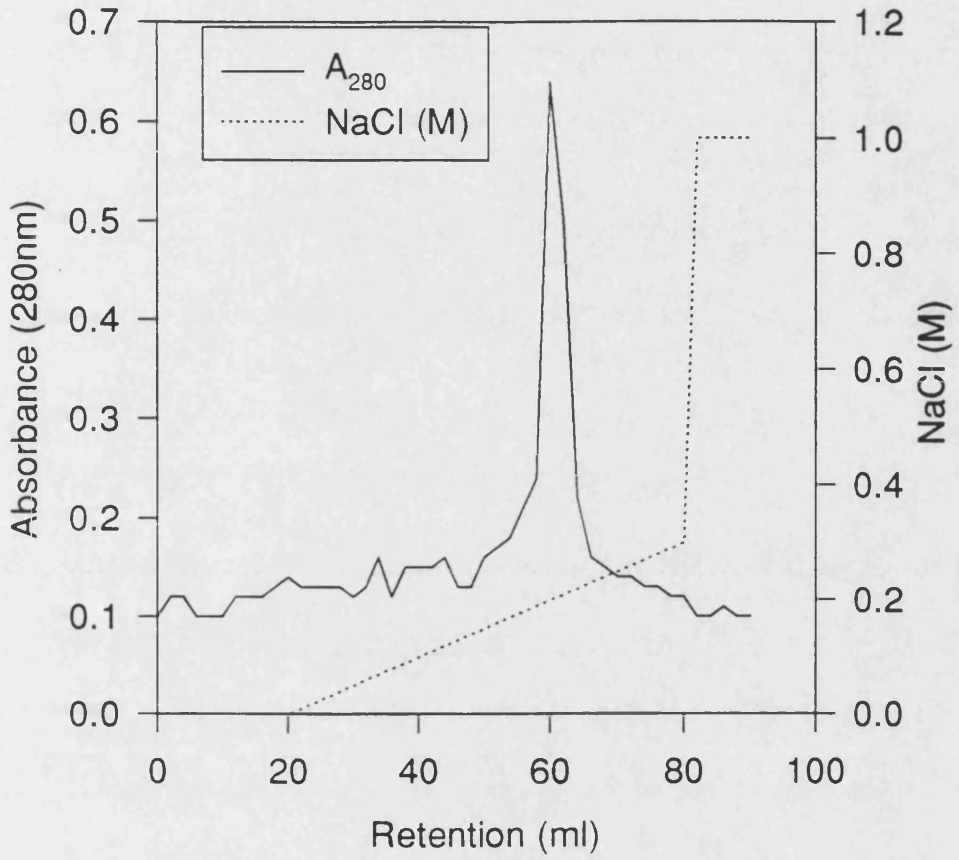

Figure 4.2 Final purification of SEA by FPLC, after previous chromatography using Red A. The 20 ml HiLoad S Sepharose high performance 16/10 column (Pharmacia) was equilibriated with 50 mM sodium acetate buffer *p*H 5.0. Toxin was eluted using 150 mM linear gradient of increasing NaCl concentration (up to 250 mM) at a flow rate of 2 ml/min.

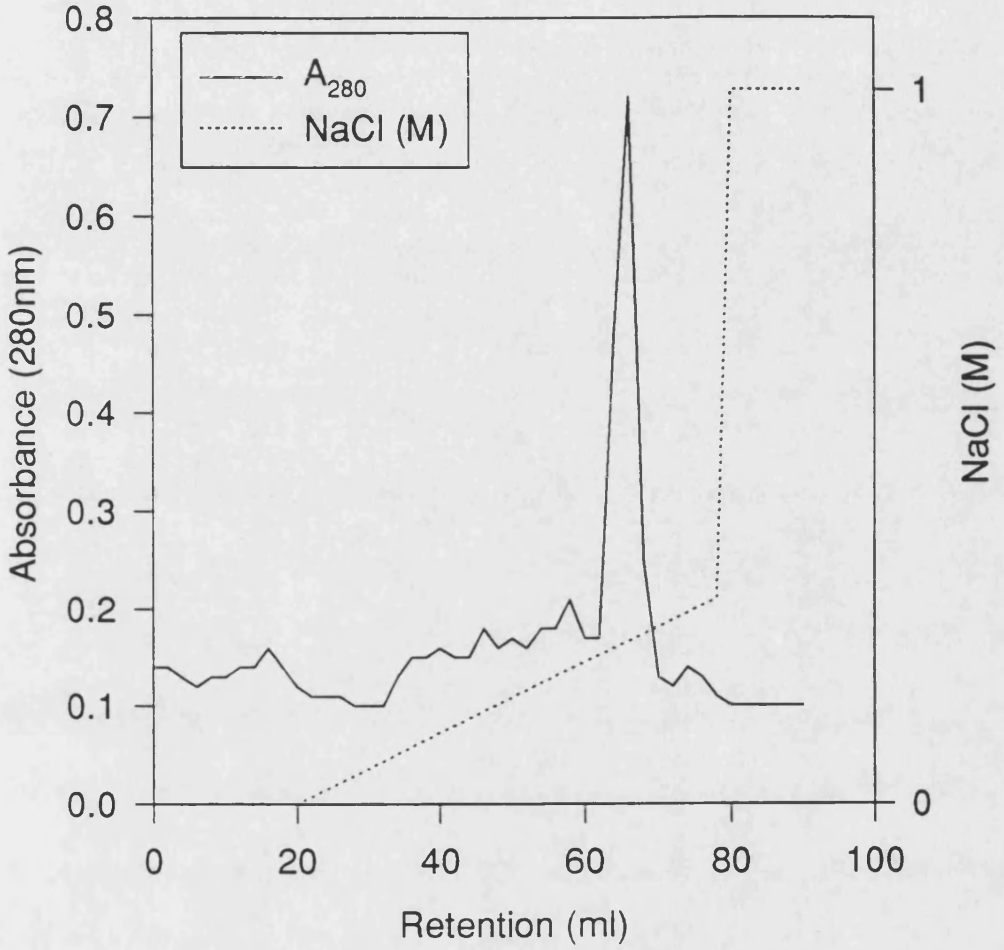

Figure 4.3 Final purification of SEB by FPLC, after previous chromatography using Red A. The 20 ml HiLoad S Sepharose high performance 16/10 column (Pharmacia) was equilibriated with 50 mM sodium acetate buffer *p*H 5.0. Toxin was eluted using 150 mM linear gradient of increasing NaCl concentration (up to 250 mM) at a flow rate of 2 ml/min.

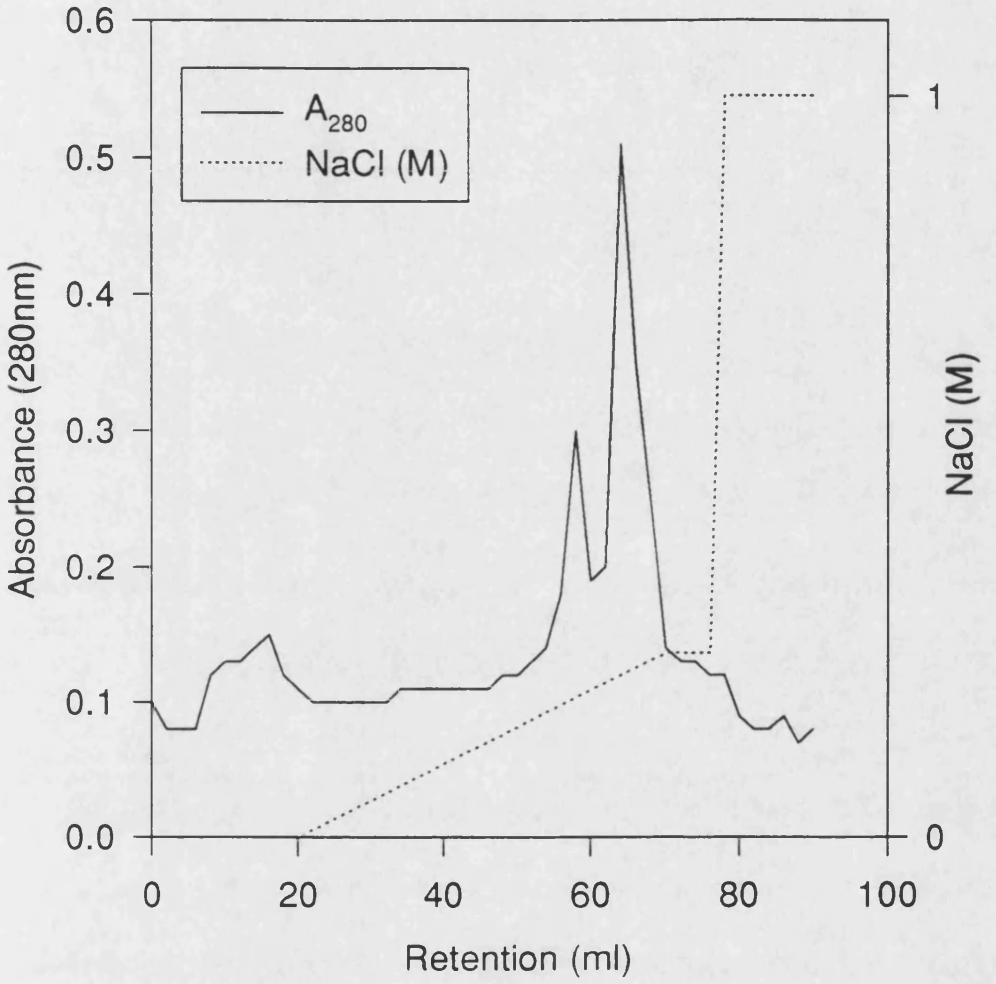

Figure 4.4 Final purification of SEC2 by FPLC, after previous chromatography using Red A. The 20 ml HiLoad S Sepharose high performance 16/10 column (Pharmacia) was equilibriated with 50 mM sodium acetate buffer *p*H 5.0. Toxin was eluted using 150 mM linear gradient of increasing NaCl concentration (up to 250 mM) at a flow rate of 2 ml/min.

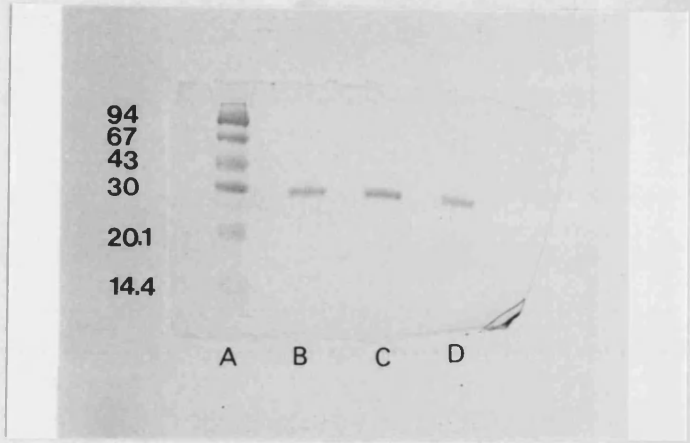

Figure 4.5 An SDS-polyacrylamide gradient 10 to 20% precast gel (Mini-PROTEAN II, BioRad) showing analysis of the final purity of SEA, SEB and SEC2 after FPLC purification. Lane A, SEA. Lane B, SEB. Lane C, SEC2. Lane D, molecular mass markers (kDa): phosphorylase *b*, 94; albumin, 67; ovalbumin, 43; carbonic anhydrase, 30; trypsin inhibitor, 20.1 and α-lactalbumin, 14.4. Lanes A to C were loaded with 10 μl of sample containing 0.5 to 1.0 mg protein per ml.

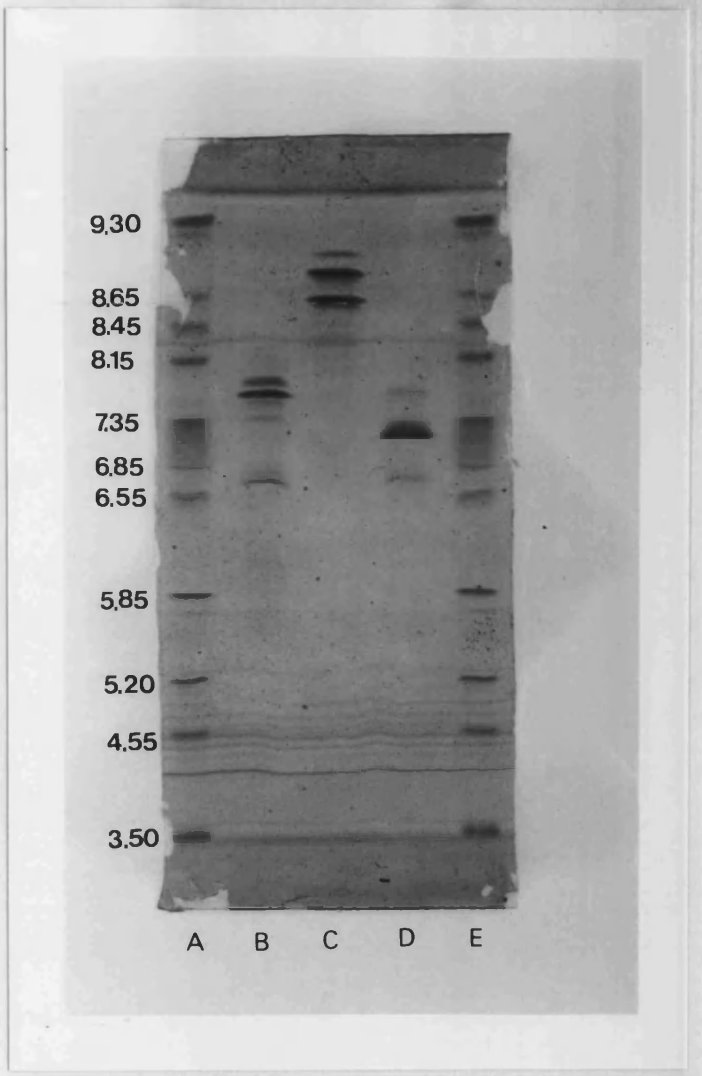

Figure 4.6 Isoelectric focusing of SEA, SEB and SEC2 after final purification by FPLC. Lanes A and E, *p*I markers: trypsinogen, 9.3; lentil lectin (basic band), 8.15; horse myoglobin (basic band), 7.35; human carbonic anhydrase B, 6.55; bovine carbonic anhydrase B, 5.85 and β-lactalbumin, 5.2. Lane B, SEA. Lane C, SEB. Lane D, SEC2.

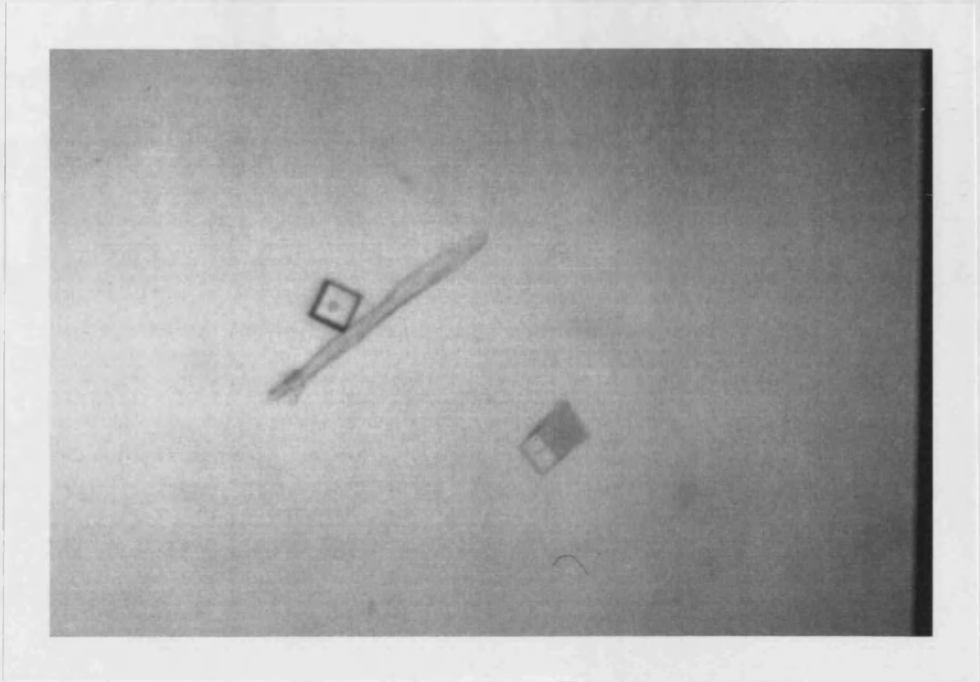

Figure 4.7 Two crystals of SEC2. The crystal dimensions are 0.3 mm × 0.4 mm × 0.8 mm.

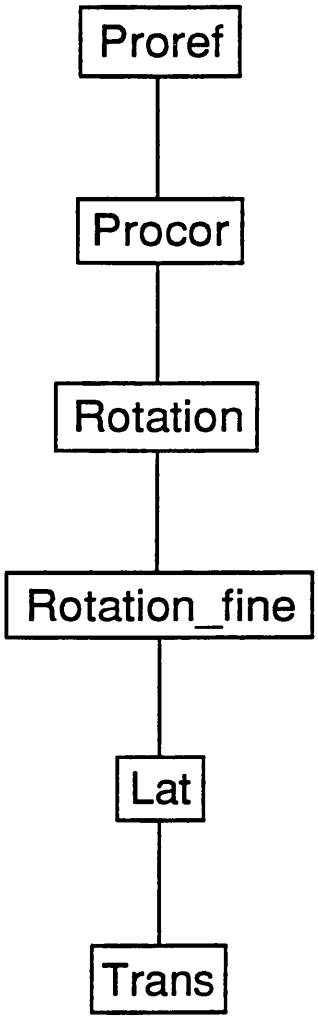

Figure 4.8 Flow diagram for SEC2 molecular replacement through the MERLOT package of programs (Fitzgerald, 1988).

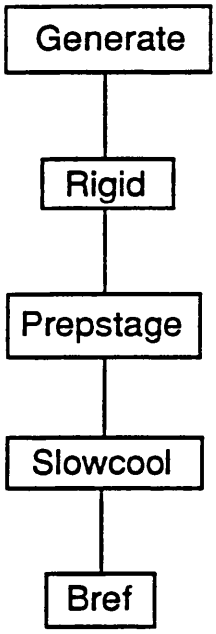

Figure 4.9 Flow diagram to show SEC2 refinement through XPLOR package of programs (Brünger, 1988).

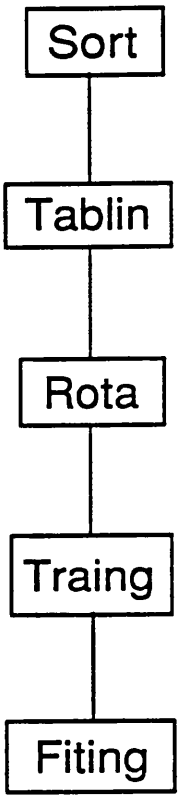

Figure 4.10 Flow diagram to show SEC2 molecular replacement through the AMoRE package of programs (Navaza, 1994).

Chapter 5

Structure-Function Studies of the Staphylococcal Enterotoxins and Toxic Shock Syndrome Toxin-1 in Relation to their Biological Activity

5.1 Emesis

One feature common to all of the SEs is the centrally located disulphide loop (Swaminathan *et al.*, 1992; Figure 3.21). Although there is some evidence to suggest that this region may be responsible for emesis, there does not appear to be a complete demarcation of this function and the T cell stimulatory effects of the SE. Thus, it is still unclear whether emesis is a result of T cell stimulation or whether these two biological phenomena are unrelated. Site-directed mutagenesis of residue Leu 48 in SEA and Phe 44 in SEB have been shown to reduce T cell proliferation but the toxins maintained their emetic properties when fed to monkeys (Harris *et al.*, 1993). This study suggested that these two activities are located at two different sites on the toxin. Mutants residues that form the disulphide bridge in SEA, Cys 106 to Ala (Grossman *et al.*, 1991), and SEC1 Cys 110 to Ala (Hovde *et al.*, 1994) both prevented emetic activity. However, when another SEC1 mutant, Cys 110 to Ser was prepared there was no appreciable loss in emetic capacity (Hovde *et al.*, 1994). It was noted that there was a 100-fold reduction in the ability of SEA mutants Cys 96 and Cys 106 to induce T cell proliferation while still binding to MHC II molecules (Grossman *et al.*, 1992). Unlike the SEs, TSST-1 does not possess any disulphide bridges and does not appear to promote emesis in individuals suffering from TSS (Spero and Morlock, 1978).

5.2 Staphylococcal Enterotoxin Binding Sites for MHC II

A number of studies have been performed to demonstrate the sites on the SEs responsible for binding to MHC II. As SED and SEE are produced only in small amounts and there is a difficulty in obtaining sufficient pure protein to carry out meaningful studies, the majority of this work has been performed on SEA and SEB. These include the use of enzymatically and chemically prepared peptide fragments and site directed mutagenesis of the toxin molecules. Deletion mutants of SEA have indicated problems associated with protein instability. For example, Hufnagle *et al,* (1991) demonstrated that removing the last C terminal amino acid of SEA did not appear to affect the biological activity of the toxin. However, deletions of three more SEA residues from the C terminal did show a loss of biological function, *ie.* it abrogated T cell activity, associated with molecule instability *ie.* a change in conformation. Fraser *et al.* (1992) demonstrated the need for Zn^{2+} ions to be present for SEA, SED and SEE for efficient binding to MHC II. This Zn^{2+} ion appears to be necessary to stabilize the SE/MHC II complex.

N terminal peptide fragments alone from SEB (residues 1 to 138) were shown to possess mitogenic activity (Buelow *et al.*, 1992). In a different experiment, the mitogenic activity of whole SEB was inhibited when a number of short SEB peptide fragments were introduced separately to holotoxin SEB which prevented binding to MHC II (Komisar *et al.*, 1994). One of these peptide fragments (90 to 114), which covered the entire disulphide loop, was shown to be the most effective in preventing MHC II binding. Swaminathan *et al.* (1992) mention two regions thought to be involved in MHC II binding. They are region 1 which include residues 9 to 23 and

region 2 which include residues 40 to 53. In the event, the crystal structure of SEB complexed to DR1 confirmed the role played by the domain 1 β barrel and β5 helix of domain 2 of SEB in binding to MHC II (Jardetzky *et al.*, 1994). The loop between β strands 1 and 2 and a portion of strand 3 were found to be the most important binding regions of SEB for MHC II. Bohach *et al.* (1989) demonstrated in SEC1 that removal of the N terminal 59 amino acid residues by trypsin, did not affect the superantigenic properties of the toxin. This C terminal fragment of SEC1 was still pyrogenic, mitogenic and in the rabbit model caused enhanced suceptability to lethal endotoxin shock. Using random mutational studies, Kappler *et al.* (1992) identified SEB residues 13 to 17 and 41 to 55 as important in MHC II binding.

Hoffmann *et al.* (1994) characterised a number of synthetic peptide fragments of SEC1 to determine those residues of the primary sequence which may be involved in MHC II binding. They deduced that three peptides 74 to 86, 148 to 162 and 156 to 171 were involved not only in T cell proliferation but also MHC II binding. From their SEC3 structure (Hoffmann *et al.*, 1994) they noted that these peptides are located around a structure called the α5 groove. They suggest that this groove could easily provide a potential binding site for the α helix of the MHC II molecule.

5.3 Toxic Shock Syndrome Toxin-1 Binding Sites for MHC II

Early experiments on the localization of biological function, made use of internal cyanogen bromide-generated fragments of TSST-1 and neutralizing monoclonal antibodies prepared against these fragments (Blomster-Hautamaa *et al.*, 1986c). These workers managed to produce three IgG

monoclonal antibodies which blocked both the TSST-1 induced mitogenic activity and the immunoglobulin suppression in mice cells. One of these fragments (14kDa), consisted of residues 33-158, which spans both domains of TSST-1.

Chemical modification of histidine and tyrosine (Kokan-Moore and Bergdoll, 1989a) or methionine (Kokan-Moore and Bergdoll, 1989b) residues showed that modification of four of the five histidine residues, with diethylpyrocarbonate, reduced its mitogenic effect by 50%. Although a monoclonal antibody was not able to react with the modified toxin, binding to polyclonal antibody preparations was not affected. The lack of reactivity with the monoclonal antibody together with far-UV CD studies, on the modified toxin molecule, indicated an increase in the α helical content after modification, suggested that there was a change in the tertiary structure of the toxin at a crucial antigenic site. Modification of only one or two of the nine tyrosines of TSST-1, using tetranitromethane was found to inhibit up to 85% of the mitogenic activity. Circular dichroism analysis of this modified protein showed a marked change in secondary structure elements which may explain the decrease in activity. Unfortunately these experiments were unable to precisely identify those residues which are involved in the mitogenic activity of the toxin. Alkylation of the methionine residues, using iodoacetic acid, revealed no change in the mitogenic activity or change in tertiary structure as demonstrated by no alteration of the binding of polyclonal antibodies, this suggested that the two methionines, located at residues 33 and 158, are not solely involved in this activity (Kokan-Moore and Bergdoll, 1989b).

Many N terminal protease-generated peptide fragments from TSST-1

have been implicated in MHC II binding. One problem associated with interpreting the data is that contamination of these peptide fragments with nanogramme quantities of the holotoxin may mask the true location of active epitopes on the peptides. To circumvent this problem such studies have been repeated with chemically synthesised peptide fragments. Synthetic peptide fragments located within domain 1 of TSST-1 that have been implicated in MHC II binding are: 34 to 43 (Murphy *et al.*, 1988), 58 to 78 (Edwin *et al.*, 1991) and 39 to 68 (Pontzer *et al.*, 1992; Soos *et al.*, 1993). Figure 5.1 illustrates the location of these sites on the TSST-1 molecule. Competitive binding studies between individual fragments and radiolabelled ^{125}I-TSST-1 for whole cell-bound MHC II molecules, revealed that a N terminal region of TSST-1 (fragment 39 to 68) may be involved in binding to MHC II molecules (Pontzer *et al.*, 1992; Soos *et al.*, 1993). Another fragment 58 to 78 (Edwin *et al.*, 1991) was itself capable of promoting *in vitro* proliferation of human peripheral mononuclear cells with concomitant induction of TNF secretion and as a result was implicated as binding directly to MHC II molecules. The range of these fragments, 34 to 78, are all located around strands β2, β3 and β4 in the concave region of the N terminal β barrel.

In contrast other workers have demonstrated that a significant portion of domain 2 is also involved in MHC II binding. For example fragments 88 to 158 (Edwin and Kass, 1989) and also 155 to 194 (Soos *et al.*, 1993) have been shown to possess superantigenic properties (Figure 5.1). The reasons for this latter observation may be the result of residues 170 to 180 which are sterically adjacent to the concave region in domain 1.

Edwin and Kass (1989) used papain generated fragments of TSST-1,

and reported that a C terminal fragment residues 88 to 158, could bind to monoclonal antibodies known to prevent mitogenic activity. From the structure of TSST-1 reported here, this peptide fragment represents an interface between domains 1 and 2 finishing at the end of strand $\beta 9$. It is not clear how this fragment alone could contain all the elements necessary for superantigenic activity.

Using monoclonal antibodies to TSST-1 and site directed mutagenesis of the toxin, Bonventre and colleagues (1988) tried to elucidate the regions of reactivity and more specifically the residues involved in TSST-1-caused mitogenicity. In their early studies they showed that some monoclonals could reduce mitogenesis in a dose dependent manner; others could prevent TSST-1 induction of interleukin-1 from human monocytes. Most significant was the ability of one monoclonal antibody, 8-5-7, to prevent the death of rabbits given a constant supply of TSST-1 by intravenous administration. The protected rabbits showed no obvious clinical signs of the renal and hepatic disorders characteristic of the controls. They used this toxin neutralizing monoclonal 8-5-7 as a probe to further investigate regions in TSST-1 that were responsible for the symptoms of toxic shock syndrome.

Site directed mutagenesis studies of TSST-1 have been based mainly within the region covering residues 34 to 158 as a result of the peptide studies described above. When the mutants which do not appear to influence mitogenicity are plotted on the TSST-1 model it is possible to identify regions which may be discounted as being crucial for superantigen activity. For example single mutants His 74 (which lies at the top of $\beta 4$ strand of the domain 1 β barrel and is exposed to the solvent) and Tyr 153 (located

within domain 2 on β9) and double mutants Tyr 51.Tyr 52 (both located in the loop linking strands β3 and β4) and Tyr 80.His 82 (both located on β5), all of which were mutated to Ala, still retained full mitogenicity. They were all indistinguishable from the native toxin when tested in rabbits (Blanco *et al.*, 1990; Bonventre *et al.*, 1993).

5.4 T Cell Receptor Binding Sites on the Staphylococcal Enterotoxins

For T cell proliferation to occur the SE must first bind to the MHC II molecule. Therefore, any experiments to locate the TcR binding sites on a SE must not effect the MHC II binding. Little information is available in terms of SE generated peptide fragments, to suggest possible TcR binding sites. Confusion has arisen from experiments which describe both domains as necessary for TcR binding. Spero and Morlock (1978) demonstrated that the N terminal fragment (6.5 kDa) of SEC1 was responsible for mitogenic activity. They showed that the C terminal (28 kDa) fragment was inactive. This is in contrast to work by Bohach *et al.* (1989) which indicated that the C terminal fragment (21 kDa) of SEC1 maintained the characteristics of the holotoxin. SEB has been studied via site directed mutagenesis studies to reveal the putative TcR binding sites. Kappler *et al.* (1992) showed that regions 1 and 3 (residues 9 to 25 and 60 and 61 respectively) had influence on the T cell activation. Asp 25 was shown to be the most important residue involved in T cell activation. This Asp residue has been conserved in all the SE (Figure 1.1) but not TSST-1.

Irwin *et al.* (1992), in a series of hybrid molecules of SEA and SEE, identified just two residues in SEA which could discriminate between Vβ3

and Vβ11. Briefly, the SEA and SEE molecules were split into thirds and the generated hybrids tested to see how they bound to MHC II and for T cell activation. SEA binds to Vβ3 molecules and SEE to Vβ11 molecules. These hybrid molecules maintained similar nanomolar binding affinities to the MHC II as well with 'normal' T cell binding characteristics. From these data the hybrids were assumed to have maintained their structural integrity. Eventually, SEA residues 220 and 221 were shown to be responsible for discriminating between the two Vβ molecules. If extrapolated to the SEB structure, these two residues are located on the loop leading to the α5 helix.

Hoffmann *et al.* (1994) recently demonstrated potential TcR binding sites by producing a number of deletion mutants in the highly conserved N terminal region of SEC1. The first mutant lacked residues 6 to 13 with the result that it induced normal T cell proliferation. However, the second mutant with deleted residues 19 to 33 was rendered non-mitogenic. Interestingly, this second mutant was capable of inhibiting native SEC1 binding to MHC II and native SEC1 induced T cell proliferation.

5.5 T Cell Receptor Binding Sites on Toxic Shock Syndrome Toxin-1

Recent work involving a number of site directed mutants of TSST-1 have been used in a rabbit infection model for toxic shock syndrome (Bonventre *et al.*, 1993). The primary objective of these studies was to compare the toxicity, mitogenic potential and also the structure-function analysis of the native toxin to that of the mutant toxins. One such mutant generated by a single point mutation at His 135 which was converted to

Ala in the mutant toxin, (H135A; Figure 5.1), which was administered to rabbits using an implanted subcutaneous chamber. The mutant retained only 10% of the mitogenic activity present in the native toxin. When two other mutant toxins were prepared by making related single conserved mutations at residue 135, one to glutamine the other to asparagine, neither had any mitogenic activity (Bonventre *et al.*, 1993).

In addition to the work by Bonventre *et al.* (1988; 1993), a number of other workers have carried out similar mutation experiments and demonstrated changes in the mitogenicity of recombinant toxins (Blanco *et al.*, 1990; Murray *et al.*, 1994). Single mutations of Tyr 115, and double mutations His 141.Tyr 144 and E132.I140, which were all converted to Ala, were found to have decreased mitogenicity but were found to be unrecognizable by monoclonal antibodies due possibly significant alterations of their 3D structure. Tyr 115 for example is located between the strands $\beta 7$ and $\beta 8$ and is exposed to the solvent. This residue may form part of the epitope recognised by the monoclonal 8-5-7. Both of the residues affected by the double mutant 141.144 are buried inside the molecule and like the 115 mutant are thought to be crucial to maintaining the tertiary structure as a monoclonal produced against the native toxin cannot recognize the mutant toxin. This mutation lies in the loop between the C terminal end of the major helix $\alpha 2$ and the $\beta 9$ strand following it.

The residues 132, 135 and 140 are all found on the major helix of domain 2 (Figure 5.1). and are positioned in the region of the molecule thought to be crucial for superantigenic activity. The mutations E132K and I140T were selected after a comparison was made between human wild type TSST-1 and ovine TSST-1 (Figure 1.1), where there are seven amino

acid changes. Ovine TSST-1 is not lethal and only slightly mitogenic when repeatedly injected in the rabbit (Lee *et al.*, 1992a).

A more recent study of site directed mutants and hybrid proteins (Deresiewicz *et al.*, 1994; Murray *et al.*, 1994) has thrown much light on what is considered to be the likely sites in TSST-1 responsible for mitogenicity and lethality. These workers used wild type TSST-1, a variant of wild type TSST-1 called TSST-O found in sheep suffering with mastitis (Ho *et al.*, 1989; Lee *et al.*, 1992b), a gene fusion product containing the N terminal region of wild type TSST-1 and containing the C terminal end of TSST-O, and finally two site directed mutagenesis proteins TSST-O K132E. The TSST-O toxin is differs from wild type TSST-1 by seven residues (Asn 19, Thr 55, Ser 57, Ile 69, Trp 80 in the N terminal domain and Lys 132 and Ile 140 in the C terminal domain (Figure 1.1). TSST-O is only weakly mitogenic and does not cause TSS in (the mini osmotic pump) rabbit model. Furthermore TSST-O is not pyrogenic and does not enhance endotoxic shock. The gene fusion protein which contained the N terminal human TSST-1 sequence together with the C terminal ovine sequence differed from wild type TSST-1 by only two residues at 132 and 140. This protein was not mitogenic nor did it produce the symptoms of TSS in rabbits. Subsequently Murray *et al.* (1994) produced single point mutants of the full TSST-O by changing residue 132 from a Lys to a Glu similar to that found in wild type TSST-1 and in a separate experiment changing residue Ile 140 in the fusion protein to a Thr. In the latter case the toxin resembled wild type TSST-1 differing at residue Lys 132 only. Both of these two mutants clearly caused TSS in rabbits and were also capable of enhancing endotoxic shock but were only partially mitogenic.

Murray *et al.* (1994) concluded that they had identified unequivocally that the C terminal domain of TSST-1 is involved in mitogenicity and that the loss of the mitogenicity of the hybrid proteins was not due to an alteration in its 3D conformation because it still reacted with both poly and monoclonal antibodies. However they did not rule out that subtle changes in the side chain residue could have dramatically altered the TcR and/or the MHC II binding region on TSST-1. Indeed their data suggested that the hybrid fusion protein was in fact less mitogenic than wild type TSST-O. Finally Murray *et al.* (1994) concluded that the five N terminal residues of TSST-O must somehow be involved in mitogenicity and that the mitogenic activity of TSST-1 is not just located in the C terminal region.

It is perhaps not coincidental that residue His 135 and other residues located on this major helix $\alpha 2$ are extremely accessible to solvent (Figure 5.1). Such direct availability to the solvent, may be important to allow the reactions involved with superantigenic mitogenicity to proceed. If the concave region of domain 1 as involved in MHC II binding, it is entirely possible that the TcR may bind on or near to residue His 135 whilst the TSST-1 molecule simultaneously binds the MHC II molecule.

5.6 Proposed Model for the TSST-1/MHC II/TcR Complex

As a result of this study a model has been proposed (Acharya *et al.*, 1994) for the trimolecular complex of TSST-1, MHC II and TcR based on site directed mutagenesis studies and crystallographic data from both TSST-1 and SEB (Swaminathan *et al.*, 1992). This model identified two regions of the TSST-1 molecule, region 1 (residues 39 to 78 and 170 to 180) and region 2 (residues Tyr 115, Glu 132, His 135 and Ile 140), that

could interact with the MHC II and TcR respectively (Figure 5.2). This model related only those gross structural features involved in superantigen interaction.

It has been suggested that region 1 of TSST-1 binds to one site on the DR1 molecule, at the end of the peptide binding cleft on DR1. This binding site is positioned exactly opposite to a site on the DR1 β chain (residues 49 to 55) which itself has been implicated in DR1 dimerization (Brown *et al.*, 1993). The TSST-1/DR1 model was still compatible with the idea of DR1 dimerization. This hypothetical assembly allowed region 2 on TSST-1 to remain accessible to the TcR. It has been postulated that the superantigens bind to the solvent exposed β sheet (BDE) of the Vβ region, as deduced from immunoglobulin modeling (Pullen *et al.*, 1990; Pullen *et al.*, 1991; White *et al.*, 1993). In addition the dimerized DR1 molecules are still available for potential binding to the CD4 coreceptor (Brown *et al.*, 1993).

5.7 Verification of the Proposed Model

Since this study was completed the 3D structure of the DR1/TSST-1 complex, to a resolution of 3.5Å, has been elucidated by the technique of X-ray crystallography (Figure 5.3; Kim *et al.*, 1994). The complex structure clearly illustrates the TSST-1 binding regions for MHC II. Figure 5.3 shows that TSST-1 binds DR1 via its N terminal β barrel and confirms both the model proposed by Acharya *et al.* (1994; this study) and peptide fragment studies (Section 5.3). The C terminal domain of TSST-1 is tilted up and away from the DR1 molecule on binding thereby allowing access for TcR binding to TSST-1. Domain 1 of TSST-1 entirely covers the α helix of

DR1α domain, makes a small number of contacts with the α helix of DR1β and most interestingly, makes contact with the bound peptide fragment. TSST-1 covers almost half the 'top' surface of the MHC II molecule.

Kim *et al.* (1994) report three major contact regions associated with DR1/TSST-1 binding. TSST-1 region I involves two loops between β1 and β2, and β3 and β4 which contact two loop regions of DR1 (between β strands 1 and 2, and 3 and 4). Region II constitutes four β strands of TSST-1 (2, 3, 4 and 5) which lie above the α helix of DR1α domain. Finally region III involves interaction between TSST-1 strands β4 and β5 and the bound peptide fragment. Table 5.1, based on Kim *et al.* (1994) illustrates the main residues involved in the DR1/TSST-1 interactions.

The crystal structure of DR1/SEB has also been determined to a resolution of 2.7Å (Jardetzky *et al.*, 1994). The DR1/TSST-1 and DR1/SEB structures are broadly similar with both superantigens binding to the side of the α helix of DR1 via their N terminal β barrel domains. However, closer inspection of these two structures reveal quite different modes of binding. TSST-1 binds DR1 at three regions (see above), and SEB binds to only two. The bound peptide fragment appears to play no part in SEB binding to DR1. In addition, when the structures of DR1/TSST-1 and DR1/SEB are compared, 11 of 17 DR1 residues bind both TSST-1 and SEB even though the complexed toxin orientations are different. Also, of 24 contacts made by TSST-1 with DR1, 13 are structurally identical with SEB in its DR1 complex (Jardetzky *et al.*, 1994).

5.8 Structural Differences Observed in Toxic Shock Syndrome Toxin-1 Due to DR1 Binding

Wild type TSST-1 coordinates (this study) were superimposed over the TSST-1 coordinates from the DR1/TSST-1 complex (Don Wiley, personal communication). This was undertaken to highlight any conformational changes that may occur on TSST-1 binding to DR1. The TSST-1 coordinates from the DR1/TSST-1 complex were superimposed over the wild type coordinates using the program ASH (Stuart *et al.*, 1979). The rms deviation for all 194 Cα atom pairs was 1.89Å. Substantial Cα rms changes (>3.5Å) from wild type occurred in four main regions: between N terminal residues 1 to 6, 76 to 79 (a loop between β3 and β4), 107 and 109 (a loop between β6 and β7) and 144 to 145 (a loop between α2 and β9). These Cα shifts are all remote from the MHC II binding site and do not appear to play a role *per se* in the binding of TSST-1 to the DR1 molecule. The rms deviation for all atoms, including side chains, was 2.4Å. Table 5.1 illustrates the most important residues located at the DR1/TSST-1 interface. The apparent lack of gross (Cα) conformational change in TSST-1 on binding indicates that major changes in TSST-1 need not occur for it to bind to the DR1 molecule.

Residues 1 to 6 in the wild type TSST-1 molecule are more closely associated with domain 2 than domain 1. In the wild type, the Cα of Ser 1 is 5.14Å away from Cα of Ser 147. However, significant changes are seen when TSST-1 is complexed to DR1. Complexed TSST-1 residues 1 to 6 now move away from residue Ser 147 and towards the DR1 peptide binding site. The Cα residue 1 in the complexed state moved approximately 10Å away from its original position. The wild type TSST-1 *B*-factors for

this region reveal rather high values all of which are greater than 40.0Å^2, with a maximum of 71.10Å^2 for Ser 1. This implies significant freedom of movement for this region. It is not clear whether this radical shift of 10.0Å is directly due to TSST-1 binding to DR1 or perhaps an artifact of crystal packing.

The shift in Cα positions for residues 107 to 109 does not immediately suggest a potential site for TcR binding being remote from the main α2 helix. The *B*-factors for these residues are between 35.31Å^2 and 61.75Å^2. This region, located in a loop between β6 and β7, may be involved in as yet unidentified binding to form a stabilization complex between the different cell types.

With residues 1 to 6 moved away from domain 2 on binding DR1, this makes residues Tyr 144 and Arg 145 exposed to the solvent. The wild type *B*-factors for these two residues range from 18.56Å^2 to 27.5Å^2. These low values are not indicative of flexibility. However, this may, in tandem with the shift of residues 1 to 6, provide the accessibility necessary for the binding of the TcR to the 'preformed' TSST-1/DR1 complex. Section 5.5 mentioned a double mutant H141A.T144A which appeared to decrease not only mitogenicity but was also unrecognisable by the monoclonal antibody 8-5-7. The residue His 144 in the DR1/TSST-1 complex was shown to alter its Cα position by a significant amount (rms deviation 4.0Å) when compared with wild type TSST-1 in the ASH study. This Tyr 144 located at a loop and not forming part of a 'regular' secondary structure element may play a role in TcR recognition of the DR1/TSST-1 complex. As with the other regions shown to possess significant changes in Cα coordinates on TSST-1 binding to DR1, further site directed mutagenesis studies are

necessary to ascertain their exact role in complex formation.

It is obvious that the peptide fragment itself plays an important role in altering the local conformation of the TSST-1 molecule around residues 76 to 79 (the loop between β3 and β4). The wild type TSST-1 molecule would make very close contacts with the peptide fragment (p13) bound to the DR1, at approximately 0.72Å^2 at Gly 77. However, when TSST-1 is in its complexed state, this same residue Gly 77 moves 'away' from the peptide fragment by 3.83Å. The *B*-factors for the wild type TSST-1 residues 76 to 79 lie in the range 31.9Å^2 to 66.29Å^2.

The very important nature of the peptide fragment in superantigenic activity has only recently been acknowledged. This has been especially highlighted in respect of the DR1/TSST-1 crystal structure. Also, the charge of the peptide fragment has influenced the crystallization of the DR1/TSST-1 complex (Kim *et al.*, 1994) as demonstrated by the requirement of isoelectric focussing to purify the DR1/peptide complex. In addition to this, the size of the bound peptide fragment may also influence the ability of the superantigen to bind to the DR1 molecule (Vignali and Strominger, 1994).

Having taken into consideration the fact that the secondary structure elements have been reduced and/or deleted in TSST-1 when compared with SEB, the way in which the TcR binds to the SAg/DR1 complex must also differ. Whereas SEB can interact with 6 human Vβ's (Table 1.3) and TSST-1 with only Vβ2 (Table 1.3), it may be possible to rationalize this from the DR1/SEB and DR1/TSST-1 complexes. In DR1/SEB structure, the 'open' nature of both the bound peptide fragment and the α helix from DR1β may allow an additional form of contact with the various Vβ

elements from the T cells. This is in contrast with the top surface of DR1 in the DR1/TSST-1 complex which is 'partially open' (Figure 5.3). This partially open DR1 surface could prevent other, as yet unknown receptors, from interacting directly with the bound peptide fragment and/or to the α helix from DR1β. This may account for only Vβ2 to interact with TSST-1 when bound to DR1. However, all these possibilities may be resolved with a detailed structure of the SAg/MHC II/TcR/peptide complex.

It is not possible at present to make a direct comparison of the *B*-factors from wild type TSST-1 with the complexed TSST-1. This is due to the DR1/TSST-1 complex being refined to 3.5Å with all *B*-factors set to 20.0Å^2. The details of binding modes could be substantiated in the future when the higher resolution (at least 2.5Å) structure becomes available for DR1/TSST-1 complex.

5.9 Future Work

Further work on TSST-1 would involve site directed mutagenesis studies of potential sites for both MHC II and TcR binding sites. In addition to this, production of individual TSST-1 domains would be of benefit to elucidating their functional roles. Co-crystallization studies of TSST-1 and monoclonal antibodies known to prevent superantigenic activity could also be pursued. Finally, a complete trimolecular complex consisting of SAg/MHC II/TcR would enhance our understanding of structure-function relationships.

Table 5.1. *Comparison of intermolecular distances between wild type TSST-1 and complex TSST-1 from DR1 residues.*

TSST-1 Residue	Location on TSST-1	DR1 Residue *	Wild Type TSST-1 Distance to DR1 Residue (Å)†	Complex TSST-1 Distance to DR1 Residue (Å)‡
D27	β1	αY13	4.50	3.60
		αQ18	3.62	4.23
		αK67	2.16	4.46
S29	β1β2 loop	αQ18	4.07	6.62
		αK67	2.76	3.89
L30	β1β2 loop	αM36	3.86	3.95
S32	β2	αA64	4.23	3.97
R34	β2	αA68	1.82	3.53
		αE71	3.23	3.03
I46	β3	αQ57	4.50	4.10
F47	β3	αK39	2.94	3.03
P48	β3β4 loop	αL60	4.28	3.78
S49	β3β4 loop	αK39	2.88	3.00
P50	β3β4 loop	αK38	2.43	3.65
		αK39	4.39	4.40
S53	β3β4 loop	αK39	5.28	3.62
K58	β3β4 loop	αQ18	7.94	5.58
		αK75	11.67	12.57

Table 5.1. *Comparison of intermolecular distances, continued.*

TSST-1 Residue	Location	DR1 Residue *	Wild Type TSST-1 Distance to DR1 Residue (Å)†	Complex TSST-1 Distance to DR1 Residue (Å)‡
Q73	β4	βL60	4.78	2.73
		βA64	3.97	2.95
T75	β4	βD66	8.19	6.12
		pA10	4.46	6.15
		pA11	3.09	3.81
		pA13	3.58	3.69
S76	β4β5 loop	pA12	1.22	6.84
		pA13	1.91	4.16

* α indicates the DR1α chain, β indicates DR1β chain and p indicates the bound peptide fragment. † coordinates from this study. ‡ coordinates from Don Wiley (personal communication).

Figure 5.1 Residues and regions on TSST-1 implicated in binding to MHC II and TcR. The TSST-1 molecule has been rotated 180° about a vertical axis. Regions implicated by peptide data in MHC II binding (Section 5.3) are coloured yellow (residues 39 - 78) and green (residues 155 - 194), the remainder of the molecule is blue. Residues implicated in mitogenic activity, based on mutational analysis (Section 5.5), are highlighted in red (Tyr 115, Glu 132, His 135, His 141 and Tyr 144). The cyan and green balls indicate the N and C termini, respectively.

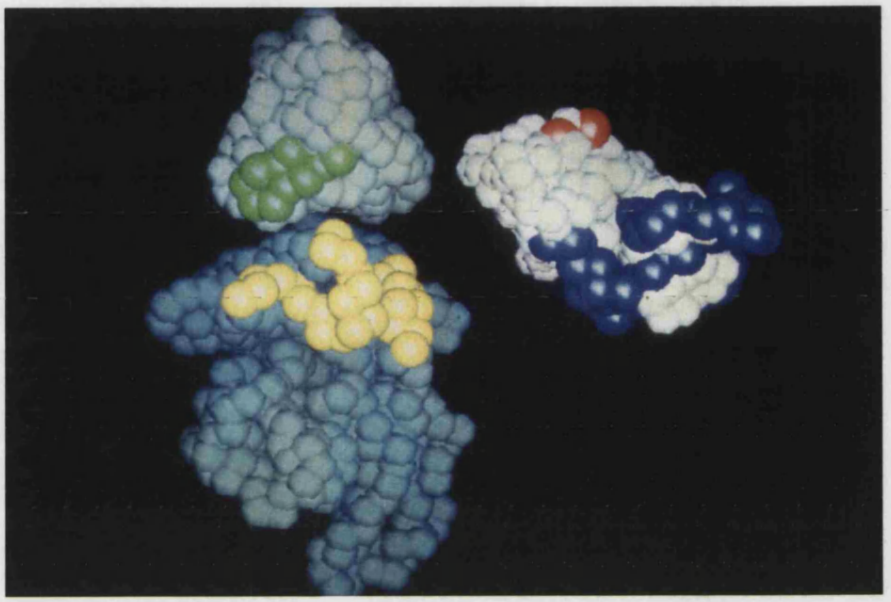

Figure 5.2 A proposed model for the interaction of TSST-1, TcR and MHC II molecules (Acharya *et al.*, 1994). The interacting faces of TSST-1 and the complexes with the MHC II/TcR molecules are represented as each having 90° rotations about a vertical axis. The molecules represented by the space filled objects are as follows: white being TSST-1, mid-blue being MHC II and the pale blue the TcR (Vα and Vβ domains). The interaction between MHC II and TcR are modelled from Bjorkman and Davis (1989) using MHC I and immunoglobulin light chain domain coordinates respectively. Site A in TSST-1 (residues 39 to 78 and 170 to 180) and site B (residues 115, 132, 135 and 140), thought to be involved in MHC II and TcR binding, are respectively coloured in dark blue and red. The yellow area on the MHC II molecule locates the α40 to α50 and β81 to β90 residues. These residues are located to one end of the peptide binding cleft. And finally, the green region of the TcR indicates the DE loop on the external β sheet of the Vβ domain (Choi *et al.*, 1990).

Figure 5.3 The DR1/TSST-1 complex determined by X-ray crystallography (Kim *et al.*, 1994; Figure from the same paper). TSST-1 is coloured red, the α1 and β1 domains of DR1 are light blue and blue, and the antigenic peptide fragment is yellow. The TSST-1 residues Y115, E132, H135, I140, H141 and Y144 have been implicated in TcR binding (Section 5.5) and are represented as ball and stick models.

Appendix A

Phosphate buffered saline (PBS)/100ml, *p*H7.4:

NaCl 8g

KH_2PO_4 0.2g

Na_2PO_4 2.9g

KCl 0.2g

Barbitone buffer, *p*H7.4:

1.2% Agarose

0.85% NaCl

0.8% Sodium barbitol

0.001% Methylate

Appendix B

1) A Summary of the Programs Used in the wild type TSST-1 Data Collection and Processing Using the Imaging Plate

IMSTILLS Using two still images 90° apart, IMSTILLS locates the direct beam coordinates, determines the background count and looks for spot intensities above a predetermined value with respect to the background count. It then decides what the median spot size is for the frame and rejects any that are too large or too small. The list of coordinates, in x and y, and their corresponding intensities for the remaining spots, is then the input for the next program REFIX and IDXREF.

REFIX A program by Kabsch (1988) which calculates an orientation matrix with information given from IMSTILLS and refines the input unit cell parameters. This orientation matrix will then be used in another program OSCGEN.

IDXREF This program indexes the diffraction spots, refines the unit cell parameters, the crystal to plate distance and also the crystal orientation from REFIX, by making use of partial reflections from data given by IMSTILLS. In order for this program to run satisfactorily, the unit cell parameters must be known to within 1% and the crystal orientation to within 1o from the data given in the still photographs.

OSCGEN This program generates a list of spots predicted to occur in further oscillation frames with their coordinates using the matrix from IDXREF.

IP-MOSFLM Using the generated list file from OSCGEN, IP-MOSFLM performs a number of operations. It measures the reflection intensities by creating a 'measurement box' around the spots. This measurement box allows the formation of an estimate for the integrated intensity of each spot which has been corrected for background. It therefore includes not only pixels which make up each spot but also a small region of the background surrounding it. Measuring the spot intensities by this method of profile fitting means that it is particularly sensitive to any errors in the predicted spot coordinates from OSCGEN. So it is vital that the unit cell parameters and crystal orientation are all known accurately in order to get positional errors of less than 50 microns.

ABSCALE Applies a number of correction factors to the data: 1) absorption, 2) Lorentz and 3) Polarization. ABSCALE calculates the correlation coefficients between a reference data set of intensities and new data. It then averages the scaled measurements and assesses any discrepancies. These corrected intensities are then written to an LCF (Labelled Column Format) file.

ROTOVATA Calculates and refines the scale and temperature factors between overlapping sets of data by the method of Fox and Holmes (1966). Use is made not only of symmetry related reflections but also any repeated fully recorded reflections which occur more than once.

AGROVATA This program applies the scale and temperature factors from ROTOVATA with a view to take account of any poor agreements between the fully recorded symmetry equivalents, by rejecting them, to give an averaged value as an output. It also adds together partially recorded

reflections.

3DSCALE A series of programs to average any symmetry repeats within a data set, consequently scaling and merging all data sets with summing of any partially recorded reflections.

DIFFER Analyses the isomorphous differences in scattering due to the binding of a heavy atom to the native protein.

PHASE Calculates the best or most probable phases.

REFINE Refines the heavy atom parameters by minimizing the lack of closure error.

GAP Averages the electron density map of the molecules related by non-crystallographic symmetry to be found in the asymmetric unit. Using each envelope-bound molecule the contents of the defined maps are then averaged (Stuart and Grimes, unpublished).

CALPHA This program uses a database to build a model of a protein using only the coordinates of the C_α atoms. In the initial steps of model building the program can remove any stereochemical strain until better ϕ, ψ angles are obtained (R.Esnouf, unpublished).

GROPAT The automated Patterson search program GROPAT was (Jones *et al.*, 1991) used to interpret the isomorphous difference Patterson maps for the heavy atom derivatives. This computer package GROPAT consists of a number of programs which establish the 'goodness of fit' of the difference Patterson map. The program generates a large number of possible

solutions and by systematically filtering out the false solutions by certain criteria . The first program GROPAT1 generates a ranked list of ~200 possible single sites judged on either self peaks or if there is more than one fixed site, the cross peaks from a 'coarse' grid search. The second program DUP then checks for duplicate solutions in one or more lists. PATREFINE instigates a refinement of each potential solution from the first list by using a finer grid and thereby optimise the agreement with the Patterson map. The fourth program GROPAIR then checks the sites in a list of cross vectors in a pairwise manner. CLUSTER checks the single site list for any potential non crystallographically related sites. Finally PREPAT will then plot the Patterson vectors for the best sites.

2) Having performed an initial manual manipulation of the model on a dedicated computer graphics system, XPLOR performs an automated refinement on it to find the global energy minimum.

GENERATE This first program analyses the model in order to generate a molecular topology file which defines the coordinates in terms of atom type, charge, angles, disulphides as well as hydrogen bonds, electrostatic and Van der Waals forces. This information is then collated into a protein structure file to be used throughout the remainder of the refinement.

CHECK This program is sometimes used in order to calculate an 'ideal' weighting factor for the structure factors used in the next stage of refinement. It also determines the initial R-factor for the model.

PREPSTAGE This performs a restrained energy minimisation to relieve bad contacts and strain from the initial rough model using a conventional

least squares refinement. The weight derived from CHECK can be added to the above equation. It gives an approximate value to the X-ray term relative to the geometric terms. Temperature factors and occupancies are usually fixed and all data above a certain σ cut-off are used. Then the conjugate gradient minimisation can be performed.

SLOWCOOL This is the simulated annealing refinement procedure using molecular dynamics. The theory behind this stage is as follows: The protein can be thought of existing in a heat bath in which the temperature increases to a certain predetermined level guaranteeing all atoms within the protein are in a state of random motion. Once at this temperature the bath is then cooled slowly, allowing the atoms to enter their lowest energy state, *ie.* a global energy minimum. This procedure is a great improvement over previous methods by providing sufficient energy for energetically unfavourable transitions to be explored (Brünger and Nilges, 1993).

BREF This performs individual B-factor refinement on all atoms within the protein to minimise the angle and bond terms to be compared against the observed structure factors.

ANALYSIS Analysis is made of the rms deviations from ideality for the whole structure for bond lengths, bond angles, impropers and dihedral angles. This can reveal how good the refinement process has progressed.

3) XDS is a suite of computer programs used for the automatic on-line processing, both collection and reduction, of X-ray diffraction data from the Siemens multiwire area detector.

XYCORR Due to the geometry of the concave multiwire area detector,

distortion of the diffraction pattern occurs. To reduce such distortion a brass plate placed in front of the detector face is exposed to a ^{55}Fe source. The brass plate information is used and a correction made for the position of each reflection from the crystal in subsequent frames.

INIT Using the first 30 frames as an input, INIT calculates the average background reading, removes any shadow produced by the backstop and determines the region of the detector exposed

COLSPOT The autoindexing routine begins using the first 30 frames. The positions of the strongest reflections above a threshold are given co-ordinates x and y. Spots on adjacent frames found to be equivalent are merged. The output is a list of coordinates, their indices and the crystal position.

IDXREF Using the output from COLSPOT the unit cell parameters, and performing an iterive least squares analysis the crystal orientation and crystal to detector distance are determined and refined. It predicts positions of reflections to be found in subsequent frames.

COLPROF Collects 3D reflection profiles using integration. Assigns those pixels which belong to a particular spot an hkl value. Any small slippage of the crystal can be accommodated here with re-refinement.

PROFIT Integrates the intensities of all reflections by fitting a '3D net' over each spot and then removing the local background count.

CORRECT The spot intensities are all scaled due to crystal degradation. Corrections are made for decay, absorption and detector surface sensitivity.

GLOREF A more accurate refinement of the unit cell parameters, crystal to detector distance and crystal rotation angle than IDXREF are estimated here because all reflections from this data collection run are used.

4) A brief explanation of the programs within MERLOT.

PROREF Processes the reflection intensity data for the unknown and is then ready for use in the other programs within MERLOT.

PROCOR The centre of mass is calculated and the molecule is then moved to the origin. Structure factors are then generated for the model.Processed coordinate data of the search model for input to the other programs in MERLOT.

ROTATION Calculates the spherical harmonic coefficients and expands the data in the form of a Bessel function. Determines the orientation of the search model in the cell of the unknown using the Fast rotation function of Crowther (1972), in terms of Eulerian angles α, β and γ on a coarse grid. A map is then made in which any peaks are indicated.

ROTATION-FINE Refines the β angle only from ROTATION using finely sampled transforms. Any peaks found in the map are indicated.

LAT Refines the α and γ angles from ROTATION using the Lattman rotation function (1972). Again a map is made and any peaks are indicated.

TRANS Calculates the positions of the search model in the cell of the unknown *ie.* translation function (Crowther and Blow, 1967). Sets up a continuous transform for subsequent programs to calculate structure fac-

tors.

5) AMoRE is a new molecular replacement computer package and involves more powerful algorithms (Dodson *et al.*, 1992; Navaza, 1994). It is a much quicker automated package of programs which allows a great many potential solutions to be explored. AMoRE makes use of a correlation coefficient as its main selection criteria for peaks as well as an R-factor value. This improved algorithm is used to calculate the structure factors of the rotated and translated search model. For a mathematical explanation the reader is invited to read the above references.

SORT This is the first of AMoREs preliminary programs which sorts, packs and assesses the quality of the data supplied such as the *hkl*s and F_{obs}.

TABLIN The second preliminary program which places the centre of mass of the search model at the origin and optimise its position there by aligning its principal axes of inertia with that of the unit cell axes. TABLIN then calculates and tabulates a continuous Fourier coefficients from the search model.

ROTA Calculates a fast rotation function based on Crowther (1972). The radius of integration used here is taken from the output of TABLIN *ie.* the distance from the centre of mass to the atom furthest away from this point. Next the structure factors for the search model are calculated. The output consists of a list of all peaks with a value greater than 50% the maximum value of the rotation function.

TRAING The whole peak list as the output of ROTA is then used as the input for TRAING. The translation function is then calculated for each line. The output of TRAING is a list of peaks, again greater than 50% the maximum for the translation function with an given correlation coefficient.

FITING This stage of AMoRE then performs a rigid body refinement of the list given as the output of TRAING.

6) Miscellaneous. **DSSP** A programm (Kabsch, 1988) which generates secondary structure features (*ie.* β sheet and α helix) from the protein coordinate file.

ASH A program which compares two protein molecules using their atomic coordinates and gives a residue by residue rms deviation (Stuart, 1979).

MOLSCRIPT A program which creates a diagram of the protein from the coordinate file (Kraulis, 1991).

PROCHECK A program which checks the stereochemical quality of the protein (Laskowski *et al.*, 1993).

References

Abe, J., Forrester, J., Nakahara, T., Lafferty, J.A., Kotzin, B.L. and Leung, D.Y.M. (1991) *J. Immunol.* **146** 3747-3750.

Achari, A, Hale, S.P., Howard A.J., Clore, G.M., Gronenborn, A.M., Hardman, K.D. and Whitlow, M. (1992) *Biochemistry* **31** 10449-10457.

Acharya, K.R., Passalacqua, E.F., Jones, E.Y., Harlos, K., Stuart, D.I., Brehm, R.D. and Tranter, H.S. (1994) *Nature* (London) **367** 94-97.

Alber, G., Hammer, D.K. and Fleischer, B. (1990) *J. Immunol.* **144** 4501-4506.

Alouf, J.E., Knöll, H. and Köhler, W. (1991) in Sourcebook of Bacterial Protein Toxins Eds J.E. Alouf and J.H.Freer. Academic Press pp367-414.

Avena, R.M. and Bergdoll, M.S. (1967) *Biochemistry* **6** 1474-1480.

Bailey, S., Dodson, E. and Phillips, S. (Eds) In *Improving Protein Phases* Proceedings of the Daresbury Study Weekend, 5-6 Febuary 1988.

Bayles, K.W and Iandolo, J.J. (1989) *J. Bacteriol.* **171** 4799-4806.

Bergdoll, M.S. (1990) In *Foodborne Diseases.* Academic Press 85-106.

Bergdoll, M.S. (1988) *Meth. Enzymol.* **165** 324-333.

Bergdoll, M.S. and Schlievert (1984) *Lancet* **2** 691.

Bergdoll, M.S. (1983) Enterotoxins. *Staphylococci and staphylococcal diseases.* Ed: C.S.F. Easmon and C.Adams. (Academic Press, London)

pp559-598.

Bergdoll, M.S., Crass, B.A., Reiser, R.F., Robbins, R.N., and Davis, J.P. (1981) *Lancet* **1** 1017-1021.

Bergdoll, M.S., Borja, C.R., Robbins, R.N. and Weiss, K.F. (1971) *Infect. Immun.* **4** 593-595.

Bergdoll, M.S. (1970) Enterotoxins. In *Microbial Toxins.* III. *Bacterial Protein Toxins,* ed. Moutie, T.C., Kadis, S.,and Ajl, S.J. 265-326. New York. Academic Press.

Bergdoll, M.S., Borja, C.R. and Avena, R.M. (1965) *J. Bacteriol.* **90** 1481-1485.

Bergdoll, M.S., Sugiyama, H. and Dack, G.M. (1959) *Arch. Biochem. Biophys.* **85** 62-69.

Betley, M.J., Soltis, M.T. and Couch, J.L. (1990) In: *Molecular Biology of the Staphylococci.* Ed. R.P.Novick. (VCH Publishers, New York). pp327-342.

Bette, M., Schafer, M.K.H., Van Rooijen, N., Weihe, E. and Fleischer, B. (1993) *J. Exp. Med.* **178** 1531-1540.

Binek, M., Newcomb, J.R., Rogers, C.M., and Rogers, T.J. (1992) *J. Med. Mirobiol.* **36** 156-163.

Bjorkman, P.J. and Davis, M.M. (1989) *Cold Spring Harb. Symp. Quant. Biol.* **LIV** 365-373.

Blackwell, C.C., Saadi, A.T., Raza, M.W., Stewart, J. and Weir, D.M. (1992) *J. Clin. Pathol.* **45** No.11 S(20-24).

Blanco, L., Choi, E.M., Connolly, K., Thompson, M.R. and Bonventre, P.F. (1990) *Infect. Immun.* **58** 3020-3028.

Blomster-Hautamaa, D.A. and Schlievert, P.M. (1988). In: *Bacterial Toxins, Handbook of Natural Toxins, Vol 4* (eds. M.C. Hardegree & A.T. Tu) pp 297-330 Marcel Dekker, New York.

Blomster-Hautamaa, D.A., Kreiswirth, B.N., Kornblum, J.S., Novick, R.P., and Schlievert, P.M. (1986a) *J. Biol. Chem.* **261** 15783-15786.

Blomster-Hautamaa, D.A., Kreiswirth, B.N., Novick, R.P., and Schlievert, P.M. (1986b) *Biochemistry* USA **25** 54-59.

Blomster-Hautamaa, D.A., Novick, R.P., and Schlievert, P.M. (1986c) *J. Immunol.* **137** 3572-3576.

Blundell, T.L. and Johnson, L.N. (1976) *Protein Crystallography.* Academic Press, London.

Bohach, G.A., Fast, D.J., Nelson, R.D. and Schlievert, P.M. (1990) *Crit. Rev. Microbiol.* **17** 251-272.

Bohach, G.A., Handley, J.P. and Schlievert, P.M. (1989) *Infect. Immun.* **57** 23-28.

Bohach, G.A., Hovde, C.J., Handley, J.P. and Schlievert, P.M. (1988) *Infect. Immun.* **56** 400-404.

Bonventre, P.F., Heeg, H, Cullen, C., and Lian, C-J. (1993) *Infect. Immun.* **61** 793-799.

Bonventre, P.F., Thompson, M.R., Adinolfi, L.E., Gillis, Z.A., and Parsonnet, J. (1988) *Infect. Immun.* **56** 135-141.

Bonventre, P.F., Weckbach, L., Staneck, J., Schlievert, P.M. and Thompson, M. (1983) *Infect. Immun.* **40** 1023-1029.

Borja, C.R. and Bergdoll, M.S. (1967) *Biochemistry* **6** 1467-1473.

Bragg, W.L. (1913) *Proc. Camb. Phil. Soc.* **17** 464.

Bränden, C.I. and Jones, A. (1990) *Nature* (London) **343** 687-689.

Braunstein, N.S., Weber, D.A., Wang, X-C., Long, E.O., and Karp, D. (1992) *J. Exp. Med.* **175** 1301-1305.

Brehm, R.D., Tranter, H.S., Hambleton, P., and Melling, J. (1990). *Appl. Environ. Microbiol.* **56** 1067-1072.

Brenner, M.B., McLean, J., Dialynas, D.P., Strominger, J.L., Smith, J.A., Owen, F.L., Seidman, J.G., Ip, S., Rosen, F. and Krangel, M.S. (1986) *Nature* (London) **372** 145-149.

Bricogne, G. (1976) *Acta. Cryst.* **A32** 832-846.

Brown, J.H., Jardetzky, T.S., Gorga, J.C., Stern, L.J., Urban, R.G., Strominger, J.L. and Wiley, D.C. (1993). *Nature* (London) **364** 33-39.

Brünger, A.T. and Nilges, M. (1993) *Quart. Rev. Biophys.* **26** 49-125.

Brünger, A.T. (1988) *J. Mol. Biol.* **203** 803-816.

Brünger, A.T., Kuriyan, J & Karplus, M. (1987) *Science* **235** 458-460.

Buelow, R., O'Hehir, R.E., Schreifels, R., Kummerehl, T.J., Reily, G., and Lamb, J.R. (1992) *J. Immunol.* **148** 1-6.

Carlsson, R., Fischer, H. and Sjögren, H-O. (1988) *J. Immunol.* **140** 2484-2488.

Casman, E.P., Bennett, R.W., Dorsey, A.E. and Issa, J.A. (1967) *J. Bacteriol.* **94** 1875-1882.

Casman, E.P. (1960) *J. Bacteriol.* **79** 849-858.

Cazenave, P.A., Marche, P.N., JouvinMarche, E., Voegtle, D., Bonhomme, F., Bandeira, A. and Coutinho, A. (1990) *Cell* **63** 717-728.

Chesney, P.J., Bergdoll, M.S., Davis, J.P. and Vergeront, J.M. (1984). *Ann. Rev. Microbiol.* **38** 315-338.

Chintagumpala, M.M., Mollick, J.A., and Rich, R.R. (1991) *J. Immunol.* **147** 3876-3881.

Choi, Y., Herman, A., DiGusto, D., Wade, T., Marrack, P. and Kappler, J. (1990) *Nature* (London) **346** 471-473.

Choi, Y., Kotzin, B., Herron, L., Callahan, J., Marrack, P. and Kappler, J. (1989) *Proc. Natl. Acad. Sci.* (USA) **86** 8941-8945.

Couch, J.L., and Betley, M.J. (1989) *J. Bacteriol.* **171** 4507-4510.

Couch, J.L., Soltis, M.T. and Betley, M.J. (1988) *J. Bacteriol.* **1702954-2960.**

Crass, B.A. and Bergdoll, M.S. (1986) *J. Infect. Dis.* **153** 918-926.

Crowther, R.A. (1972) In *The Molecular Replacement Method.* Ed: M.G.Rossmann 174-178. New York: Gordon and Breach.

Dack, G.M., Cary, W.E., Woolpert, O. and Wiggers, H.S. (1930) *Prevent. Med.* 4 167.

Davis, J.P., Chesney, P.J., Wand, P.J. and LaVenture, M. (1980) *N. Engl. J. Med.* **303** 1429-1436.

Dellabona, P., Peccoud, J., Kappler, J., Marrack, P., Benoist, C. and Mathis, D. (1990) *Cell* **62** 1115-1121.

Deresiewicz, R.L., Woo, J.H., Chan, M., Finberg, R.W. and Kasper, D.L. (1994) *Biochemistry* **33** 12844-12851.

Devereux, J., Haeberli, P. and Smithies, O. (1984) *Nucleic Acid Res.* **12** 387-395.

Dodson, E.J., Glover, S. and Wolf, W. (eds.) (1992) in *Molecular Replacement* CCP4 Daresbury Study Weekend. SERC Daresbury Laboratory, Warrington WA4 4AD, UK.

Dohlsten, M., Hedlund, G., Åkerblom, E., Lando, P.A., and Kalland, T. (1991) *Proc. Natl. Acad. Sci.* (USA) **88** 9287-9291.

Ducruix, A. and Geige, R. (1992) In *Crystallization of Nucleic Acids and*

Proteins. A Practical Approach. IRL Press.

Edwin, C., Swack, J.A., Williams, K., Bonventre, P.F., and Kass, E.H. (1991) *J. Infect. Dis.* **163** 524-529.

Edwin, C., and Kass, E.H. (1989) *Infect. Immun.* **57** 2230-2236.

Fast, D.J., Schlievert, P.M. and Nelson, R.D. (1989) *Infect. Immun.* **57** 291-294.

Ferrick, D.A., Ohashi, P.S., Wallace, V., Schilham, M. and Mak, T.W. (1989) *Immunol. Today.* **10** 403-407.

Fischer, H., Dohlsten, M., Lindvall, M., Sjögren, H-O. and Carlsson, R. (1989) *J. Immunol.* **142** 3151-3157.

Fitzgerald, P.M.D. (1988). *J. Appl. Crystallogr.* **21** 273-278.

Fleischer, B. and Schrezenmeier, H. and Conradt, P. (1989) *Cell. Immunol.* **120** 92-101.

Fleischer, B. and Schrezenmeier, H. (1988) *J. Exp. Med.* **167** 1697-1707.

Fraser, J.D., Urban, R.G., Strominger, J.L., and Robinson, H. (1992) *Proc. Natl. Acad. Sci.* (USA) **89** 5507-5511.

Fraser, J.D. (1989) *Nature* (London) **339** 221-223.

Garbe, P.L., Arko, R.J., Reingold, A.L., Graves, L.M., Hayes, P.S., Hightower, A.W., Chandler, F.W., and Broome, C.V. (1985) *J. Am. Med. Assoc.* **253** 2538-2542.

Gascoigne, N.R.J. and Ames, K.T. (1991) *Proc. Natl. Acad. Sci.* (USA) **88** 613-616.

Germain, R.N. and Margulies, D.H. (1993) *Ann. Rev. Immunol.* **11** 403-450.

Goodfellow, J., Hendrick, K and Hubbard, R. (eds.) (1989) in *Molecular Simulations and Protein Crystallography.* CCP4 Daresbury Study Weekend. SERC Daresbury Laboratory, Warrington WA4 4AD, UK. DL/SCI/R23 ISSN 0144-5677.

Green, D.W., Ingram, V.M. and Perutz, M.F. (1954) *Proc. Roy. Soc. London.* **A225** 287.

Grossman, D., Lamphear, J.G. and Mollick. J.A. (1992) *Infect. Immun.* **60** 5190-5196.

Grossman, D., Van, M., Mollick, J.A., Highlander, S.K., and Rich, R.R. (1991) *J. Immunol.* **147** 3274-3281.

Hansson, J., Ericsson, P.O., Dohlsten, M., Sjogren, H.O., Kalland, T. and Hedlund, G. (1992) *Immunol. Lett.* **34** 229-236.

Harlos, K. (1992) *J. Appl. Crystallogr.* **25** 536-538.

Harris, T.O., Hufnagle, W.O. and Betley, M.J. (1993) *Infect. Immun.* **61** 2059-2068.

Helliwell, J.R. (1992) *Macromolecular Crystallography with Synchrotron Radiation.* Cambridge University Press, Cambridge.

Herman, A., Kappler, J.W., Marrack, P., and Pullen, A.M. (1991a) *Annu. Rev. Immunol.* **9** 745-72.

Herman, A., Labrecque, N., Thibodeau, J., Marrack, P., Kappler, J.W., and Sekaly, R.P-. (1991b) *Proc. Natl. Acad. Sci.* (USA) **88** 9954-9958.

Hermann, T., Accolla, R.S. and MacDonald, H.R. (1989) *Eur. J. Immunol.* **19** 2171-2174.

Hewitt, C.R.A., Lamb, J.R., Hayball, J., Hill, M., Owen, M.J., and O'Hehir, R.E. (1992) *J. Exp. Med.* **175** 1493-1499.

Ho, G., Campbell, W.H. Bergdoll, M.S. and Carlson, E. (1989) *J. Clin. Microbiol.* **27** 210-212.

Hoffmann, M.L., Jablonski, L.M., Crum, K.K., Hackett, S.P., Chi, Y-i., Stauffacher, C.V., Stevens, D.L., and Bohach, G.A. (1994) *Infect. Immun.* **62** 3396-3407.

Holbrook, M.R., Yong, K.E., Gibbon, L.G., Webster, C.A., Tranter, H.S., Arbuthnott, J.P. and Todd, I. (1993) *FEMS Immunol. Medicinal Microbiol.* **7** 169-174.

Hovde, C.J., Marr, J.C., Hoffmann, M.L., Hackett, S.P., Chi, Y-i., Crum, K.K., Stevens, D.L., Stauffacher, C.V. and Bohach, G.A. (1994) *Molec. Microbiol.* **13** 897-909.

Huang, I.Y., Hughes, J.L., Bergdoll, M.S. and Schantz, E.J (1987) *J. Biol. Chem.* **262** 7006-7013.

Huang, I.J. and Bergdoll, M.S. (1970) *J. Biol. Chem.* **245** 3518-3525.

Hudson, K.R., Robinson, H. and Fraser, J.D. (1993) *J. Exp. Med.* **177** 175-184.

Hufnagle, W.O., Tremaine, M.T and Betley, M.J. (1991) *Infect. Immun.* **59** 2126-2134.

Hynes, T.R. and Fox, R.O. (1991) *Proteins, Strut. Funct. Gen.* **10** 92-105.

Iandolo, J.J. and Tweten, R.K. (1988) In *Methods in Enzymology*, Vol 165, *Microbial Toxins: Tools in Enzymology* (ed. S. Harshman), pp 43-52. Academic Press, San Diego.

Ikejima,T., Dinarello, C.A., Gills, D.M. and Wolff, S.M. (1984) *J. Clin. Invest.* **73** 1312-1320.

Irwin, M.J., Hudson, K.R., Fraser, J.D., and Gascoigne, N.R.J. (1992) *Nature* (London) **359** 841-843.

Jancarik, J. and Kim, S-H. (1991) *J. Appl. Cryst.* **24** 409-411.

Janeway, C.A.Jr., Yagi, J., Conrad., P.J., Katz, M.E., Jones, B., Vroegop, S. and Buxser, S. (1989) *Immunol. Rev.* **107** 61.

Jardetzky, T.S., Brown, J.H., Gorga, J.C., Stern, L.J., Urban, R.G., Chi, Y-I., Stauffacher, C., Strominger, J.L. and Wiley, D.C. (1994) *Nature* (London) **368** 711-718.

Johnson, L.P. and Schlievert, P.M. (1984) *Mol. Gen. Genet.* **194** 52-56.

Jones, E.Y., Davis, S.J., Williams, A.F., Harlos, K. and Stuart, D.I. (1992) *Nature* (London) **360** 232-239.

Jones, E.Y. & Stuart, D.I. In *Isomorphous Replacement and Anomalous Scattering* (eds Wolf, W., Evans, P.R. & Leslie, A.G.W.) 39-47 SERC Daresbury Laboratory, Warrington, 1991.

Jones, A. (1985) *Meth. Enzym.* **115** 157-171.

Kabsch, W. (1988). *J. Appl. Cryst.* **21** 67-71.

Kabsch, W. and Sander, (1988) *Biopolymers* **22** 2577-2637.

Kalland, T., Dohlstein, M., Lind, P., Sundstedt, A., Abrahamsen, L., Hedlund, G., Bjork, P., Lando, P.A. and Bjorklund, M. (1993) *Medical Oncology and Tumor Pharmacotherapy* **10** 37-47.

Kappler, J.W., Herman, A., Clements, J. and Marrack, P. (1992) *J. Exp. Med.* **175** 387-396.

Kappler, J., Kotzin, B., Herron, L., Gelfand., E.W., Bigler, R.D., Boylston, A., Carrel, S., Posnett, D.N., Choi, Y. and Marrack, P. (1989) *Science* **244** 811-814.

Karp, D.R. and Long, E.O. (1992) *J. Exp. Med.* **175** 415-424.

Karp, D.R., Teletski, C.L., Scholl, P., Geha, R., and Long, E.O. (1990) *Nature* (London) **346** 474-476.

Karplus, M., Brünger, A.T., Elber, R. and Kuriyan, J. (1987) *Cold Spr. Harb. Symp. Quant. Biol.* **LII** 381-390.

Kim, J., Urban, R.G., Strominger, J.L. and Wiley, D.C. (1994) *Science* **266** 1870-1874.

Kirkpatrick, S., Gelatt, C.D. and Vecchi, M.P. (1983) *Science* **220** 671-680.

Kokan-Moore, N.P., and Bergdoll, M.S. (1989a) *Infect. Immun.* **57** 1901-1905.

Kokan-Moore, N.P., and Bergdoll, M.S. (1989b) *Rev. Infect. Dis.* **11** (Suppl 1) S125-S129.

Komisar, J.L., Small-Harris, S. and Tseng, J. (1994) *Infect. Immun.* **62** 4775-4780.

Kotb, M. (1992) *Cur. Opin. Infect. Dis.* **5** 364-374.

Kotzin, B.L., Leung, D.Y.M., Kappler, J. and Marrack, P. (1993) *Adv. Immunol.* **54** 99-166.

Kraulis, P.J. (1991). *J. Appl. Crystallogr.* **24** 946-950.

Kunstmann, G., Schröder, E., Habasch, H., and Pulverer, G. (1989) *Zbl. Bakt.* **271** 486-492.

Lagoo, A.S., LagooDeenadayalan, S., Lorentz, H.M., Byrne, J., Barber, W.H. and Hardy, K.J. (1994) *J. Immunol.* **152** 1641-1652.

Laskowski, R.A., MacArthur, M.W., Moss, D.S. and Thornton, J.M. (1993) *J. Appl. Crystallogr.* **26** 283-291.

Lattman and Love (1970). *Acta. Cryst.* **B26** 1854-1857.

Lee, P.K., Kreiswirth, B.N., Deringer, J.R., Projan, S.J., Eisner, W., Smith., B.L., Carlson, E., Novick, R.P., and Schlievert, P.M. (1992a) *J. Infect. Dis.* **165** 1056-1063.

Lee, V.T., Chang, A.H. and Chow, A.W. (1992b) *J. Infect. Dis.* **166** 911-915.

Lee, P.K., Deringer, J.R., Kreiswirth, B.N., Novick, R.P and Schlievert, P.M. (1991) *Infect. Immun.* **59** 879-884.

Love, D. (Ed) in *the CCP4 Suite-Computer Programs for Protein Crystallography* SERC Daresbury Laboratory, Warrington, England. 1993.

Machin, P.A. (1985) in *Molecular Replacement.* CCP4 Daresbury Study Weekend. SERC Daresbury Laboratory, Warrington WA4 4AD, UK. DL/SCI/R23 ISSN 0144-5677.

Madden, D.R., Garboczi, D.N. and Wiley, D.C. (1993) *Cell* **75** 693-708.

Malam, J.E., Carrick, G.F., Telford, D.R., Morris, J.A. (1992) *J. Clin. Pathol.* **45** 716-721.

Marrack, P. Winslow, G.M., Choi, Y., Scherer, M., Pullen, A., White, J. and Kappler, J.W. (1993) *Immunol. Rev.* **131** 79-92.

Marrack, P and Kappler, J. (1990). *Science* **248** 705-711.

Marrack, P., Blackman, M., Kushnir, E. and Kappler, J. (1990) *J. Exp. Med.* **171** 455-464.

Marrack, P. and Kappler, J. (1987) *Science* **238** 1073-1079.

Matthews, B.W. (1968). *J. Mol. Biol.* **33**, 91-97.

McPherson, A. (1990) *Eur. J. Biochem.* **189** 1-23.

McPherson, A. (1982). In *The Preparation and Analysis of Protein Crystals.* John Wiley & Sons, New York.

McRee, D. (1993) *Practical Protein Crystallography* Academic Press, San Diego.

Meyer, R.F. and Palmieri, M.J. (1980) *Appl. Environ. Microbiol.* **40** 1080-1085.

Micusan, V.V and Thibodeau, J. (1994) *Sem. Immunol.* **5** 3-11.

Miethke, T., Duschek, K., Wahl, C., Heeg, E. and Wagner, H (1993) *Eur. J. Immunol.* **23** 1494-1500.

Miethke, T., Wahl, C., Heeg, K., Echtenacher, B., Krammer, P.H., Wagner, H. (1992) *J. Exp. Med.* **175** 91-98.

Mittrücker, H-W., and Fleischer, B. (1992) *Cell. Immunol.* **139** 108-117.

Mollick, J.A., Chintagumpala, M., Cook, R.G. and Rich, R. (1991) *J. Immunol* **146** 463-468.

Mollick, J.A., Cook, R.G., and Rich, R.R. (1989) *Science* **244** 817-820.

Morio, T., Geha, R.S. and Chatila, T.A. (1994) *Eur. J. Immunol.* **24** 651-658.

Mourad, W., Scholl, P., Diaz, A., Geha, R., and Chatila, T. (1989) *J. Exp.*

Med. **170** 2011-2022.

Murphy, B.G., Kreiswirth, B.N., Novick, R.P. and Schlievert, P.M. (1988) *J. Infect. Dis.* **158** 549-555.

Murray, D.L., Prasad, G.S., Earhart, C.A., Leonard, B.A.B., Kreiswirth, B.N., Novick, R.N., Ohlendorf, D.H., and Schlievert, P.M. (1994) *J. Immunol.* **152** 87-95.

Murzin, A.G. (1993). *EMBO J.* **12** 861-867.

Murzin, A.G. (1992). *Nature* (London) **360** 635.

Naidu, A.S., Eriksson, K.-O., Hallberg, T., Lindeberg, J., Liao, J,-L., Yao, K., Wadström, T. and Hjerten, S. (1989). *APMIS* **97** 1088-1096.

Navaza, J. (1994) *Acta. Cryst.* **A50** 157-163.

Norton, S.D., Schlievert, P.M., Novick, R.P., and Jenkins, M.K. (1990) *J. Immunol.* **144** 2089-2095.

Ochi, A., Migita, K., Xu, J. and Siminovitch, K. (1993) *J. Immunol.* **151** 3180-3186.

Otinowski, Z. (1993) in: Sawyer, L., Isaacs, N. and Bailey, S. Data Collection and Processing. Proceedings of the CCP4 Study Weekend, 29-30 January 1993.

Overington, J.P. (1992) *Curr. Opin. Strut. Biol.* **2** 349-401.

Palkama, T. and Hurme, M. (1993) *Hum. Immunol.* **36** 259-267.

Palliard, X., West,S.G., Lafferty, J.A., Clements, J.R., Kappler, J.W., Marrack, P. and Kotzin, B.L. (1991) *Science* **253** 325-329.

Panina-Bordignon, P., Fu, X.T., Lanzavecchia, A. and Karr, R.W. (1992) *J. Exp. Med.* **176** 1779-1784.

Parsonnet, J., Hickman, R.K., Eardley, D.D. and Pier, G.B. (1985) *J. Infect. Dis.* **151** 514-522.

Passalacqua, E.F., Brehm, R.D., Acharya, K.R., and Tranter, H.S. (1993) *J. Mol. Biol.* **233** 170-172.

Passalacqua, E.F., Brehm, R.D., Acharya, K.R., and Tranter, H.S. (1992) *J. Mol. Biol.* **228** 983-986.

Peavy, D.L., Adler, W.H. and Smith, R.T. (1970) *J. Immunol.* **105** 1453-1458.

Petsko, G.A. (1985) *Meth. Enzymol.* **114** 147-157.

Poindexter, N.J., and Schlievert, P.M. (1986) *J. Infect. Dis.* **153** 772-779.

Pontzer, C.H., Irwin, M.J., Gascoigne, N.R.J. and Johnson, H.M. (1992) *Proc. Natl. Acad. Sci.* USA **89** 7727-7731.

Pontzer, C.H., Russell, J.K., and Johnson, H.M. (1991) *Proc. Natl. Acad. Sci.* USA **88** 125-128.

Pontzer, C.H., Russell, J.K., and Johnson, H.M. (1989) *J. Immunol.* **143** 280-284.

Pullen, A.M., Bill, J., Kubo, R.T, Marrack, P. and Kappler, J.W. (1991) *J. Exp. Med.* **173** 1183-1192.

Pullen, A.M., Wade, T., Marrack, P. and Kappler, J.W. (1990) *Cell* **61** 1365-1374.

Ramachandran, G.N. and Sasisekharan, V. (1968) *Adv. Prot. Chem.* **23** 283.

Ramesh, N., Spertini, F., Scholl, P., and Geha, R. (1992) *J. Immunol.* **148** 1025-1030.

Reeves, M.W., Arbo, R.J., Chandler, F.W. and Bridges, N.B. (1986) *Infect. Immun.* **51** 431-439.

Reiser, R.F., Robbins, R.N., Noleto, A.L., Khoe, G.P. and Bergdoll, M.S. (1984) *Infect. Immun.* **45** 625-630.

Reiser, R.F., Robbins, R.N., Khoe, G.P. and Bergdoll, M.S. (1983) *Biochemistry* **22** 3907-3912.

Reynolds, D., Tranter, H.S., Sage, R. and Hambleton, P. (1988) *Appl. Environ. Microbiol.* **54** 1761-1765.

Rosenthal, L.A., Taub, D.D., Moors, M.A. and Blank, K.J. (1992) *Immunopharmacol.* **24** 203-217.

Rossi, G.L. (1992) *Cur. Opin. Struct. Biol.* **2** 816-820.

Rossmann, M.G. (1972) *The Molecular Replacement Method.* A Collection of papers on the use of Non Crystallographic Symmetry. Gordon and

Breach Publishers.

Rosten, P.M., Bartlett, K.H., and Chow, A.W. (1989) *Revs. Infect. Dis.* **11** (Suppl 1) S100-S116.

Russell, J.K., Jarpe, M.A., and Johnson, H.M. (1992) *Biochem. Biophys. Res. Commun.* **182** 1016-1024.

Rust, C.J.J., Verreck, F., Vietor, H., and Koning, F. (1990) *Nature* (London) **346** 572-574.

Schantz, E.J., Rossler, W.G., Woodburn, M.J., Lynch, J.M., Jacoby, H.M., Silverman, S.J., Gorman, J.C. and Spero, L. (1972) *Biochemistry* **11** 360-366.

Schantz, E.J., Rossler, W.G., Wagman, J., Spero, L., Dunnery, D.A. and Bergdoll, M.S. (1965) *Biochemistry* **4** 1011-1016.

Schlievert, P.M. (1989) *Rev. Infect. Dis.* S107-S109.

Schlievert, P.M. (1986) *Lancet* **1** 1149-1150.

Schlievert, P.M. (1984) *Surv. Synth. Path. Res.* **3** 54-62.

Schlievert, P.M. (1983) *J. Infect. Dis.* **147** 391-398.

Schlievert, P.M. (1982) *Infect. Immun.* **36** 123-128.

Schlievert, P.M. (1981) *Infect. Immun.* **31** 732-736.

Schlievert, P.M., Shands, K.N., Dan, B.B., Schmid, G.P., and Nishimura, R.D. (1981) *J. Infect. Dis.* **143** 509-516.

Schmidt, J.J and Spero, L. (1983) *J. Biol. Chem.* **258** 6300-6306.

Scholl, P.R., Trede, N., Chatila, T.A., and Geha, R.S. (1992) *J. Immunol.* **148** 2237-2241.

Scholl, P., Diez, A., Mourad, W., Parsonnet, J., Geha, R.S. and Chatila, T. (1989a) *Proc. Nat. Acad. Sci.* (USA) **86** 4210-4214.

Scholl, P.R., Diez, A., and Geha, R.S. (1989b) *J. Immunol.* **143** 2583-2588.

Scholl, P.R., Sekaly, R.P., Diez, A., Glimcher, L.H. and Geha, R.S. (1990) *Eur. J. Immunol.* **20** 1911-1916.

Schwab, J.H., Brown, R.R., Anderle, S.K., Schlievert, P.M. (1993) *J. Immunol.* **150** 4145-4159.

See, R.H. and Chow, A.H. (1992) *Infect. Immun.* **60** 3456-3459.

See, R.H., Krystal, G., and Chow, A.W. (1990) *Infect. Immun.* **58** 2392-2396.

Seth, A, Stern, L.J., Ottenhoff, T.H.M., Engel, I., Owen, M.J., Lamb, J.R., Klausner, R.D. and Wiley, D.C. (1994) *Nature* (London) **369** 324-327.

Shands, K.N., Schmid, G.P., Dan, B.B., Blum, D., Guidotti, R.J., Hargrett, N.T., Anderson, R.L., Hill, D.L., Broome, C.V., Band, J.D. and Fraser, D.W. (1980) *New. Engl. J. Med.* **303** 1436.

Sixma, T.K., Pronk, S.E., Kalk, K.H., van Zanten, B.A.M., Berghuis, A.M. and Hol, W.G.J. (1992). *Nature* (London) **355** 561-564.

Sixma, T.K., Pronk, S.E., Kalk, K.H., Wartna, E.S., van Zanten, B.A.M., Witholt, B. and Hol, W.G.J. (1991) *Nature* (London) **351** 371-377.

Sloane, R., de Azavedo, J.C.S., Arbuthnott, J.P., Hartigan, P.J., Kreiswirth, B., Novick, R., and Foster, T.J. (1991) *FEMS Microbiol. Lett.* **78** 239-244.

Soos, J.M., Russell, J.K., Jarpe, M.A., Pontzer, C.H. and Johnson, H.M. (1993) *Biochem. Biophys. Res. Comm.* **191** 1211-1217.

Spero, L. and Morlock, B.A. (1978) *J. Biol. Chem.* **253** 8787-8791.

Staneck, J.L., and Bonventre, P.F. (1984) *Surv. Synth. Path. Res.* **3** 38-53.

Stein, P.E., Boodhoo, A., Tyrrell, G.J., Bronton, J.L. and Read, R.J. (1992). *Nature* (London) **355** 748-750.

Stelma, G.N. and Bergdoll, M.S. (1982) *Biochem. Biophys. Res. Comm.* **105** 121-126.

Stuart, D.I., Levine, M., Muirhead, H. and Stammers, D.K. (1979) *J. Mol. Biol.* **134** 109-142.

Sugiyama, H., McKissic, E.M., Bergdoll, M.S. and Heller, B. (1964) *J. Infect. Dis.* **114** 111-118.

Swaminathan, S., Furey, W., Pletcher, J., and Sax, M. (1992) *Nature* (London) **359** 801-806.

Telford, D.R., Morris, J.A. and Hughes, P. (1989) *J. Infect. Dis.* **28** 163-

172.

Todd, J.K., Fishaut, M., Kapral, F & Welch, T. (1978). *Lancet* **2** 1116-1118.

Tranter, H.S. and Brehm, R.D. (1994) *Rev. Med. Microbiol.* **5** 56-64.

Tsukihara, T., Fukuyama, K., Nakamura, M., Katsube, Y., Tanaka, N., Kakudo, M., Wada, K., Hase, T. and Matsubara, H. (1981) *J. Biochem.* (Tokyo) **90** 1763

Turner, T.N., Smith, C.L. and Bohach, G.A. (1992) *Infect. Immunol.* **60** 694-697.

Uchiyama, T., Yan, X-J., Imanishi, A., Kawachi, M., Araake, R., Tachihara, K., Shinagawa, K. and Kanagawa, O. (1991) *Cell. Immunol.* **133** 446-455.

Uchiyama, T., Imanishi., Saito, S., Araake, M., Yan, X.J., Obata, F., Kashiwagi, N and Inoko, H. (1989) *Eur. J. Immunol.* **19** 1803-1809.

Vignali, D.A. and Strominger, J.L. (1994) *J. Exp. Med.* **179** 1945-1946.

jay-Kumar, S., Bugg, C.E. and Cook, W.J. (1987) *J. Mol. Biol.* **194** 531

Vijay-Kumar, S., Bugg, C.E. and Cook, W.J. (1987) *J. Mol. Biol.* **194** 531

Wang, B.C. (1985). *Meth. Enzym* **115** 90-111.

White, J., Pullen, A., Choi, Y., Marrack, P. and Kappler, J.W. (1993) *J. Exp. Med.* **177** 119-125.

White, J., Herman, A., Pullen, A.M., Kubo, R., Kappler, J.W., and Marrack, P. (1989) *Cell* **56** 27-35.

Wolf, W., Evans, P.R. and Leslie, A.G.W. (Eds) in *Isomorphous Replacement and Anomalous Scattering* Proceedings of the Daresbury Study Weekend, 25-26 January 1991.

Wood, S.C. and Holsapple, M.P. (1993) *Fund. Appl. Toxicol.* **20** 280-287.

Yagi, J., Baron, J., Buxser, S and Janeway, C.A. (1990) *J. Immunol.* **144** 892-901.

Zehavi-Willner, T., Shenberg, E. and Barnea, A. (1984) *Infect. Immun.* **44** 401-405.

Reprinted from *J. Mol. Biol.* (1992) **228**, 983–986

Purification, Crystallization and Preliminary X-ray Analysis of Toxic Shock Syndrome Toxin-1 from *Staphylococcus aureus*

Edward F. Passalacqua, Rossalyn D. Brehm, K. Ravi Acharya and Howard S. Tranter

J. Mol. Biol. (1992) **228**, 983–986

Purification, Crystallization and Preliminary X-ray Analysis of Toxic Shock Syndrome Toxin-1 from *Staphylococcus aureus*

Edward F. Passalacqua[1], Rossalyn D. Brehm[2], K. Ravi Acharya[1]† and Howard S. Tranter[2]

[1]*Department of Biochemistry, University of Bath Claverton Down, Bath BA2 7AY, Avon, U.K.*

[2]*Division of Biologics, PHLS Centre for Applied Microbiology and Research Porton Down, Salisbury SP4 0JG, Wiltshire, U.K.*

(Received 28 July 1992; accepted 7 August 1992)

High yields of toxic shock syndrome toxin-1, from *Staphylococcus aureus*, have been purified (>99%) using a novel, simple, two-step procedure involving dye ligand chromatography. Crystals suitable for X-ray diffraction work were obtained by vapour diffusion using ammonium sulphate and polyethylene glycol as precipitants. They belong to the orthorhombic space group $C222_1$, with unit cell dimensions $a = 108{\cdot}6$ Å, $b = 177{\cdot}6$ Å and $c = 97{\cdot}5$ Å, with three molecules per asymmetric unit. The crystals diffract to at least 2·5 Å resolution and are suitable for three-dimensional X-ray structural analysis.

Keywords: toxic shock syndrome toxin-1; toxin purification; dye ligand chromatography; crystallization; X-ray diffraction

Toxic shock syndrome toxin-1 (TSST-1‡) is an extracellular protein produced by some, but not all, strains of *Staphylococcus aureus* (Chesney *et al.*, 1984). It is recognized as the major factor responsible for toxic shock syndrome, an acute life-threatening multisystem disease (Todd *et al.*, 1978). The disease is characterized by high fever, hypotension, scarlatiniform erythematous rash, desquamation of the skin and dysfunction of three or more organs, including the gastro-intestinal tract, liver, kidney, muscles, the blood and the central nervous system. The majority of cases are epidemiologically associated with tampons used in menstruating young women (Shands *et al.*, 1980). However, about 15% to 30% of cases occur in male or female individuals with focal, non-genital wounds or soft tissue infections (Schlievert, 1983). Other toxins such as the staphylococcal exterotoxins A, B and C are also capable of causing toxic shock-like illness (De Azavedo, 1989).

Studies with TSST-1 and the functionally related staphylococcal enterotoxins (SE) have also revealed them to be highly potent polyclonal activators of T cells in the presence of cells bearing class II antigens of the major histocompatability complex (MHC; Wood *et al.*, 1991). The toxins act at nanomolar concentrations and are not processed internally in comparison with nominal antigens. Each toxin type is capable of stimulating a subpopulation of peripheral T lymphocytes possessing a specific variable β (Vβ) gene segment. This property, together with the resultant release of cytokines, is characteristic of a group of molecules called superantigens (Marrack & Kappler, 1990) Currently, these molecules are the subject of intense study as workers attempt to correlate immunological and pathological activity with molecular structure.

TSST-1 is a single-chain polypeptide consisting of 194 amino acid residues; the predicted M_r from the gene sequence is 22,049 (Blomster-Hautamaa *et al.*, 1986), although values of 22,000 to 24,000 have been reported following SDS/polyacrylamide gel electrophoresis (PAGE) of purified protein (Reiser *et al.*, 1983). There is little sequence homology between the SE and TSST-1 based on amino acid or nucleotide data (Blomster-Hautamaa *et al.*, 1986; Goshorn & Schlievert, 1989). Indeed, the absence of cysteine residues and emetic activity can be used to differentiate TSST-1 from the SE. However, TSST-1 and the SE show striking similarities in biological properties that may be a function of the three-dimensional arrangement of the molecular structure of these toxins. Using far ultraviolet light circular dichroism spectra, Singh *et al.* (1988) were able to identify a similarity in secondary structure between TSST-1 and the enterotoxins but there is no

† Author for correspondence.

‡ Abbreviations used: TSST-1, toxic shock syndrome toxin-1; SE, staphylococcal enterotoxins; MHC, major histocompatability complex; SRD, single radial immunodiffusion.

0022-2836/92/230983-04 $08.00/0

information available on the tertiary structure of these molecules. An early report on the crystallization of SEB (Swaminathan *et al.*, 1988) has not revealed an insight on the molecular structure of these toxins. However, more recently the crystallization of SEC3 was reported (Bohach *et al.*, 1992) which identified both triclinic and tetragonal forms of crystal with one toxin molecule per asymmetric unit.

The present study describes the production of diffraction quality crystals of TSST-1 which will be used to determine the three-dimensional structure of this molecule. Such studies, together with similar ones using the SE, may provide information on these toxins to explain their biological relatedness in the absence of any obvious sequence homology. Furthermore, structural information may be useful in studying the binding domains of the toxin with the MHC II complex and T cells especially since the probable three-dimensional structure of the MHC class II molecule has been elucidated (Brown *et al.*, 1988). The toxin in this work was purified by a modification of the dye ligand chromatography method developed initially for the staphylococcal enterotoxins (Reynolds *et al.*, 1988; Brehm *et al.*, 1990). This method is particularly suited for the present study due to its ability to give large amounts of highly purified toxin.

Staphylococcus aureus strain MN8 was used for the production of TSST-1. The strain was grown in medium containing 20·0 g/l of proteose peptone no. 3 (Difco Laboratories) and 20·0 g/l of N-Z amine A (Sheffield Products) adjusted to pH 7·0 and sterilized by autoclaving (121 °C for 20 min). A seed inoculum (400 ml), prepared in a 2 l flask was shaken (200 revs/min) at 37 °C overnight and used to inoculate a 35 l Chemap AG fermenter containing 25 l of the same medium to which 0·03% (final concentration) polypropylene glycol 2000 antifoam (KW; Revai Chemicals Ltd) had been added. The culture was grown in the fermenter for 19 hours with a stirrer speed of 280 revs/min and in the presence of an O_2/CO_2 (1:1) mixture sparged at 2 l/min.

Bacterial cells were removed and the culture filtrate concentrated to 1 l by cross-flow filtration with a Pellicon system (Millipore U.K. Ltd: Brehm *et al.*, 1990). To prevent protease activity and growth contamination during downstream processing, 0·5 M-EDTA was added to the culture filtrate to a final concentration of 2 mM. The concentrated culture supernatant fluid containing 1·5 mg/ml TSST-1 was dialysed overnight at 4 °C against 20 mM-potassium phosphate buffer, pH 6·5.

A portion (300 ml) of the dialysed culture filtrate containing 0·3 g TSST-1 was diluted with 1·5 volumes of 20 mM-phosphate buffer, pH 6·5, and loaded onto a 500 ml Red A column (4·5 cm × 31 cm; Amicon Ltd) which had been pre-equilibrated with 20 mM-phosphate buffer, pH 6·5. The column was washed with 1·4 l of the equilibration buffer followed by the same volume of 60 mM-potassium phosphate buffer, pH 6·5. Toxin

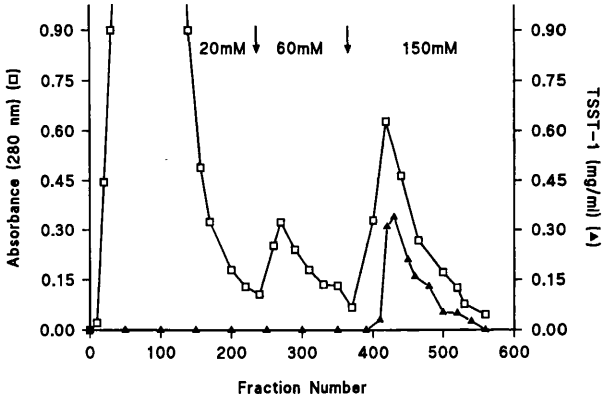

Figure 1. Dye ligand chromatography of TSST-1 on Red A. The column (4·5 cm × 31 cm) was equilibrated in 20 mM-potassium phosphate buffer, pH 6·5, and eluted with a stepwise increase in molarity of phosphate buffer, pH 6·5. Fractions (10 ml) were collected at a flow rate of 40 ml/h (during binding) and 80 ml/h (during elution).

was eluted with 2 l of 150 mM-potassium phosphate buffer, pH 6·5 (Fig. 1). The protein content of fractions was estimated by measuring the A_{280} with a PU 8600 UV/VIS spectrophotometer (Pye-Unicam) and toxin content determined by single radial immunodiffusion (SRD; Meyer & Palmieri, 1980) using polyclonal rabbit anti-TSST-1. Fractions containing toxin were pooled and concentrated by ultrafiltration (Minitan system, Millipore U.K. Ltd) using 10,000 molecular weight cut off membranes (PLGC). Recovery of TSST-1 from the Red A column was estimated to be 80%.

Concentrated toxin fractions collected from the Red A column were refractionated by fast protein liquid chromatography. For this, the fractions were dialysed against 50 mM-sodium acetate buffer, pH 5·0, overnight at 4 °C. After dialysis, 30 ml portions were injected into a 20 ml HiLoad S Sepharose, high performance 16/10 column (Pharmacia), previously equilibrated with 50 mM-sodium acetate buffer, pH 5·0. The column was eluted with a 150 ml linear gradient of increasing NaCl concentration (up to 250 mM) at a flow rate of 2 ml/min. The toxin eluted as a single peak at 170 mM-NaCl in 50 mM-sodium acetate buffer, pH 5·0. All fractions that gave an absorbance (A_{280}) of greater than 0·1 unit were collected and tested (SRD) against anti-TSST-1. After elution the column was regenerated with 30 ml of equilibration buffer containing 1 M-NaCl. The overall process yield was 60%. The purified toxin was dialysed against MilliQ water (18 MΩ cm^{-1}) then 1 mg amounts were put into small vials and lyophilized. The concentration of the pure toxin was determined by using the extinction coefficient $E^{1\%}_{1\,cm}$ of 9·5 at 280 nm (Reiser *et al.*, 1983). Analysis of the final toxin by SDS/PAGE indicated that the toxin was >99% pure (Fig. 2).

Crystals of purified TSST-1 were grown at ambient temperature using the hanging-drop

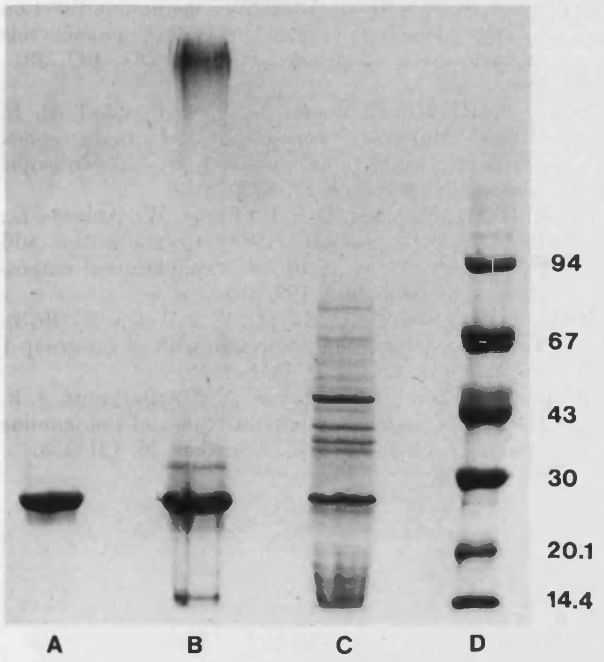

Figure 2. SDS/polyacrylamide gradient (8 to 18%) gel analysis of stages in the purification of TSST-1. Lane A, pooled fractions from fast protein liquid chromatography. Lane B, pooled fractions eluted from Red A. Lane C concentrated culture supernatant fluid. Lane D, molecular mass markers (kDa): phosphorylase b, 94; albumin, 67; ovalbumin, 43; carbonic anhydrase, 30; trypsin inhibitor, 20·1; and α-lactalbumin, 14·4. Lanes A to C were loaded with 10 μl of sample containing 0·5 to 1·0 mg protein per ml.

method (McPherson, 1982) in 24-well Linbro plastic tissue culture plates (Flow Labs). Equal volumes (4 to 5 μl) of purified protein (20 mg/ml) and reservoir solution were mixed on plastic coverslips (Thermanox) and the coverslips inverted over the wells and sealed using silicone grease. Crystals suitable for diffraction were produced when the reservoir solution (1 ml) consisted of 0·1 M-acetate buffer, pH 4·6, with 0·2 M-ammonium sulphate and 23% to 25% polyethylene glycol 3350 (Sigma) as co-precipitants. Parallelepiped crystals appeared between seven and ten days and growth reached a maximum (0·3 mm × 0·4 mm × 0·8 mm) after three weeks (Fig. 3).

Crystals were mounted in a thin walled quartz capillary tube and data were collected on a Siemens area detector mounted on a Rigaku rotating anode X-ray source using CuK_α radiation operating at 50 kV and 80 mA. The crystals were well ordered and diffracted to at least 2·5 Å resolution (1 Å = 0·1 nm) with little sign of decay after exposure for 48 hours. They belong to orthorhombic space group $C222_1$ ($a = 108{\cdot}6$ Å, $b = 177{\cdot}6$ Å, $c = 97{\cdot}5$ Å). Assuming a trimer per asymmetric unit, the specific volume of the protein is 3·55 $Å^3$/Da, which falls within the range normally observed for protein crystals, and corresponds to a 65% (v/v) solvent content (Matthews, 1968).

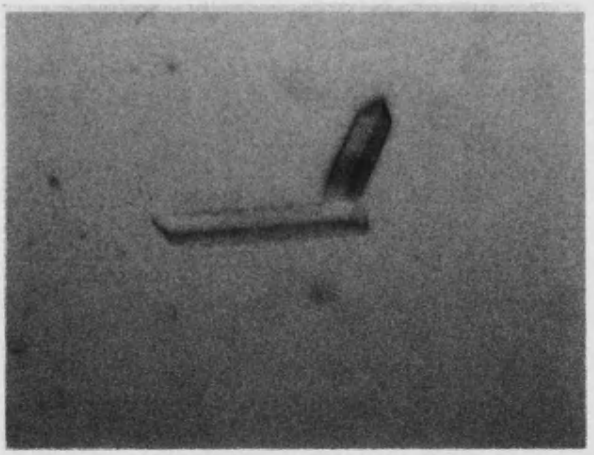

Figure 3. Orthorhombic crystals of toxic shock syndrome toxin-1.

A preliminary 2·8 Å data set has been collected and a search for suitable heavy-atom derivatives is in progress.

We thank the Science & Engineering Council, U.K. for a CASE award to E.F.P. and Professor A. R. Rees for support and encouragement. We acknowledge the technical expertise of Mr Roger Rhind-Tutt and Miss Alison Carter for the fermentation.

References

Blomster-Hautamaa, D. A., Kreiswirth, B. N., Kornblum, J. S., Norvick, R. P. & Schlievert, P. M. (1986). The nucleotide and partial amino acid sequence of toxic shock syndrome toxin-1. *J. Biol. Chem.* **261**, 15783–15786.

Bohach, G. A., Chi, Y.-I. & Stauffacher, C. V. (1992). Crystallisation and preliminary X-ray diffraction analysis of staphylococcal enterotoxin type C. *Proteins*, **13**, 152–157.

Brehm, R. D., Tranter, H. S., Hambleton, P. & Melling, J. (1990). Large-scale purification of staphylococcal enterotoxins A, B and C_2 by dye ligand affinity chromatography. *Appl. Environ. Microbiol.* **56**, 1067–1072.

Brown, J. H., Jardetzky, T., Saper, M. A., Samraoui, B., Bjorkman, P. J. & Wiley, D. C. (1988). A hypothetical model of the foreign antigen binding site of class II histocompatibility molecules. *Nature (London)*, **332**, 845–850.

Chesney, P. J., Bergdoll, M. S., Davis, J. P. & Vegeront, J. M. (1984). The disease spectrum, epidemiology and etiology of toxic-shock syndrome. *Annu. Rev. Microbiol.* **38**, 315–338.

De Azavedo, J. C. S. (1989). Animal models for toxic shock syndrome: overview. *Rev. Infect. Dis.* **11**, (Suppl. 1), S205–209.

Goshorn, S. C. & Schlievert, P. M. (1989). Bacteriophage association of streptococcal pyrogenic exotoxin type C. *J. Bacteriol.* **171**, 3068–3073.

Marrack, P. & Kappler, P. (1990). The staphylococcal enterotoxins and their relatives. *Science*, **248**, 705–711.

Matthews, B. W. (1968). Solvent content of protein crystals. *J. Mol. Biol.* **33**, 491–497.

McPherson, A. (1982). In *The Preparation and Analysis of Protein Crystals*. John Wiley & Sons, New York.

Meyer, R. F. & Palmieri, M. J. (1980). Single radial immunodiffusion method for screening staphylococcal isolates for enterotoxin. *Appl. Environ. Microbiol.* **40**, 1080–1085.

Reiser, R. F., Robbins, R. N., Khoe, G. P. & Bergdoll, M. S. (1983). Purification and some physiochemical properties of toxic shock toxin. *Biochemistry*, **22**, 3907–3912.

Reynolds, D., Tranter, H. S., Sage, R. D. & Hambleton, P. (1988). Novel method for purification of staphylococcal enterotoxin A. *Appl. Environ. Microbiol.* **54**, 1761–1765.

Sands, K. N., Schmid, G. P., Dan, B. B., Guidotti, R. J., Hargrett, N. T., Anderson, R. L., Hill, D. L., Broome, C. V., Band, J. D. & Fraser, D. W. (1980). Toxic shock syndrome in menstruating women: its association with tampon use and *Staphylococcus aureus* and the clinical features in 52 cases. *New Eng. J. Med.* **303**, 1436–1442.

Schlievert, P. M. (1983). Alteration of immune function by staphylococcal pyrogenic exotoxin C: possible role in toxic-shock syndrome. *J. Infect. Dis.* **147**, 391–398.

Singh, B. R., Kokan-Moore, N. P. & Bergdoll, M. S. (1988). Molecular topography of toxic shock syndrome toxin 1 as revealed by spectroscopic studies. *Biochemistry*, **27**, 8730–8735.

Swaminathan, S., Yang, D. S. C., Furey, W., Abrams, L., Pletcher, J. & Sax, M. (1988). Crystallization and preliminary X-ray study of staphylococcal enterotoxin B. *J. Mol. Biol.* **199**, 397.

Todd, J. K., Fishaut, M., Kapral, F. & Welch, T. (1978). Toxic shock syndrome associated with phage-group-1 *staphylococci*. *Lancet*, ii, 1116–1118.

Wood, A. C., Todd, I., Cockayne, A. & Arbuthnott, J. P. (1991). Staphylococcal enterotoxins and the immune system. *FEMS Microbiol. Immunol.* **76**, 121–133.

Edited by A. Klug

Reprinted from *J. Mol. Biol.* (1993) **233**, 170–172

Crystallization and Preliminary X-ray Analysis of a Microbial Superantigen Staphylococcal Enterotoxin C2

Edward F. Passalacqua, Rossalyn D. Brehm, K. Ravi Acharya and Howard S. Tranter

J. Mol. Biol. (1993) **233**, 170–172

Crystallization and Preliminary X-ray Analysis of a Microbial Superantigen Staphylococcal Enterotoxin C2

Edward F. Passalacqua[1], Rossalyn D. Brehm[2], K. Ravi Acharya[1]† and Howard S. Tranter[2]

[1]*Department of Biochemistry, University of Bath Claverton Down, Bath, Avon BA2 7AY, U.K.*

[2]*Division of Biologics, PHLS Centre for Applied Microbiology and Research, Porton Down Salisbury, Wilts SP4 0JG, U.K.*

(Received 16 April 1993; accepted 26 April 1993)

High yields of staphylococcal enterotoxin C2, from *Staphylococcus aureus*, have been purified using dye ligand chromatography. Crystals suitable for X-ray diffraction work were obtained by vapour diffusion using ammonium sulphate and polyethylene glycol as precipitants. They belong to the tetragonal space group $P4_122$ with unit cell dimensions $a=b=43{\cdot}2$ Å and $c=290{\cdot}9$ Å with one molecule per asymmetric unit. The crystals diffract to at least 2·8 Å resolution and are suitable for three-dimensional X-ray structural analysis.

Keywords: Staphylococcal enterotoxin; crystallization; X-ray diffraction; superantigen

The staphylococcal enterotoxins (SEs‡) are a family of structurally related proteins produced by *Staphylococcus aureus* which cause food poisoning and various forms of gastro-intestinal illness (Bergdoll, 1990). The toxins may also be involved in other forms of acute disease because of their ability to induce lymphocyte mitogenesis, immunosuppression, cytokine production, fever and to enhance endotoxin shock, properties they share with the pyrogenic toxins (SPEs) produced by *Streptococcus pyrogenes* (Alouf *et al.*, 1991). Collectively these toxins are known also as microbial superantigens because of their ability to stimulate T cells bearing particular T-cell receptor Vβ regions (Kappler *et al.*, 1989). Recently it has been shown that class II major histocompatibility complex (MHC) molecules are the specific receptors responsible for antigen presentation to the T cells (Fraser, 1989); unlike classically presented antigens however, the SEs are not processed prior to binding (Fleischer & Schrezenmeier, 1988).

The SEs can be classified into five serologically distinct groups SE (A to E) with molecular masses in the range 27 to 30 kDa. Due to differences in minor epitopes SEC can be subdivided into SEC1, SEC2 and SEC3 (Bergdoll, 1979). An examination of amino acid sequences has revealed a high degree of homology, ranging from 30 to 86%, among the toxins (Marrack & Kappler, 1991). SEA is more related to SED and SEE whereas SEB has greater homology with SEC. Until recently all attempts to assign biological activity to areas within the enterotoxin molecules had come from the use of synthetic peptides (Pontzer *et al.*, 1989) or interpretation of secondary structure from circular dichroism and tryptophan quenching studies (Singh *et al.*, 1988; Singh & Betley, 1989). However the crystal structure of SEB has just been reported (Swaminathan *et al.*, 1992) which consists of two domains within the enterotoxin molecule and provides information concerning the stereochemistry of putative MHC II and T cell receptor binding sites. Recently conditions for the crystallization of SEC3 have been reported (Bohach *et al.*, 1992) together with those for crystallization of toxic shock syndrome toxin-1, a toxin which shares similar biological properties with the enterotoxins but has very little sequence homology (approx. 24%; Passalacqua *et al.*, 1992). The X-ray crystallographic studies on these toxins should provide information on the three-dimensional structure of the molecules which would enable the identification of areas of common structural features within the different toxins. In this communication we describe the production of crystals of SEC2 suitable for X-ray diffraction.

† Author to whom all correspondence should be addressed.

‡ Abbreviations used: SE, staphylococcal enterotoxin; MHC, major histocompatibility complex.

0022-2836/93/170170-03 $08.00/0

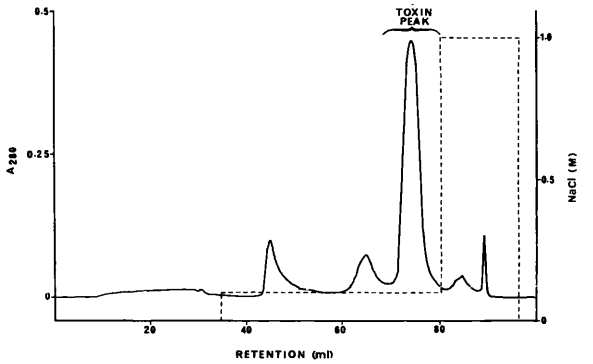

Figure 1. Final purification of SEC2 by FPLC after initial chromatography on Red A. The column (20 ml) HiLoad S Sepharose, high performance 16/10 (Pharmacia) was equilibrated with 50 mM sodium acetate buffer (pH 5·0). Toxin was eluted using 100 mM NaCl in 50 mM sodium acetate buffer (pH 5·0) at a flow rate of 2 ml/min. (——, A_{280}; – – – –, NaCl concentration).

These crystals will be used to determine the three-dimensional structure of the SEC2 molecule and define regions of antigenic variability known to exist among the SEC molecules.

Staphylococcal enterotoxin C2 was produced during the fermentation of *S. aureus* 361 (supplied by M. S. Bergdoll, Food Research Institute, Department of Food Science and Industry, University of Wisconsin, Madison) in a 15 litre Biostat E fermenter as previously published (Brehm *et al.*, 1990). Toxin was initially purified from concentrated spent culture fluid by dye ligand chromatography on Red A gel (Amicon Ltd.). For crystallization the toxin was refractionated by fast protein liquid chromatography. Toxin was dialysed overnight at 4 °C against 50 mM sodium acetate buffer (pH 5·0) and 20 ml portions were injected onto a 20 ml HiLoad S Sepharose, high performance 16/10 column (Pharmacia) previously equilibrated with the same buffer. The column was eluted with 100 mM NaCl in 50 mM sodium acetate buffer (pH 5·0) at a flow rate of 2 ml/min. All fractions that gave an absorbance (A_{280}) of >0·1 unit were collected and tested in a single radial immunodiffusion test using rabbit anti-SEC2 (Meyer & Palmieri, 1980). Toxin eluted as the major peak (Fig. 1) and after dialysis against MilliQ water (18 MΩ cm^{-1}) was distributed (2 mg) into small vials, lyophilized and stored at −20 °C. After elution the column was regenerated with 16 ml of euqilibration buffer containing 1 M NaCl. Analysis of the final toxin by SDS PAGE indicated that the toxin was >99% pure.

Crystals of purified SEC2 were grown at ambient temperature using the hanging drop method (McPherson, 1982) in 24-well Linbro plastic tissue culture plates (Flow Labs). Equal volumes (3 to 5 μl) of the protein (2 mg/ml) and reservoir solution were mixed on plastic coverslips (Thermanox) and the coverslips inverted over the wells and sealed using silicone grease. Crystals suitable for diffraction were produced when the reservoir solution (1 ml) consisted of 0·1 M cacodylate buffer (pH 6·5) with 0·15 M ammonium sulphate, 0·02% sodium azide and 25 to 28% polyethylene glycol 8000 (Sigma) as co-precipitants. Rectangular crystals appeared between 3 and 4 weeks and growth reached a maximum (0·3 mm × 0·4 mm × 0·8 mm) after 6 to 8 weeks.

Crystals were mounted in a thin walled quartz capillary tube and data collected on a Siemens area detector mounted on a Siemens rotating anode X-ray source using CuK_α radiation operating at 50 kV and 76 mA. The crystals were well ordered and diffracted to at least 2·8 Å resolution with little sign of decay after exposure for 50 hours. They belong to tetragonal space group $P4_122$ ($a=b=$ 43·2 Å, $c=290·9$ Å). Assuming a monomer per asymmetric unit, the specific volume of the protein is 2·46 $Å^3$/Da, which falls within the range normally observed for protein crystals, and corresponds to a 50% (v/v) solvent content (Matthews, 1968).

A preliminary 2·9 Å data set has been collected and a search for suitable heavy atom derivatives is in progress.

We thank the Science & Engineering Research Council, U.K. for a CASE award to E.F.P. and Professor A. R. Rees and Dr P. Hambleton for support and encouragement. We acknowledge the technical expertise of Mr Roger Rhind-Tutt and Miss Alison Carter for the fermentations.

References

Alouf, J. E., Knoll, H. & Kohler, W. (1991). The family of mitogenic, shock-inducing and superantigenic toxins from staphylococci and streptococci. In *Sourcebook of Bacterial Protein Toxins* (Alouf, J. E. & Freer, J. H., eds), pp. 367–414, Academic Press, London.

Bergdoll, M. S. (1979). Staphylococcal intoxications. In *Foodborne Infections and Intoxications* (Reimann H. & Bryan, F. L., eds), pp. 443–494, Academic Press, New York.

Bergdoll, M. S. (1990). Mechanisms of action, diagnostic and rapid methods of analysis of *Staphylococcus aureus* enterotoxins. In *Microbial Toxins in Foods and Feeds* (Pohland, A. E., Dowell, V. R. & Richard, J. L., eds), pp. 45–56, Plenum Press, New York & London.

Bohach, G., Chi, Y.-I. & Stauffacher, C. V. (1992). Crystallisation and preliminary X-ray diffraction analysis of staphylococcal enterotoxin type C. *Proteins*, **13**, 152–157.

Brehm, R. D., Tranter, H. S., Hambleton, P. & Melling, J. (1990). Large-scale purification of staphylococcal enterotoxins A, B and C_2 by dye ligand affinity chromatography. *Appl. Environ. Microbiol.* **56**, 1067–1072.

Fleischer, B. & Schrezenmeier, H. (1988). T-cell stimulation by staphylococcal enterotoxins. Clonally variable response and requirement for major histocompatibility complex II molecules on accessory or target cells. *J. Exptl Med.* **167**, 1697–1708.

Fraser, J. D. (1989). High affinity binding of staphylococcal enterotoxins A and B to HLA-DR. *Nature (London)*, **339**, 221–223.

Marrack, P. & Kappler, J. (1991). The staphylococcal enterotoxins and their relatives. *Science*, **248**, 705–711.

Matthews, B. W. (1968). Solvent content of protein crystals. *J. Mol. Biol.* **33**, 491–497.

McPherson, A. (1982). *The Preparation and Analysis of Protein Crystals*, John Wiley & Sons, New York.

Meyer, R. F. & Palmieri, M. J. (1980). Single radial immunodiffusion method for screening staphylococcal isolates for enterotoxin. *Appl. Environ. Microbiol.* **40**, 1080–1085.

Kappler, J., Kotzin, B., Herron, L., Gelfand, E. W., Bigler, R. D., Boylston, A., Carrel, S., Posnett, D. N., Choi, Y. & Marrack, P. (1989). V beta-specific stimulation of human T cells by staphylococcal toxins. *Science*, **244**, 811–813.

Passalacqua, E. F., Brehm, R. D., Acharya, K. R. & Tranter, H. S. (1992). Purification and crystallisation of toxic shock syndrome toxin-1 from *Staphylococcus aureus*. *J. Mol. Biol.* **228**, 983–986.

Pontzer, C. H., Russell, J. K. & Johnson, H. (1989). Localisation of an immune functional site on staphylococcal enterotoxin A using the synthetic peptide approach. *J. Immunol.* **143**, 280–284.

Singh, B. R. & Betley, M. J. (1989). Comparative structural analysis of staphylococcal enterotoxins A and E. *J. Biol. Chem.* **264**, 4044–4411.

Singh, B. R., Kokan-Moore, N. P. & Bergdoll, M. S. (1988). Molecular topography of toxic shock syndrome toxin 1 as revealed by spectroscopic studies. *Biochemistry*, **27**, 8730–8735.

Swaminathan, S., Furey, W., Pletcher, J. & Sax, M. (1992). Crystal structure of staphylococcal enterotoxin B, a superantigen. *Nature (London)*, **359**, 801–805.

Edited by A. Klug

Structural basis of superantigen action inferred from crystal structure of toxic-shock syndrome toxin-1

K. Ravi Acharya*, Edward F. Passalacqua*, E. Yvonne Jones†, Karl Harlos†, David I. Stuart†, Rossalyn D. Brehm‡ & Howard S. Tranter‡

* School of Biology and Biochemistry, University of Bath, Claverton Down, Bath BA2 7AY, UK
† Oxford Centre for Molecular Sciences and Laboratory of Molecular Biophysics, Rex Richards Building, South Parks Road, Oxford OX1 3QU, UK
‡ Division of Biologics, PHLS Centre for Applied Microbiology and Research, Porton Down, Salisbury SP4 0JG, UK

SUPERANTIGENS stimulate T cells bearing particular T-cell receptor *Vβ* sequences[1,2], so they are extremely potent polyclonal T-cell mitogens. T-cell activation is preceded by binding of superantigens to class II major histocompatibility complex (MHC) molecules[3]. To further the structural characterization of these interactions, the crystal structure of a toxin associated with toxic-shock syndrome, TSST-1, which is a microbial superantigen, has been determined at 2.5 Å resolution. The N- and C-terminal domains of the structure both contain regions involved in MHC class II association; the C-terminal domain is also implicated in binding the T-cell receptor. Despite low sequence conservation, the TSST-1 topology is similar to the structure reported for the superantigen staphylococcal enterotoxin B[4]. But TSST-1 lacks several of the structural features highlighted as central to superantigen activity in the staphylococcal enterotoxin B and we therefore reappraise the structural basis of superantigen action.

Toxic-shock syndrome toxin-1 (TSST-1) is secreted by *Staphylococcus aureus* and is important in the genesis of human toxic-shock syndrome[5]. The protein has 194 residues and is

monomeric in solution (data not shown). The crystal structure determination is described in Table 1. The two domains of TSST-1 are packed tightly together to form a compact molecule of dimensions ~45 × 45 × 58 Å^3 (Fig. 1). After a short N-terminal portion, which spans the domain interface and includes an α-helix (α1), the polypeptide folds in a continuous 'roll' of β-strands (β1 − β5) to form the distinctive β-barrel of the N-terminal domain. This motif has also been noted in four other proteins of unrelated sequence[6], including two bacterial toxins, the heat-labile toxin and verotoxin-1 from *Escherichia coli*. A piece of extended chain caps one end of the β-barrel in TSST-1, replacing the α-helix observed in the other structures. However, the topology and positioning of the structural elements is conserved (Fig. 1). In TSST-1, the concave β1β2β3 face of this domain is distinguished by a prominent clustering of solvent-accessible hydrophobic residues (Fig. 2*a*). The C-terminal domain is composed of one particularly long α-helix (α2) with a highly twisted β-sheet (β6–β12) cupped around it (Fig. 2*b*). As the N-terminal domain packs against the other face of α2, this helix serves as the 'backbone' of the molecule. The overall topology of the C-terminal domain is unique so far to the microbial superantigens, although it may be considered to be an elaborated form of the β-grasp motif[6].

Figure 2*a* shows the buried residues of TSST-1 and, on the basis of the structure, possible linear epitopes can be suggested. Data for the location of biologically active sites on TSST-1 are related to the structure shown in Fig. 3*a* and *b*. Two results are specific for MHC class II binding. A peptide corresponding to residues 58–78, which reacts with neutralizing monoclonal antibodies against whole TSST-1 and demonstrates some of the immunoregulatory properties of the whole molecule, has been implicated in binding to MHC class II molecules[7]. Similarly, peptides 39–68 and 155–194 have been reported to compete with whole TSST-1 for MHC class II binding[8]. Thus, many of the data on specific binding to MHC class II molecules centre on residues 39–78 in the N-terminal β-barrel domain. In contrast, a C-terminal 12K fragment (M_r 12,000; residues 88–194, in effect the C-terminal domain) of TSST-1 has been reported to have mitogenic activity and to contain the epitope for antibody 8-5-7, which is able to neutralize the major clinical signs of toxic-shock syndrome[9,10]. As superantigen/MHC class II binding is a prerequisite of subsequent T-cell antigen receptor (TCR) binding and mitogenic activity, this fragment must retain some MHC class II binding affinity in addition to the TCR binding site. Site-directed mutagenesis[11–13] has implicated residues Tyr 115, Glu 132, His 135, Ile 140, His 141 and Tyr 144 in mitogenic activity. Tyrosine 115 is exposed to solvent in the β7β8 loop and as mutation to alanine abrogates antibody 8-5-7 binding, it appears to contribute directly to this key neutralizing epitope. Glutamic acid 132, His 135 and Ile 140 are all located on helix α2 and are exposed to solvent. It has been reported[12] that replacement of residue His 135 by alanine abolishes mitogenic activity, although the mutant protein is still recognized by antibody 8-5-7. Residues 141 and 144 are both buried, and mutation of these residues may well result in conformational changes influencing the nature of the molecular surface in the region of the α2β9 loop (situated above Tyr 115 in the orientation of Fig. 3*a*, *b*). The extent of such changes is not sufficient to impinge on the 8-5-7 epitope for His 141 but may be for the deeply buried Tyr 144 (ref. 11). In total, the available data for the superantigenic activity of TSST-1 appear to cluster into two sites, one (site A) involving the concave face of the N-terminal β-barrel, the other (site B) containing α2 and the β7β8 and α2β9 loops in the C-terminal domain. Site A is associated with MHC class II binding. But as the C-terminal domain alone[9], and a portion of the polypeptide chain between residues 155 and 194 in particular, have also been implicated in MHC binding[8], we predict that the residues between 170 and 180, where the chain packs closely against the concave face of the N-terminal β-barrel (Fig. 3*a*, *b*), form part of site A. Data for site B do not distinguish between MHC class II or TCR binding, but we suggest that its position (diametrically opposed on the TSST-1 molecule to site A) makes it the likely site of TCR interaction.

TSST-1 shares little amino-acid sequence identity (~24%) with the staphylococcal enterotoxins (SEs: SEA–SEE) but shares similar biological functions. A comparison on the basis of secondary structure assignments is shown for TSST-1 and SEB in Fig. 2*b*. The smaller protein, TSST-1, has the same core topology as SEB but is extensively truncated in several loop

TABLE 1 Statistics for crystallographic structure determination

Diffraction data

Dataset	d_{min} (Å)	No. of measurements	Unique reflections (% complete)	R_{merge} (all data)	MFID
Native (IP Lab 1)	3.5	20,717	11,231 (94)	7.5	—
Native (IP Lab 2)	2.5	49,530	29,155 (87)	7.5	—
Native (IP Lab 1+2)	2.5	70,247	30,007 (89)	8.6	—
Uranyl acetate	3.5	11,104	9,186 (77)	8.4	29.9
Uranyl fluoride	3.5	13,938	10,536 (88)	4.5	17.1

MIR phasing

Derivative	No. of sites	R_c to 6.0 Å (3.5 Å)	Phasing power to 6.0 Å (3.5 Å)
Uranyl acetate (10 mM)	5	0.55	1.9
Uranyl fluoride (10 mM)	3	0.49 (0.56)	2.1 (1.7)

Solvent flattening

d_{min} (Å)	Pre-Wang FM	% Solvent	Wang R factor	Phase change	Wang FM
6.0	0.60	65	26.3	41.3°	0.78
3.5	—	65 (55)	22.6 (18.7)	50.5° (48.3)	0.77 (0.80)

TSST-1 was purified and crystallized as described[24]. The crystals belong to orthorhombic space group $C222_1$ (cell dimensions a=108.6, b=177.6, c=97.5 Å) with 3 molecules per asymmetric unit, but possess pseudo-hexagonal symmetry space group $P6_322$ (cell dimensions $a=b$=104.1, c=97.5 Å; with 1 molecule per asymmetric unit). Diffraction data from native crystals (3.5 Å and 2.5 Å resolution) and from two heavy-atom derivatives (3.5 Å resolution) were collected using an MAR-research imagining-plate system with CuK_α X-rays generated by a Rigaku RU200 rotating anode with a graphite monochromator. Data were processed using the MOSFLM package (A. Leslie) ($R_{merge}=\sum(|I_{obs}-\bar{I}|)/\sum\bar{I}$; MFID, mean fractional isomorphous difference). Heavy-atom sites were identified using the automatic Patterson search program GROPAT[25] and difference Fourier analyses. Heavy-atom parameters were refined and MIR phases calculated using the programs REFINE and PHASE (P. Shaw, unpublished) respectively (R_c: Cullis R-factor for centric reflections; phasing power: mean value of the heavy-atom structure factor amplitudes divided by the residual lack-of-closure error). The MIR phases were improved by solvent flattening (65% solvent) to give a 3.5 Å electron density map from which we established the relationship between the non-crystallographically related molecules. The pseudo-symmetry arises because the orthorhombic asymmetric unit contains one half of a crystallographic dimer and one non-crystallographic dimer arranged on a pseudo-hexagonal net (FM, mean figure of merit; Wang R factor, crystallographic R factor between observed structure factor amplitudes and those calculated from the solvent-flattened map; phase change, difference between MIR phases and phases from the solvent flattened map). *Ab initio* phase extension to 2.5 Å was achieved using the GAP program suite (D.I.S. and J. Grimes, unpublished) by 3-fold real-space averaging, which resulted in an R-factor and correlation coefficient of 0.31 and 0.91, respectively, between observed data and data obtained by inversion of the averaged solvent-flattened map. Owing to the 3-fold averaging, the 2.5 Å resolution electron density map was quite clear. Initially a skeletal model for one monomer (all 194 residues) was fitted to the 2.5 Å electron density map (program FRODO[26]) and the appropriate amino-acid sequence incorporated using the program CALPHA (R. Esnouf, unpublished). The structure was refined by simulated annealing with strict non-crystallographic symmetry constraints (program XPLOR[27]). In the final round, the non-crystallographic constraints were relaxed and the 3 molecules were individually checked and refined with non-crystallographic restraints. The current model, which includes 4,677 non-hydrogen atoms (for 3 molecules), has a crystallographic R factor of 0.213 for all data to 2.5 Å (15.6% for $F\geqslant3\sigma$). No bound waters have been modelled, although a correction for the bulk solvent has been made. The root-mean-square (r.m.s.) deviation from ideal values for bond lengths is 0.011 Å and for bond angles is 2.68°. The r.m.s. deviation of atomic coordinates for all atoms between monomer pairs 1–2, 1–3 and 2–3 are 0.13, 0.15, 0.15 Å, respectively. With the exception of Ser 86 (ϕ=61°, ψ=−157°), main-chain torsion angles for all residues lie within allowed regions of the Ramachandran plot. Atomic coordinates will be deposited in the Brookhaven Protein Data Bank.

regions, including some that incorporate secondary structure elements. Thus there are no structural equivalents in TSST-1 for much of the SEB N-terminal region, including SEB α1. Similarly, helices α3 and α5, situated in loops between β3β4 and β10β11 in SEB, are respectively lost and truncated to a single turn of 3_{10} helix in TSST-1, whereas the β2β3 and β4β5 loops are markedly shorter. This latter loop is often referred to as the 'cysteine loop' of the SEs, and residues in this region have been implicated in SE emetic activity[14]. The lack of emetic activity in TSST-1 is consistent with the marked difference we observe between TSST-1 and SEB structures in this region. The many alterations in TSST-1 as compared with SEB, particularly in the N-terminal region and SEB α5, both of which are situated at the domain interface, also have considerable bearing on the superantigenic sites, as predicted from inspection of the SEB structure[4]. Inhibition of intact SEA by synthetic peptides has implicated the N-terminal domain of SEA in MHC class II binding[15,16]. Mutagenesis[17] of the solvent-accessible Asn 23 of SEB implicates α2 of that molecule in TCR binding. Data from the same study for the exposed hydrophobic residue Phe 44 (in SEB) associate the β1β2 turn with MHC class II binding. This study also demonstrated $V\beta$-specific binding effects at the tip of the β2β3 loop and some MHC class II binding dependency on α1 (SEB); these areas have no structural equivalents in TSST-1. In SEA, mutants that affect $V\beta$ specificity[18] map onto residues just preceding the start of α5 in SEB; again, there are no structural equivalents in TSST-1. With the exception of Asn 23 (SEB), mutations in SEA and SEB reported to affect TCR binding abrogate binding to only some of the $V\beta$ elements known to recognize the native protein.

Many of the detailed elements of both TCR and MHC binding sites appear to be altered between TSST-1 and the SE family, as represented by SEB. Overall, the evidence for MHC class II binding to these microbial superantigens focuses onto the front (α5 in SEB) face of the molecule (Fig. 3*a*, *b*), which includes the concave surface of the β1β2β3 sheet in the N-terminal domain. It is therefore of particular interest that this surface, delineated by the β1β2, β3β4 and β4β5 loops, is the site of oligonucleotide or oligosaccharide binding in the structurally analogous domains of other proteins[6]. The specific site of TCR binding involves several amino acids on the top and back (α4 in SEB) face of the molecule (Fig. 3*a*, *b*) and appears to vary between different superantigens and/or different TCR $V\beta$ variants.

Any discussion of superantigen binding must consider the structure of the MHC class II and TCR molecules. MHC class II/superantigen binding is believed to involve regions to the side of the antigen-binding cleft[19,20]. Superantigen binding to the TCR is thought to be to the solvent-exposed face of a β-sheet (the BED β-sheet) in the $V\beta$ component of the TCR $V\alpha V\beta$ dimer[21,22]. Combination of these observations with a model for the MHC/TCR antigen recognition complex enables us to represent superantigen action schematically (Fig. 3*c*)[23]. Figure 3*d* shows that these proposed sites of interaction between TSST-1 and the MHC and TCR molecules are entirely consistent with such a model. In the absence of high-resolution evidence for the structure of the ternary complex, such models may prove helpful for understanding the microbial superantigen mechanism of pathogenicity and enable therapeutic compounds to be engineered that target appropriate epitopes derived from the molecular structures of these toxins. □

FIG. 1 The polypeptide fold for TSST-1. Helices are coloured red (3_{10} helices being drawn more thinly than α-helices), β-strands green and loops yellow. Blue and red balls represent N and C termini, respectively.

a

```
          1        10        20        30        40        50
TSST-1  STNDNIKDLL DWYSSGSDTF TNSEVLDNSL GSMRIKNTDG SISLIIFPSP
          *   * **   ** ***     * **       * * * ** *** *   *
              <---------> <-----------> <-----> <----->
                  α1          β1          β2        β3

         51        60        70        80        90       100
          YYSPAFTKGE KVDLNTKRTK KSQHTSEGTY IHFQISGVTN TEKLPTPIEL
                    *** **     *       * ** ******          *
                  <-----------------> <----------->
                           β4              β5

        101       110     + 120       130  +  +    + +  +  150
          PLKVKVHGKD SPLKYWPKFD KKQLAISTLD FEIRHQLTQI HGLYRSSDKT
           * * *            *    *  ******* * ** ***   **** *
          <-----> <-->       <-----><----------------->
            β6     β7          β8          α2

        151       160       170       180       190  194
          GGYWKITMND GSTYQSDLSK KFEYNTEKPP INIDEIKTIE AEIN
            * ***       * *         *   * * *  **
          <-----> <----->     <---> <-><-><-------->
            β9      β10       3₁₀-1  β11 ↑   β12
                                     3₁₀-2
```

b

SEB		TSST-1	
Secondary structure	Residues	Secondary structure	Residues
α1	12-17	-	-
α2	21-29	α1	7-15
β1	33-39	β1	18-29
β2	48-52	β2	32-37
β3	63-68	β3	41-47
α3	70-78	-	-
β4	81-89	β4	60-75
β5	112-120	β5	79-89
β6	127-138	β6	101-106
β7	141-151	β7	109-111
β8	154-156	β8	119-124
α4	157-172	α2	125-140
β9	182-190	β9	152-158
β10	195-200	β10	161-166
α5	210-217	3_{10}-1	173-177
β11	222-225	β11	181-182
-	-	3_{10}-2	183-185
β12	229-236	β12	186-193

FIG. 2 *a*, Amino-acid sequence of TSST-1. Positions of the secondary structural elements in TSST-1 (based on program DSSP) are indicated, and solvent-inaccessible residues (less than 20 Å^2) of exposed surface) are indicated by asterisks. Residues implicated in mitogenic activity (based on site-directed mutagenesis) are represented by plus signs. *b*, Comparison of the secondary structural elements for SEB[4] and TSST-1.

Received 8 June; accepted 2 November 1993.

1. White, J. *et al. Cell* **56,** 27–35 (1989).
2. Janeway, C. A. *et al. Immun. Rev.* **107,** 61–88 (1989).
3. Fleischer, B. & Schrezenmeier, H. *J. exp. Med.* **167,** 1697–1707 (1988).
4. Swaminathan, S. *et al. Nature* **359,** 801–806 (1992).
5. Marrack, P. & Kappler, J. *Science* **248,** 705–711 (1990).
6. Murzin, A. G. *Nature* **360,** 635 (1992).
7. Edwin, C. *et al. J. infect. Dis.* **163,** 524–529 (1991).
8. Şoos, J. M. *et al. Biochem. biophys. Res. Commun.* **191,** 1211–1217 (1993).
9. Edwin, C. & Kass, E. H. *Infect. Immun.* **57,** 2230–2236 (1989).
10. Bonventre, P. F. *et al. Infect. Immun.* **56,** 135–141 (1988).

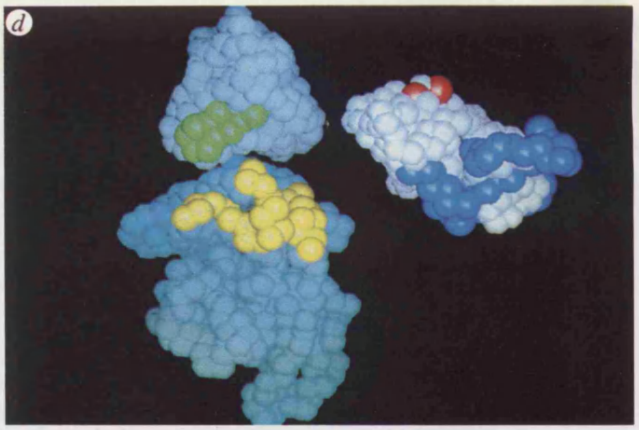

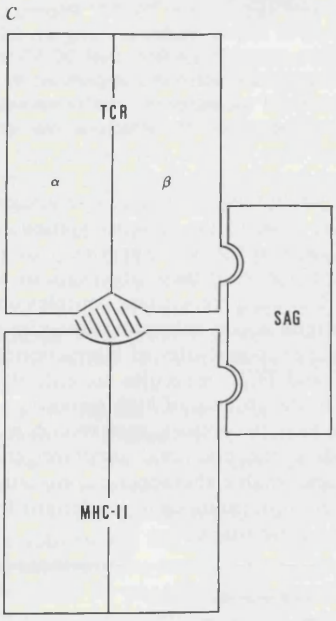

FIG. 3 MHC class II and TCR binding to TSST-1. *a* and *b*, Residues on TSST-1 implicated in these interactions. In *a*, the molecule is viewed as in Fig. 1; in *b*, the molecule has been rotated by 180° about a vertical axis. The regions implicated by peptide data in MHC class II binding are coloured yellow (residues 39–78) and green (residues 155–194)[8], the rest of the molecule in blue. Residues implicated in mitogenic activity (based on mutational analysis[11–13]) are highlighted in red. The cyan and green balls represent the N and C termini, respectively. *c*, Standard schematic representation of superantigen (SAG) function (cross-hatched region represents the MHC-bound peptide). *d*, Possible model for the interaction of TSST-1 with MHC and TCR molecules. The interacting faces of both the MHC–TCR complex and the TSST-1 are revealed by (opposed) 90° rotations of each about a vertical axis. The mid-blue, pale blue and white space-filled objects represent the MHC molecule, the TCR molecules ($V\alpha$ and $V\beta$ domains), and the TSST-1 molecule, respectively. The MHC/TCR interactions are modelled after ref. 28 using MHC class I and immunoglobulin light-chain dimer as representative coordinates. The yellow area on the MHC molecule maps the location of the regions α40 to α50 and β81 to β90. Such an area is consistent with available data on superantigen binding[19,20] but places particular emphasis on residues around one end of the peptide-binding cleft. The green region of the TCR molecule marks the DE loop on the external β-sheet surface of the $V\beta$ domain[29]. Two opposed sites on the TSST-1 molecule, site A (represented by residues 39–78 and 170–180) and site B (indicated by residues 115, 132, 135 and 140), which we propose interact with the MHC class II and TCR molecules, are highlighted in dark blue and red, respectively. This model merely serves to relate gross structural features; data are drawn from studies using several different superantigens so details of binding are expected to vary. However, to within the low resolution of this exercise, such superantigen interactions are compatible with the standard models of MHC/TCR complex formation. Our model involves superantigen binding at a site on the end of the MHC class II molecule peptide-binding cleft opposite the region (β49 to β55) recently implicated in MHC class II dimerization[30]. The side of the MHC class II molecule proposed[30] as the binding site of CD4 also remains accessible in our model. Thus, this form of superantigen binding could simply act as an additional stabilizing component in the multimolecular aggregations of MHC class II, TCR and CD4 molecules proposed by Brown *et al.*[30].

11. Blanco, L. *et al. Infect. Immun.* **58,** 3020–3028 (1990).
12. Bonventre, P. F. *et al. Infect. Immun.* **61,** 793–799 (1993).
13. Murray, D. L. *et al.* Abstr. *93rd gen. Mtg Am. Soc. Microbiol.*, Atlanta, Georgia, 64 (1993).
14. Spero, L., Johnson-Winegar, A. & Schmidt, J. J. in *Bacterial Toxins, Handbook of Natural Toxins* Vol. 4 (eds Hardegree M. C. & Tu A. T.) 131–163 (1988).
15. Griggs, N. D. *et al. J. Immun.* **148,** 2516–2521 (1992).
16. Pontzer, C. H., Russell, J. K. & Johnson, H. M. *Proc. natn. Acad. Sci. U.S.A.* **88,** 125–128 (1991).
17. Kappler, J. W. *et al. J. exp. Med.* **175,** 387–396 (1992).
18. Irwin, M. J. *et al. Nature* **359,** 841–843 (1992).
19. Braunstein, N. S. *et al. J. exp. Med.* **175,** 1301–1305 (1992).
20. Panina-Bordignon, P. *et al. J. exp. Med.* **176,** 1779–1784 (1992).
21. Pullen, A. M. *et al. Cell* **61,** 1365–1374 (1990).
22. Pullen, A. M. *et al. J. exp. Med.* **173,** 1183–1192 (1991).
23. Woodland, D. L. & Blackman, M. A. *Immun. Today* **14,** 208–212 (1993).
24. Passalacqua, E. F. *et al. J. molec. Biol.* **228,** 983–986 (1992).
25. Jones, E. Y., Walker, N. P. C. & Stuart, D. I. *Acta crystallogr.* A**47,** 753–770 (1991).
26. Jones, A. *Meth. Enzym.* **115,** 157–171 (1985).
27. Brünger, A. T., Kuriyan, J. & Karplus, M. *Science* **235,** 458–460 (1987).
28. Bjorkman, P. J. & Davis, M. M. *Cold Spring Harb. Symp. quant. Biol.* **LIV,** 365–373 (1989).
39. Choi, Y. *et al. Nature* **346,** 471–473 (1990).
30. Brown, J. H. *et al. Nature* **364,** 33–39 (1993).

ACKNOWLEDGEMENTS. We thank A. R. Rees and P. Hambleton for support and encouragement, V. Subramanian, T. Edwards, H. Reyburn and S. Davis for discussion, P. Artymuik for the database search, and the SERC for a studentship to E.F.P.; D.I.S. is a member and E.Y.J. an associate member of the Oxford Centre for Molecular Sciences supported by the SERC and MRC. E.Y.J. is supported by a Royal Society University Research Fellowship and K.H. by the OCMS.